REAL-TIME HUMAN HAND POSE ESTIMATION AND TRACKING USING DEPTH SENSORS

by

Mustafa Furkan Kıraç

B.S., Mechanical Engineering, Boğaziçi University, 2000

M.S., Systems and Control Engineering, Boğaziçi University, 2002

Submitted to the Institute for Graduate Studies in
Science and Engineering in partial fulfillment of
the requirements for the degree of
Doctor of Philosophy

Graduate Program in Computer Engineering

Boğaziçi University

2013

ACKNOWLEDGEMENTS

I would like to dedicate this thesis to my now passed away grand mother, and my way-ahead-of-his-time grand father for their invaluable positive effects on me, for teaching me with unconditional love. I would like to thank my parents for their unending love and support, even sometimes there were kilometers between us. I wish to thank the following people for having helped me in one way or another during the course of my thesis. First of all, my supervisor, Prof. Lale Akarun, for having believed in me for a long time, starting from my master thesis committee. She has envisioned the direction to be investigated accurately, since 2000. Her constructive criticisms and encouragements made me feel I have learned a lot during this project. Yunus Emre, for being a great technical advisor, an awesome friend, and an exceptional coder. Gaye, for being her, and for her tolerance to Yunus Emre and I, during hard coding hours. All the members of PILAB, especially İsmail for his wide and spreading creative enthusiasm; Alp for extraordinary fast solutions; Barış Evrim, Barış Kurt, Neşe, Heysem, and Umut(s) for always studying in the lab, Cem for igniting me. Özer, for being an extraordinary friend, for his spreading joy, for our brainstorming sessions, for our unending ridiculous jokes, and long walks. Prof. Oğuz Sunay, Prof. Tanju Erdem, and Prof. Reha Civanlar; for believing in me, and together with Özer providing me the beginning of a life-long journey as a member of Computer Science Department of Özyeğin University. Alihan, Bilgin and Ersin, for their precious talks, long walks, and for being there. Finally, I would like to thank my thesis committee; Prof. Bülent Sankur for his very detailed guidance, Prof. Taylan Cemgil for his tolerance to my heuristics, Prof. Albert Ali Salah for his game changer insights, and Prof. Tanju Erdem for supporting me during my difficult times.

ABSTRACT

REAL-TIME HUMAN HAND POSE ESTIMATION AND TRACKING USING DEPTH SENSORS

The human hand has become an important interaction tool in computer systems. Using the articulated hand skeleton for interaction was a challenge until the development of input devices and fast computers. In this thesis, we develop model-based super real-time methods for articulated human hand pose estimation using depth sensors. We use Randomized Decision Forest (RDF) based methods for feature extraction and inference from single depth image. We start by implementing shape recognition using RDFs. We extend the shape recognition by considering a multitude of shapes in a single image representing different hand regions centered around different joints of the hand. The regions are utilized for joint position estimation by running mean shift mode finding algorithm (RDF-C). We combine shape recognition and joint estimation methods in a hybrid structure for boosting the quality. RDFs, when used for pixel classification are not resistant to self-occlusion. We overcome this by skipping the classification, and directly inferring the joint positions using regression forests. These methods assume joints are independent, which is not realistic. Therefore, we conclude our single image based framework by considering the geometry constraints of the model (RDF-R+). The accuracies at 10 mm acceptance threshold are acquired for synthetic and real datasets. Comparing RDF-C and RDF-R+ methods respectively, we report significant accuracy increase. We finally extend single image methods to tracking dynamic gestures. We learn the grasping motion from synthetic data by extracting a manifold, and fix RDF estimations by projecting them onto the manifold. We then track the projections by using a Kalman Filter.

ÖZET

DERİNLİK ALGILAYICILARI İLE GERÇEK ZAMANLI İNSAN EL POZU KESTİRİMİ VE İZLEMESİ

İnsan eli bilgisayar sistemlerinde önemli bir iletişim aracı olmuştur. Eklemli iskelet modelleri ile giriş aygıtlarının ve hızlı bilgisayarların gelişimine kadar çalışma yapılamamıştır. Bu tezde derinlik algılayıcıları ile insan el pozu kestirimi için gerçek zaman ötesinde çalışan model tabanlı eklem metodları geliştirdik. Derinlik imgesinden öznitelik özütleme ve çıkarımı için Rasgele Karar Ağaçları (RDF) kullandık. RDF'leri şekil tanıma için uygulayarak başladık. Şekil tanımayı aynı derinlik resminde eklemler etrafında merkezlenmiş birden fazla şekli destekler biçimde geliştirdik. Mean shift algoritması kullanarak bu bölgelerin merkezlerindeki eklemleri kestirdik (RDF-C). Şekil tanıma ve eklem kestirimini birleştirip melez ağaçlarla kaliteyi arttırdık. RDF'ler piksel tanıma ile kullanıldığında kapatma durumlarına dayanıklı değiller. Bu problemi tanıma adımını atlayarak ve eklemleri kestirirken bağlanım kullanarak aştık. Bu metodlar gerçekçi olmayan biçimde eklemleri bağımsız olarak kabul ediyorlar. Bu yüzden tek resim tabanlı yöntemimizi modelin geometrik özelliklerini kullanarak geliştirdik (RDF-R+). 10 mm kabul eşiğinde doğruluk değerlerini sentetik ve gerçek veriler üzerinde hesapladık. RDF-C ve RDF-R+ metodlarını kıyasladığımızda doğruluk değerlerinin büyük artış gösterdiğini gözlemledik. Son olarak, tek resim temelli metodlarımızı dinamik hareketler izlemek için geliştirdik. Sentetik veriden kavrama hareketinin manifoldunu öğrendik. RDF kestirimlerimizi manifold üzerine izdüşümleyerek düzelttik ve Kalman süzgeci ile izledik.

TABLE OF CONTENTS

LIST OF FIGURES

LIST OF TABLES

1. INTRODUCTION

1.1. Motivation

An important area of research for the last four decades has been human computer interaction. Improvement of work efficiency and quality depends on the enhancement of communication between humans and computers. For that reason, new mice and keyboards are still being designed. In spite of the new designs, the use of classical input devices has become a bottleneck when compared to the capabilities of today's computers. Natural interfaces which make use of speech, touch, and gestures are sought. Speech recognition has been widely used and has proved its success in recognizing a multitude of languages. Touch interfaces have become mainstream with the invention of touch enabled LCD tablets. After the release of multi-touch enabled devices, touching has become a big part of our lives. Even babies are able to touch and pan these devices before they are able to talk. However, the real breakthrough will be through the use of the human hand gestures as an input device.

Gesture based communication is very intuitive for humans. A simple way to employ gesture recognition is by tracking the position of hands and detecting a gesture. Detecting and tracking the centers of naked hands are relatively simpler when compared to detecting the exact configuration of the articulated pose. Unfortunately, most of the hand gestures require the exact detection of the hand pose and tracking the pose variations in a robust fashion. Even in the presence of powerful CPUs, articulated hand pose extraction is a very difficult problem. Moreover, the hand is a small limb that produces self-occluded poses during gesture performance.

With the introduction of inexpensive depth cameras, the human computer interaction field has been revolutionized; and it is now feasible to establish methods employing computer vision based interaction. Bypassing the illumination based problems encountered on the images captured by conventional cameras, new depth cameras have made it possible to establish very fast and less power hungry methods. Unfortunately,

inexpensive depth cameras that are widely used still work on low resolution.

1.2. Definition of the Problem

The major problem attacked in this thesis is to capture the skeletal pose configuration of the hand in super real-time once its single depth image is available, as illustrated in Figure 1.1. Recognition of the hand shape and the associated articulation of the hand shape is a well-known way of capturing the skeleton. The skeletal configuration is available as meta-data during the training. In this method, the training phase only learns the differentiation of different silhouettes of shapes. This kind of method is named as "shape recognition" in this thesis. Unfortunately, shape recognition is not flexible enough to be extended to all kinds of hand configurations. It works for a limited number of different poses of the hand. As the number of poses becomes higher than 100, distinction between different shape silhouettes of the hand becomes difficult, and the shape recognition performance of the algorithms starts to decrease. Alternative methods for finding the locations of the different joints of a hand without using shape recognition are essential. Pose estimation is the problem of estimating the the coordinates of different hand joints. For a limited number of different hand poses, the shape recognizers are adequate while we need pose estimators for more flexible and accurate results.

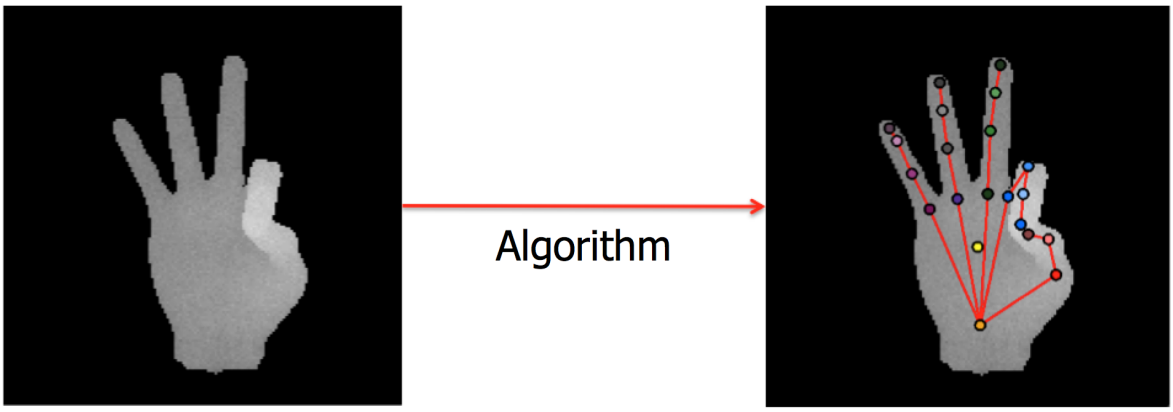

Figure 1.1. Problem definition: (a) depth image captured, (b) skeletal configuration of all the joints are extracted.

Extracting the hand joints independently from a single depth image present an-

other difficult problem. Some of the joints whose coordinates are to be found may not be visible in the image due to self-occlusion. Unfortunately, most of the gestures produce occluded depth images where a large proportion of the hand parts are unseen. The additional challenge is to extract the articulated hand pose from self-occluded, noisy, and low resolution hand depth images, with algorithms that are suitable for real-time implementation on current CPUs and/or GPUs.

In addition to that, most of the time, gesture recognition is a preliminary step to another task. Therefore, real-time extraction of the articulated hand pose should not consume all the processing power of the computer so that other algorithms that depend on the extracted pose sequences can operate within feasible amount of idle CPU cycles. We need to solve most of the task at the training phase so that the inference step requires minimal amount of processing power. For that reason, the speed requirement is "super-real time", rather than real-time.

1.3. Real-time Hand Pose Estimation with Advances in Sensors

Dynamic hand gesture and hand shape tracking is a tedious task. The problem is hard due to the deformable nature of the hand. If the joint estimates are known, it is possible to track the joints in real-time as presented in [1]. Even after manual initialization such a system depends on extreme GPU parallelization and special hardware. Heavily depending on the temporal domain information also induces errors that accumulate over time during tracking. Re-initialization of the joint estimates are required from time to time. Unfortunately, detecting pose configuration from a single image is a challenging problem. Achieving this in real-time is another difficulty. In addition to that, dynamic gesture detection may be the preliminary step of an application, hence, the application's extra processing demands should be met. In an application such as a game, there are other processing demands.

Competition of gaming consoles produced a new set of requirements which rely on qualitative body and hand pose estimation in a fast manner. Although real-time estimation of joints in human body or human hand is difficult enough, this is not fast

enough from the perspective of gaming industry. Gaming consoles need great amounts of power to be allocated normally for running the artificial intelligence logic of the game and supporting the game scenario by generating realistic computer graphics. These tasks normally spend most of the processing power already. Hence, in reality game developers need every bit of CPU/GPU cycle for squeezing all the power from the console for providing a competitive and profitable game. Human body and hand pose estimation must be solved not in real-time but in super real-time, freeing most of the power of the CPU/GPU to the game itself. Unfortunately, preliminary preprocessing step of foreground and background segmentation is an involved task on its own when working with color cameras. Background clutter poses a challenging computer vision problem and cannot be solved in super real-time using today's computers. Depth sensors have provided an easy solution to this problem since they are both bypassing the illumination problem and the background segmentation problem. Unfortunately, depth sensors were quite expensive, which is not acceptable by game industry, and they were gathering low resolution imagery. Recently, new cost-efficient depth sensors [2] have provided a very cost effective solution to this problem. They used structured infrared pattern projection to the environment from which they rendered the environment's depth map in real time. The sensor is very cheap and is bundled with Microsoft Xbox Gaming Console starting from 2011.

Recent advances have shown that using random classification forests on depth images is a suitable choice for hand pose skeleton extraction, since the recognition phase is very fast and requires minimal time complexity. A method which works on single depth images for human body pose estimation has been presented by [3] and revolutionized the game industry with the help of Kinect. Randomized decision trees are demonstrated for their extreme parallelism, resilience to over-fitting, and quality estimations as presented in [4]. Since both quality tracking and automatic initialization of the hand both demand good and fast single frame observations, we choose an adaptation of the randomized forest methodology to human hand as shown in [5].

1.4. Summary of Contributions

The basic idea explored in this thesis is that the notion of fast joint estimation of articulated shapes can be, and should be, learned from synthetic examples of an articulated model. Specifically, we develop new approaches that learn an embedding of the 3D data where real data performance of the learned model is fast and high. We start by modeling the human hand in 3D by rigging a skeleton to it. The created hand synthesizer is capable of representing most configurations that a human hand can be in. A crucial practical advantage of the synthesizer approach is that any articulated 3D model which is represented by a 3D mesh model with a skeleton can be animated for generating big amounts of qualitative synthetic training samples, which in turn can be used for training an expert suitable for parallel recognition. In some of the applications reported here, we use our training approach, and achieve state-of-the-art performance in super real-time.

We then develop and implement a family of algorithms for learning such an embedding. The algorithms offer a trade-off between simplicity and speed of learning on the one hand and accuracy and flexibility of the learned concept on the other hand. We then describe four applications of our learning approach in computer vision: for a classification task of different shape regions by visual similarity, for a pixel classification based hand pose estimation, for a regression task of estimating articulated human hand pose from images, and for a tracking task of specific human hand gesture from videos.

In the context of single frame estimation by regression, the novelty of our approach is that it relies on learning an embedding that directly reflects model's constraints in the target space by using multi-modality of individual estimates of different joints. For instance, in the case of the human hand, this means that the estimated coordinates of different joints are always compatible with the bone hierarchy and the length of bones of the object.

In the context of tracking, we propose a novel embedding which represents both the prior knowledge of a dynamic gesture and the constraints of the model. Tracking

runs on the extracted manifold using a standard Kalman Filter that extremely improves the joint estimation accuracy if the possible gestures are known beforehand.

1.5. Organization of the Thesis

Chapter 3 provides the background for the thesis research. It describes the prior work in related areas, with particular emphasis on the two ideas that inspired our learning approach: randomized forests and manifold extraction for dynamic gestures. Chapter 2 mentions about the 3D model designed for generating synthetic training data. Chapter 4 describes the basic randomized decision forest usage for detecting shapes from depth images. Armed with these algorithms we develop super real-time approaches for two computer vision domains. In Chapter 5 and Chapter 6 we describe methods for estimating articulated pose of human hand figure from a single depth image. In Chapter 7 a method for extracting non-linear manifolds is utilized for tracking pre-learned dynamic gestures. We conclude with the discussion of the presented approaches and the most important directions for future work in Chapter 8.

2. MODELING OF THE HUMAN HAND

In this thesis, we study on fitting a hierarchical model to a single depth camera image of a human hand and track the articulated motion during a specific dynamic gesture. Human hand is a highly deformable object. Labeling 3D coordinates of hand joints in depth images is a tedious task. Moreover, inferring the 3D coordinates from a single depth image is a hard problem even for a human. The amount of data that is necessary for a qualitative training is vast, hence, manual labeling is infeasible. Synthetic data generation has already been considered by [6] and found to be effective, even better than real data at times. Being able to generate synthetic human hand data requires a detailed study of 3D modeling and animation. Fortunately once a synthesizer is designed, the difficult problem of collecting training data along with ground truth labels is achieved. In this chapter, we describe the development of a 3D human hand rigged with a skeleton that can be animated so that it can represent the poses of a real human hand.

2.1. Introduction

The skeleton of the human hand consists of 27 bones as shown in Figure 2.1: the eight short bones of the wrist or carpus organized into a proximal row, which articulates with the skeleton of the forearm, and a distal row, which articulates with the bases of the metacarpal bones (i.e. the bones of the palm or "hand proper").

The articulations are:

- interphalangeal articulations of hand (the hinge joints between the finger bones)
- metacarpophalangeal joints (where the fingers meet the palm)
- intercarpal articulations (where the palm meets the wrist)
- wrist (may also be viewed as belonging to the forearm).

The average length of an adult male hand is 189 mm, while the average length of an

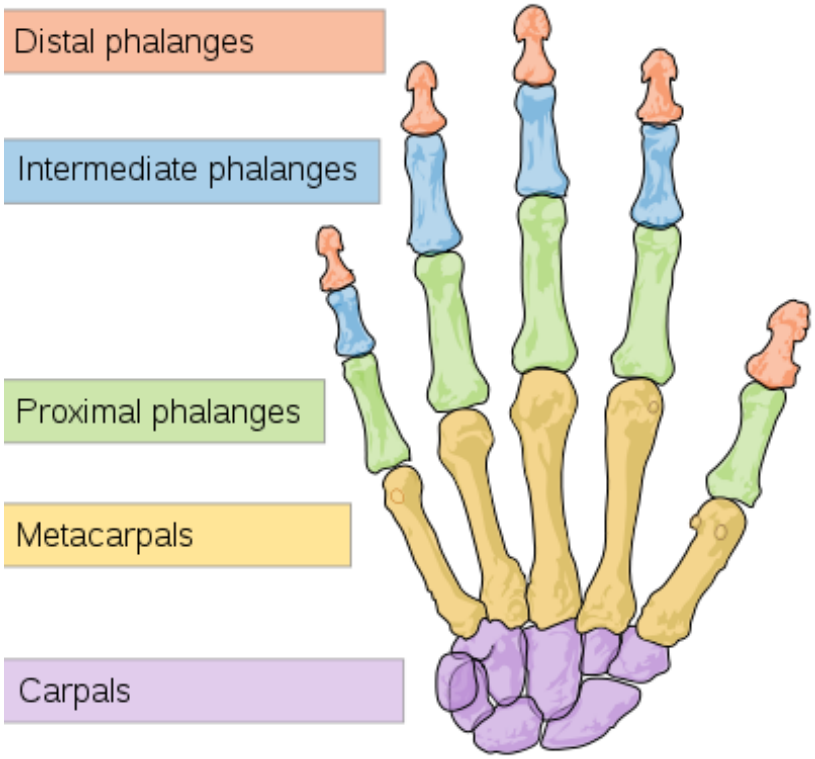

Figure 2.1. Anatomy of the human hand.

adult female hand is 172 mm. The average hand breadth for adult males and females is 84 and 74 mm respectively. The ratio of the length of 2nd finger to the length of the 4th finger (noted 2D:4D) in adults is affected by the level of exposure to male sex hormones of the embryo in utero. This digit ratio is below one for both sexes but it is lower in males than in females on average.

The size of the human hand is the most significant feature among many minor differences from person to person. In this study we assume a mean human hand that is suitable for all of the samples. At the testing time, the size of the hand is calibrated to the data which is to be recognized in real-time.

One of the very early hand animations using a computer is presented in a short movie "A Computer Animated Hand". It is a 1972 American computer-animated film produced by Edwin Catmull and Fred Parke. Produced during Catmull's tenure at the University of Utah, the short was created for a graduate course project. After

creating a model of Catmull's left hand, 350 triangles and polygons were drawn in ink on the model. The model was digitized and laboriously animated in a three dimensional animation program that Catmull wrote [7].

After four decades, in computer graphics, various hand models have been developed for several typical applications. An example of a realistic model of a human hand includes muscle architecture, muscle contraction, mechanical properties, muscle deformation models [8]. Computer modeled hands are required for different scientific disciplines. In computer graphics, the major aim is to represent the exteriors of the hand as realistic as possible. The interaction of the hand model with its surroundings is also important. In the field of medical research, scientists also require volumetric modeling of the hand. They want to cut a slice and examine the interiors of the model as required. In the field of computer vision, we require a good combination of surface modeling with the least possible resources.

The most prominent application areas of hand models are model-based tracking, interactive grasping, and simulation systems used for e.g. surgery planning. Heap *et al.* [9] have built a statistical hand shape model from simplex meshes fitted to MRI data for their tracking system. For model-based finger motion capturing, Lin *et al.* [10] employ a learning approach for the hand configuration space to generate natural movement.

2.1.1. Hand Modeling in Computer Graphics

The modeling aim in computer graphics is to render the surface model as complex as possible, making it photo realistic. Good interpolative behavior is also essential in-between the key-frames of the designed animation as first illustrated in the work of Badler *et al.* [11]. [12] further enhanced the concept of local deformations associated with joint motion. The 3D hand model for computer graphics and computer animation is usually created by thousands of smooth polygons, skin deformations at the joints, and the model will be skinned by realistic textures [7, 13, 14]. Some successful human hand models incorporate features such as nails and skin bulging. Usually these kinds

of 3D hand models are created by professional 3D softwares, such as, AutoCAD, 3D Studio MAX, Poser, etc. In old days, the 3D hand data was gathered using archaic electromagnetic sensors such as the Polhemus 3-SPACE [15]. In order to acquire the accurate 3D hand model data, usually a plaster caste of the human hand was required. Because of the long durations required during the scanning phase, the hand model was needed to be still in the same pose for minutes.

2.1.2. Hand Modeling in Medical Research

3D human hand models are also extremely useful for the medical research with different uses. Researchers are not mainly concerned about the exteriors of the model. Interior modeling with utmost detail is the major concern. Medical research requires a very detailed volumetric internal model which includes bones, tendons, veins, etc. Most of these 3D hand model's data are gathered from X-ray or Computed Tomography (CT) [16], or cadavers [17]. Most of these 3D human hand models are used in clinical and medical education, such as tendon displacement and range of motion of joints. Thompson *et al.* [18] designed a bio-mechanical workstation with interactive graphics for hand surgery. It was used to apply mathematical modeling and describe the kinematics of the hand and its resultant effect on hand function. Methods were developed to portray kinematic information such as muscle excursion and effective moment arm and extended to yield dynamic information such as torque and work. In 2003, Albrecht *et al.* [19] presented a human hand model with the underlying anatomical muscle structure. This 3D human hand model's motion is controlled by the muscle contraction amounts. They employ a physically based hybrid muscle model to convert these contraction values into movement of the skin and the bones. Consequently, this model can simulate the muscle deformation of the human hand.

2.1.3. Hand Modeling in Computer Vision

There are multitudes of different 3D hand models developed using computer graphics. Most of the time, 3D hand models used are created by complex modeling primitives such as NURBS (non-uniform rational b-splines). Complex surfaces can

make the hand model look very realistic [20]. In our problem, we work with low resolution depth images. We don't depend on complex representations of the surface. A standard polygon mesh with enough triangles will suffice. Moreover, we will not be relying on renders of the hand model during inference. Synthesizer outputs will be needed only in our training phase. If the renders of the 3D hand model were required during testing, it would be better to further simplify the hand model. Redrawing the model using different pose configurations during testing stage may be essential if we were to use analysis-by-synthesis approach. For instance, a particle filter based shape recognizer or pose estimator would create different particles, hence renders of the model, and observe the particles [21]. The main idea about the analysis-by-synthesis approach is to analyze the model's posture by synthesizing the 3D model of the human hand and then varying its parameters until the model and the real human hand match as close as possible [22]. As a result, a sufficient 3D hand model with less parameters and realistic simulation can increase the tracking algorithm's accuracy and speed.

2.2. A Skeleton Model for the Human Hand

The main component of our system is a prototype hand model with anatomical structure, which is denoted as our reference hand model in the following. The building blocks of our reference hand model are: the skin surface, which is represented by a triangle mesh consisting of 12000 triangles; the skeleton of the hand, composed of 21 triangle meshes corresponding to the individual bones of the human hand; a joint hierarchy, which matches the structure of the skeleton, with an individually oriented coordinate system at each joint center defining valid axes of joint rotation. For the purposes of our study we do not need a set of virtual muscles, which are embedded in between the skin surface and the skeleton nor a mass-spring system, interlinking the skin, skeleton, and muscles. The skeleton model is directly rigged to the mesh. The model is animated using a custom software developed during this study. Software can generate simulated depth and ground truth label images calibrated with a real camera model and train classifiers and/or regressors.

We use a 3D skinned mesh model with a hierarchical skeleton, consisting of 19

bones corresponding to the bones in Figure 2.1 except carpals. Carpals are modeled by using only one joint. Our skeleton structure consists of 15 joints and 21 different regions as viewed in Figure 2.2. Hand regions are chosen in a way to ensure that skeleton joints are at the centers of their corresponding regions. Hence, the thumb contains three parts and all the other fingers contain four parts. The palm has been divided into two different regions, namely, upper and lower palm, so that the topology of the hand can alternatively be inferred better during recognition, if required. The model is animated and rendered with a depth shader or with a texture to generate depth images and labeled images, respectively.

Skeletal rigging process is enhanced by using weighting pixels that are close to the hand joints. Each pixel can belong to more than one parent joint with a different weight. This weighting process produces better deformations as the hand is animated. Skeletal animation is done using the Ogre Game Development framework [23]. 3D rendering is done using OpenGL.

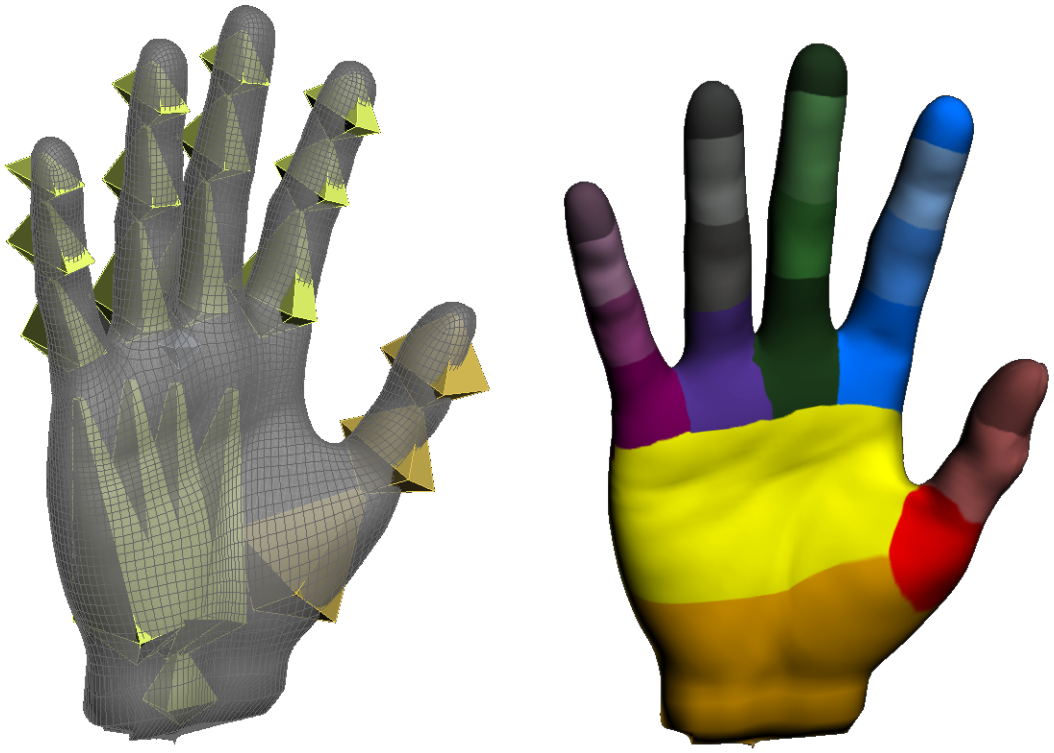

(a) (b)

Figure 2.2. The 3D hand skeleton model and its labeled parts are illustrated.

2.3. Customization for Different Hands

The framework normally uses a single skeleton rigged hand mesh. Although this work concentrates on a single hand shape, the hand model is parameterized so that the length of the fingers, size of the palm, etc., can be easily modified. The model is easily customizable for different variations of the human hand.

Synthesized data generation details are discussed in Section 6.3. Generated images and animated skeleton joint coordinates are used as ground truth during training.

3. BACKGROUND

In this chapter, we review the techniques that are used in articulated pose modeling, pose configuration estimation, and dynamic gesture tracking both for human body and human hand. We speak briefly about the sensors and how new sensors contributed to developing faster and affordable algorithms.

Hand gestures are a natural part of human interaction. In addition to their complementary roles in speech based interaction, they play a primary role when speech is absent, as in sign language based interaction. Attempts to use the hand gesture modality in human computer interaction (HCI) has intensified research efforts for articulated hand pose tracking and hand shape recognition in the last decade. Hand gesture tracking meant to track the centroid of the hand and capture dynamic gestures in time. However most of the information passed during a sign language interaction is gathered from the pose configuration of the hand. High degree of articulation poses a challenging task for capturing the exact pose of the hand in a fast manner.

Recent advances have been made on the depth camera front. Achievements in the field of high-speed depth sensors has greatly facilitated the image processing and segmentation part of the task. Usually, time-of-flight depth cameras were used to acquire depth (range) images. Two developments have recently accelerated implementations of HCI using human body and hand gestures: The first is the release and widespread acceptance of the Kinect [2] depth sensor. With its ability to generate depth images independent of external illumination conditions, this sensor makes the human body and hand detection and segmentation a simple task. The second development is the emergence of fast discriminative approaches using simple depth features coupled with GPU implementation; enabling real-time human body pose extraction [3, 24].

The last decade witnessed the step by step attack to the real-time pose estimation problem both for human body and human hand. Some of the roots of the pose estimation problem comes from object classification. Classification of smaller parts of

an object can be combined into a bigger agenda as presented by Fergus *et al.* [25]. They capture scale invariant features from a dataset in an unsupervised fashion. They then utilize these constellation of small object parts for object classification. Winn *et al.* [26] use conditional random fields in a similar fashion for detecting partially occluded objects. Liu *et al.* [27] use time-of-flight cameras to acquire depth images for hand gesture recognition. Their hand detection method is based on measuring the shape similarity by thresholding the depth data and using Chamfer distance. They recognize gestures using shape, location, trajectory, orientation and speed features of the hand. Grest *et al.* [28] use non-linear optimization techniques to iteratively fit a 3D body model to depth images in near real-time. Knoop *et al.* [29] use sensor fusion from different cues such as time-of-flight depth cameras, stereo cameras, and monocular images for capturing the human body pose by using a 3D model. Zhu *et al.* [30] utilize depth images and tracking for labeling the upper body of a human. Body parts classification is achieved by reducing the labeling problem to linear programming. Inverse kinematics is also incorporated for better tracking. First the pixels are classified as belonging to a body part, then the upper body pose is estimated. Bourdev *et al.* [31] propose a two-layer supervised classification/regression model for detecting people and localizing body components. The first layer consists of classifiers that specializes on detecting local patterns in the image. The second layer combines the output of the classifiers in a max-margin framework. Siddiqui *et al.* [32] use a data driven MCMC approach to find an optimal pose based on a likelihood that compares synthesized depth images to the observed depth image. They incorporate extra data from head and torso estimators for fast convergence of their method. Plagemann *et al.* [33] concentrate on real-time localization of important body parts such as head, hands, and feet in depth images. They both estimate the location and orientation of hands in a probabilistic manner. Ganapathi *et al.* [34] use time-of-flight cameras for model based tracking of human body using Bayesian networks. They coarsely find important body part locations and use the noisy observations as input to their probabilistic tracking framework. Suryanayaran *et al.* [35] use depth for dynamically recognizing scale and rotation invariant poses. Using a volumetric shape descriptor formed by augmenting a 2D image, they classify six signature hand poses. Shotton *et al.* [3, 6] use classification forests for human pose estimation using depth data. Doliotis *et al.* [36] train a shape

classifier from synthesized depth images and try to segment and recognize American Sign Language shapes. In [37], Gallo *et al.* use depth images along with PCA and Flusser moments for detection of predefined shape postures. Billiet *et al.* [38] extract finger alignments after segmenting the hand, and use a rule-based approach for representing hand poses. Some works make use of disparities to get depth information, and some works use color and depth data together for estimating hand poses [39, 40]. Liang *et al.* [40] use a model based estimation framework which utilizes both the color and depth cues for tracking fingertips. They then employ articulated ICP for tracking the full hand pose.

The state-of-the-art approaches for human body pose estimation generally use the Kinect [2] camera. They employ a variety of techniques: Shotton *et al.* [3] use a large amount of labeled synthetic images to train a randomized decision forest (RDF) [41] for the task or body part recognition. In a later study, Girschick *et al.* [24] use the same methodology, but let each pixel vote for joint coordinates; and learn the voting weights from data. Ye *et al.* [42] rely on pre–captured motion exemplars to estimate the body configuration as well as the semantic labels of the point cloud. Lopez *et al.* [43] use an upper body model and tracks it using a hierarchical particle filter. Although these ideas may be extended to extracting the 3D pose of the hand, the problem is made more difficult by the increased pose variability and self-occlusion.

There are also tracking based skeleton extraction methods in the literature. Most skeleton tracking algorithms estimate a skeleton by exploiting kinematic constraints and dynamics of the object: Bregler *et al.* [44] propose new linear update equations of motion for tracking the walking videos of humans. They assume walking motion is involving minimal acceleration and they model by a twist motion model. Their initialization is costly and all the remaining tracking purely depends on the initialization step. Sigal *et al.* [45] use belief propagation over particle sets of body parts. They learn conditional probabilities of body connections from motion captured training data. The parts of body are sampled from a 3D articulated human model. Simple bottom–up body part detectors are also implemented for automatic re-initialization and recovery from tracking errors. They run their algorithm by using four calibrated color cameras

with successful results. Wang *et al.* [46] employ a nearest neighbor pose classification from a sampled synthetic hand pose dataset. Their tracking framework depends on using a color glove specially designed for easily recovering the hand regions from color images. They then utilize inverse kinematic constraints for fine tuning the captured pose. Brubaker *et al.* [47] use sequential Monte Carlo tracking with kinematic constraints for tracking walking motion in monocular video. These algorithms can achieve high frame rates by using temporal domain information between frames. Unfortunately, without constant re-initialization, these tracking algorithms are going to lose track eventually.

There are several surveys on hand pose estimation and gesture recognition [48, 49]. Erol *et al.* [48] review hand pose estimation methods. They investigate both partial and full pose estimation methods. They categorize the full pose estimation methods into single frame and model-based tracking methods. Most of the works in the literature focus on grayscale or color based methods. These works use either single or multiple cameras. Athitsos *et al.* [50] create a large synthetic hand pose database using an articulated model and estimate 3D hand pose from a single frame cluttered image by finding the closest match. [51] recovers hand pose from a single frame using an RVM-based learning method. In order to overcome the self-occlusion problem, multiple views are combined. Oikonomidis *et al.* [1] use Particle Swarm Optimization for solving the 3D hand pose recovery problem. [52] works on monocular videos for 3D hand pose estimation. They track hand poses using a generative model-based method. Thippur *et al.* [53] use visual shape descriptors for describing the hand shape. Hand pose estimation studies have initially relied on 2D models [48]. Although pose variability and occlusion limit the success of 2D approaches, successful partial models have been defined [54].

Stenger *et al.* [55] use a 27 DOF 3D hand model composed of quadrics. They utilize fast projection of quadrics on a 2D screen and edge detection as the features for observing the hand from color images. They successfully track the pose configuration by using an unscented Kalman filter. Rosales *et al.*designed a Specialized Mapping Architecture (SMA) where a regression based method is employed for mapping hand

silhouettes to pose configurations [56]. They rendered hands using commercial library [57]. A stochastic learning method is used to capture the mappings from the synthesized data. In testing time, they segment the hands from color images, and feed the extracted silhouettes to the SMA architecture for estimating pose configuration. Mo *et al.* [58] work on low-resolution depth images acquired from a laser-based camera. Their algorithm requires manual initialization and uses basic sets of finger poses for interpolating a hand pose. Malassiotis *et al.* [59] use depth images generated from synthetic 3D hand models. They rely on depth cameras for successful segmentation of hands. They then recognize German Sign Language hand shapes from depth images.

These approaches have achieved good performances even in the presence of occlusions and pose changes, though their time performances have limited their application in real-time HCI applications. In a recent study, Oikonomidis *et al.* [1] present a solution that makes use of both depth and color images. They propose a generative single hypothesis model-based pose estimation method. They use particle swarm optimization for solving the 3D hand pose recovery problem, and report accurate and robust tracking in near real–time (15 fps), with a GPU based implementation.

Our work [5] has adapted the method in [3] to hand pose estimation with successful results. They further enhanced randomized decision forest based hand pose estimation by using multiple layers of forests. Clustering the hand pose configurations and training a specialized RDF for each different cluster yielded better results. They also utilized an RDF for detecting the cluster of the depth image in inference [60]. A similar approach is also used in [61], which detects the hands in the first layer and then classifies hand shapes in the second layer. Method of Keskin *et al.* [62] classifies hand shapes in the first layer and then estimates the hand pose in the second layer.

Recent emphasis on manifold based tracking is also producing attention. Manifold extraction techniques have evolved in last two decades considerably. Machine learning can often be visualized in three major categories. Firstly, a dataset is considered as inputs and outputs in supervised learning. Secondly, a required goal is bound with a reward in reinforcement learning. And in unsupervised learning, the objective is

to extract the structure of the underlying dataset. In manifold extraction, an approach to unsupervised learning, we represent the original data Y, in a lower dimensional embedded space X. Probabilistic variables in the lower dimensional space are named as latent variables. Mackay [63] proposed Density networks, and employed a multi-layer perceptron (MLP) to provide mapping from latent space to the data space. A prior distribution is placed over the latent-space and the latent-spaces posterior distribution is approximated by sampling. Bishop *et al.* [64] used a radial basis function (RBF) network instead of an MLP for faster training times. This model later became the generative topographic mapping (GTM) [65] where the latent-space was uniformly sampled, and a mixture model was fitted via the expectation-maximization (EM) algorithm. The latent space uniform grid layout is shared with the self organizing map (SOM) of Kohonen *et al.* [66]. These methods represent the latent space as a grid, however, point representations of the latent-space are useful because they allow for non-linear models. Points are easier to map through the non-linear mapping to the data-space. Standard statistical tools that rely on linear mappings, such as principal component analysis (PCA) and factor analysis (FA) may not be able to reflect the structure of the data in a low dimensional embedding. PCA seeks a lower dimensional sub-space in which the variance of the data is maximized. For visualization purposed, generally a 2D sub-space is sought. However, two dimensions may not be enough to capture the variability in the data. Structure of the data is most probably not captured. PCA also has a latent variable model representation shown by Tipping *et al.* [67]. It is strongly related to Factor Analysis (FA). Other famous works that focused on forming the proximity matrix include Isomap by Tenenbaum *et al.* [68], and usage of spectral clustering in Shi *et al.* [69].

Reducing the pose space dimensionality is favorable since human activities are often observed to be located on a low dimensional latent space [70, 71]. Manifold tracking depends on three main steps. First, a mapping between original pose space to manifold must be available. Second, a mapping from manifold to original space must also be defined. Third, how tracking occurs within the manifold must be defined. PCA is linear and not adequate since the mapping from original space to manifold space is almost always non-linear. Locally Linear Embedding (LLE) or Isomap can

capture this non-linear embedding, but they are not invertible. Inverse mapping is more important since the tracking is to be done in the manifold space. Gaussian Process Latent Variable Models [72] and Locally Linear Coordination (LLC, [73]) provide the inverse mapping. Sminchisescu *et al.* [74] extract the underlying manifold by using spectral embedding, a type of Gaussian mixture model. Inverse mapping is provided by the learned Radial Basis Functions, after which the tracking is done by a linear dynamical model. Urtasun *et al.* [75] utilize a GPLVM to learn prior models for 3D human tracking. GPLVMs are used easily in combination with gradient descent based optimization schemes since they generate smooth mappings between manifold and pose space. In later works [76, 77], a Gaussian Process Dynamical Model (GPDM) is learned from training data, which also learns a latent space dynamic model. Work by Moon *et al.* [78] has examined the contribution of dynamics in the human motion tracking. Tian *et al.* [79] use a GPLVM for 2D pose estimation. Particle filtering is used, where the particles are sampled in the latent manifold space. On the other hand, Li *et al.* [80] use LLC for learning the mappings. Their mapping is designed in a way so that close points in the latent space map to close poses in the original pose space. Therefore, a simple dynamical model could be used. In more recent approaches, Ek *et al.* [81] design a shared GPLVM model which describes a method for recovering 3D human body pose from silhouettes. Method encapsulates both pose and silhouette features, and is generative,which allows to model the ambiguities of a silhouette representation in a principled way. A dynamical model is learned for overcoming the ambiguities using temporal consistency. Lee *et al.* [82] model hand shape variations using 4D torus manifolds. They estimate the camera view angles, pose configuration of the hand at the same time using Particle Filters that run on the extracted manifold. Advantages and disadvantages of various embedding techniques are illustrated in Table 3.1.

In this thesis, we are going to discuss the key approaches required for estimation of hand joints both in a single image setup and temporal domain tracking without a need for regular re-initialization. The basis of the methodologies that is going to be developed for single image estimation depends on Randomized Decision Forests. Tracking in the time domain makes use of low dimensional manifold learning.

Table 3.1. Overview of the relationship between embedding algorithms. A ✓ symbol indicates the algorithm exhibits that property, an S indicates that there is an interpretation of the algorithm that supports the property. $\mathbf{X}$ is the embedded space. $\mathbf{Y}$ is the data-space. *Nonlinear*: method allows for nonlinear embeddings, *Probabilistic*: method is probabilistic, *Convex*: method has a unique solution [72].

	Proximity	$\mathbf{X} \rightarrow \mathbf{Y}$	$\mathbf{Y} \rightarrow \mathbf{X}$	Nonlinear	Probabilistic	Convex
PCA	S	✓	✓		S	✓
Factor Analysis		✓	✓		✓	✓
Kernel PCA	✓		✓	✓		✓
MDS	✓			✓		
Sammon mapping	✓			✓		
Neuroscale	✓		✓	✓		
Spectral clustering	✓			✓		✓
GTM		✓		✓	✓	
GPLVM	S	✓		✓	✓	

3.1. Summary

In this chapter, we have reviewed methods for shape classification and joint estimation from single image. We also investigated the manifold extraction based tracking schemes in the context of which we develop our learning approach. In the next chapters, we adapt existing approaches in the literature, and customize them for the human hand. Step by step, we improve the quality and add our novel contributions.

4. SHAPE CLASSIFICATION FROM SINGLE DEPTH IMAGE

The RDF model, which has been used for body pose estimation in [3] has been adapted to a number of hand related tasks. One of our first attempts has been hand shape classification [62]. In this chapter, we first present a shape classifier, which is an adaptation of the RDF based pose estimation method of [3] to generic shapes. We call this new type of RDF an RDF for shape classification (RDF-S).

The performance of the shape classification method is evaluated on real and synthetic images, respectively. In particular, RDF-S is tested on the publicly available ASL dataset of [83] and is shown to achieve a success rate of 97.8%. Multi-user ASL letter recognition is a difficult task, and comparable good results to ours have been reported in the literature on other datasets. [84] provides a good review of ASL letter recognition on depth data.

4.1. Randomized Decision Forest (RDF)

A decision tree is used for inferring a set of posterior probabilities for the input. It consists of internal nodes and leaf nodes; where the internal nodes propagate the data to one of its children. In the binary case, decisions to split the data are simply yes/no decisions. Leaf nodes do not make a decision but give statistical information about the nature of the data. The type of statistical information depends on the application.

In randomized decision trees, the decisions on internal nodes are made by selecting a random subset of the features. The aim is to reach leaf nodes that are as pure as possible. A pure node consists of samples of only one class. Thus, the features are selected to yield maximum information gain, in other words, minimum entropy. The

decision rule is usually of the form:

$$f_n(v) < \tau_n \tag{4.1}$$

where $f_n(v)$ is a split function, v is the feature vector and τ_n is a threshold, at split node n. A split function is a real valued function on a subset of features.

During training, the split functions and thresholds of nodes are chosen to satisfy the minimum entropy condition. On the leaf nodes, statistics are collected using the data associated with that node. In the case of classification, this is usually a histogram of the class labels of the leaf node data.

Randomized Decision Forest (RDF) is an ensemble of decision trees. Each tree can be trained on the same or slightly different datasets. During testing, the given sample is processed in each tree separately. The statistics on the reached leaves are combined for a common response. In classification problems, this is usually done by accumulating normalized histograms in the leaves as shown by Shotton *et al.* [3]. Same approach for estimating human body pose has been applied to estimation of human hand pose [5].

4.2. Pixel Training and Classification using RDF (RDF-C)

During training, at each node of a randomized decision tree, a random subset of features must be selected and a decision must be made using this subset. The training data consists of large number of pixels of different depth images. Given a depth image I, features are computed as

$$F_{\boldsymbol{u},\boldsymbol{v}}(I,\boldsymbol{x}) = I\left(\boldsymbol{x} + \frac{\boldsymbol{u}}{I(\boldsymbol{x})}\right) - I\left(\boldsymbol{x} + \frac{\boldsymbol{v}}{I(\boldsymbol{x})}\right) \tag{4.2}$$

where $\boldsymbol{u}$ and $\boldsymbol{v}$ are offsets relative to the pixel position $\boldsymbol{x}$, and they are normalized by the depth at $\boldsymbol{x}$, $I(\boldsymbol{x})$. The node data consisting of $(I,\boldsymbol{x})$ pairs are split into two sets

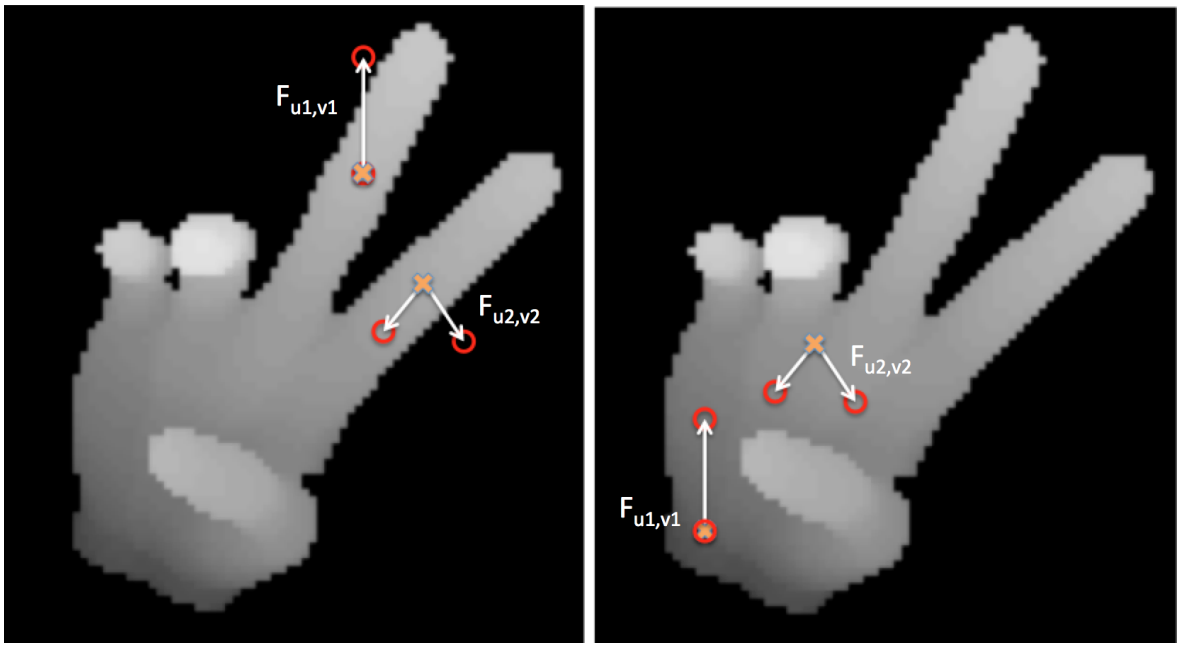

Figure 4.1. Orange crosses are the pixels to be classified. Red circles are the offset vectors from the classified pixels as in Figure 4.1. left) Two depth features give a high depth response. right) Same features in different places give smaller depth response.

for each child as

$$C_L(\boldsymbol{u}, \boldsymbol{v}, \tau) = \{(I, \boldsymbol{x}) \mid F_{\boldsymbol{u},\boldsymbol{v}}(I, \boldsymbol{x}) < \tau\} \tag{4.3}$$

$$C_R(\boldsymbol{u}, \boldsymbol{v}, \tau) = \{(I, \boldsymbol{x}) \mid F_{\boldsymbol{u},\boldsymbol{v}}(I, \boldsymbol{x}) >= \tau\}. \tag{4.4}$$

Since it is desired to split the data into child nodes with similar data at leaf nodes, the tuple $((\boldsymbol{u}, \boldsymbol{v}, \tau))$ that gives the maximum information gain is chosen among randomly created tuples. Maximum information gain is found using entropy. First, a candidate split is found and the total decrease in entropy that results from this split is calculated. The split score is

$$S(\boldsymbol{u}, \boldsymbol{v}, \tau) = H(C) - \sum_{s \in \{L,R\}} \frac{|C_s(\boldsymbol{u}, \boldsymbol{v}, \tau)|}{|C|} H(C_s(\boldsymbol{u}, \boldsymbol{v}, \tau)) \tag{4.5}$$

where $H(K)$ is the Shannon entropy estimated using the normalized histogram of the labels in the sample set K. Then, the candidate tuple that yields the maximum score

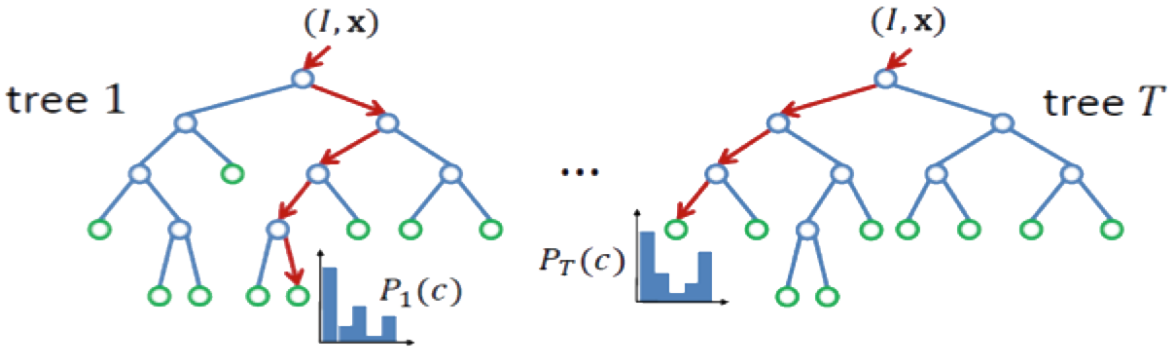

Figure 4.2. RDF classification of a pixel x in image I is illustrated for different trees.

is chosen for the particular node.

In classification, a pixel $(I, \boldsymbol{x})$ is pushed down the tree until a leaf node is reached. At each leaf node, a histogram represents the posterior probabilities $P(c_i|I, \boldsymbol{x})$ for each class c_i learned during the training phase. The final decision is made by averaging the posterior probabilities estimated by the trees of the forest as illustrated in Figure 4.2:

$$P(c_i|I, \boldsymbol{x}) = \frac{1}{N} \sum_{n=1}^{N} P_n(c_i|I, \boldsymbol{x}) \tag{4.6}$$

where N is the number of trees in the forest.

4.3. Shape Recognition using Randomized Decision Forest for Pixel Classification (RDF-C)

Shape recognition is the act of assigning a class label c to an input image I representing a certain shape. We propose an RDF model that uses scale invariant features extracted from depth images to infer the shape class. Inspired by the part classification approach of [3] and [5], we formulate an RDF for shape classification, in which each pixel votes for a shape label. The final class label is determined by majority vote. Per pixel classification is done by RDF-C.

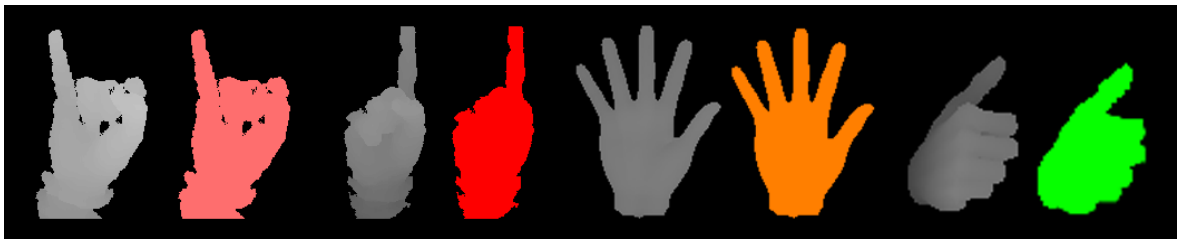

Figure 4.3. Sample RDF-S training images: The first four images are real depth images and their labels, and the rest of the images are synthetic depth images and their labels.

4.4. Randomized Decision Forest for Shape Classification (RDF-S)

An RDF-C assigns each pixel in an input image to a shape class. In order to determine a final shape label for a specific input image, the posterior probabilities of each pixel in the image are averaged, and the label that maximizes this term is selected:

$$c^* = \arg\max_{c_i} \frac{1}{M} \sum_{m=1}^{M} P(c_i | I, \boldsymbol{x_m}) \tag{4.7}$$

where M is the number of foreground pixels in the input image, and c^* is the determined shape class label.

4.4.1. Shape Classification Performance

The accuracy of the RDF-S is tested on a dataset consisting of 65K depth images corresponding to 24 of the 26 ASL letters (omitting non–static letters j and z) performed by five subjects [83]. Pugeault *et al.* reported their results on this dataset using both leave–one–subject–out cross–validation and by using half of the set for training and half for validation. For the former validation technique, we employed four trees of depth 20, and sampled 1000 features at each node. RDF-S achieved a recognition rate of 84.3%, while Pugeault *et al.* [83] report 47%. For the latter, an RDF-S consisting of a single tree reached 97.8%, compared to 69% using only depth features, and 75% using both depth and color features [83]. Moreover, an RDF-S can be trained easily using real images since image labels are consisting of pixels which are all set as the

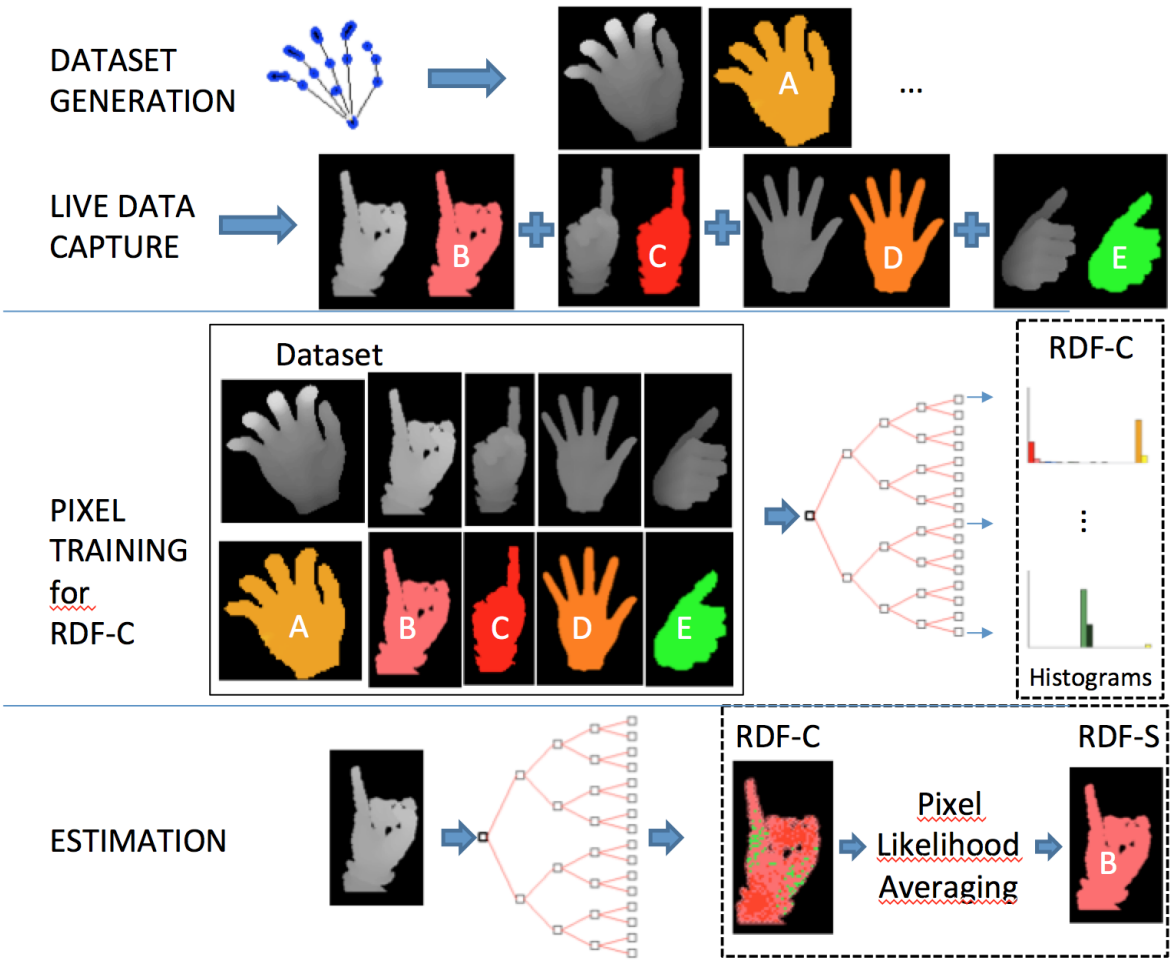

Figure 4.4. Overview of the RDF-S based pixel training and shape classification.

same shape labels. Our system achieves significantly better recognition results, and only has difficulty differentiating between the poses that correspond to the ASL letters M, N and T, as is evident from the confusion matrix depicted in Figure 4.5. The ASL letters M, N and T are very similar, as viewed in Figure 4.6.

4.4.2. Shape Classification Results

Hand shape recognition can also be achieved by using the 3D coordinate estimates of hand joints as presented in [5]. However shape recognition is a different and simpler problem than joint estimation. In this chapter, we attempted to tackle the shape recognition problem directly by applying it to single depth images of the human hand. We utilized RDF-S based hand shape classification method that achieves very

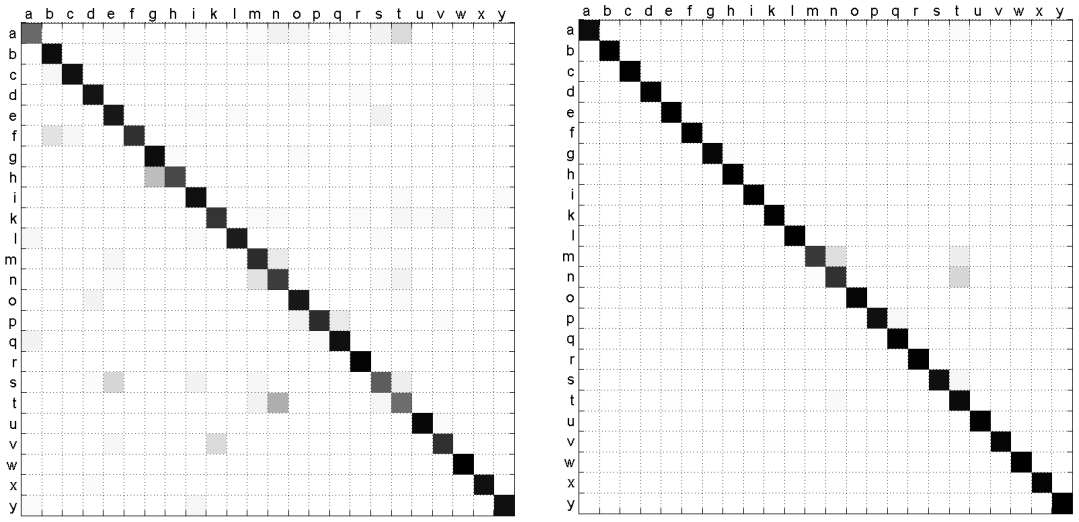

(a) (b)

Figure 4.5. Confusion matrix for the ASL letter classification task using RDF-S on SURREY dataset [83]. (a) Leave-one-subject-out with a success rate of 84.3%. (b) Half training-half validation, with a success rate of 97.8%. The main source of error is the similarity of the letter poses for M, N and T.

high recognition rates on real datasets. Specifically, our shape classification method contrasts the approach in [5] in that: (i) it does not rely on the efficiency of the hand pose estimation module; (ii) the models can be trained using real data, which simplifies the training process and gives more accurate results; (iii) evaluation is faster; (iv) fewer samples are needed for training.

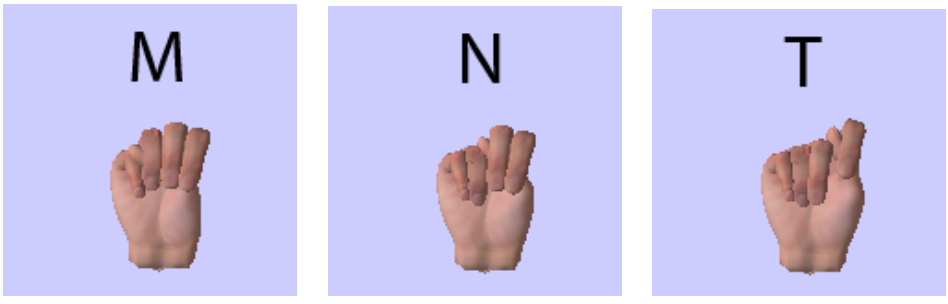

(a) (b) (c)

Figure 4.6. ASL letters (a) M, (b) N, and (c) T. These shapes differ only slightly and they are the main cause for error during hand shape classification.

5. HAND POSE ESTIMATION FROM SINGLE DEPTH IMAGE USING PIXEL CLASSIFICATION

In Chapter 4, we have described the use of RDFs for hand shape classification. However, our main goal is articulated hand pose estimation. This chapter gives the details of the hand pose estimation method which employs pixel classification that is described in Section 4.1. Section 5.1 explain the use of random decision forests for hand pose estimation based on classification (RDF-C). We then extend the idea of shape recognition to recognizing hand parts, as published in [3, 33, 25, 26, 31].

5.1. Hand Pose Estimation using Randomized Decision Forest for Classification (RDF-C)

Shotton *et al.* [3] used RDF-C for human body pose estimation. Keskin *et al.* [5] adapted that method to the hand pose estimation problem. The aim of the method is to find the formerly trained corresponding pixel regions closest to each joint. However, since some classification errors are anticipated, it would be better to find the mode of the pixel positions instead of the mean. For this purpose, first the training data pixels are labeled to define the area around the joints. A decision forest is trained using this data. On the leaves, histograms are calculated using the classes of the pixels. Training and testing framework of an RDF with a sample human hand model is demonstrated in Figure 5.1.

For a given depth image, the RDF-C algorithm yields posterior probabilities of each pixel for each class after classification. The resulting probability surfaces are generally multi-modal. Thus, simple averaging is not a suitable operation. For overcoming the high impact of misclassified pixels on the centroid of the pixel locations of the same class, a method that is more robust to false positives than averaging, must be used. In this situation, mode finding is preferred instead of averaging. A local mode finding approach, such as mean shift, can be used. The posterior probabilities assigned to

each pixel are used to estimate the joint positions as in [5]. The mean shift local mode finding algorithm [85] is used to estimate the mode of the probability density of each class label.

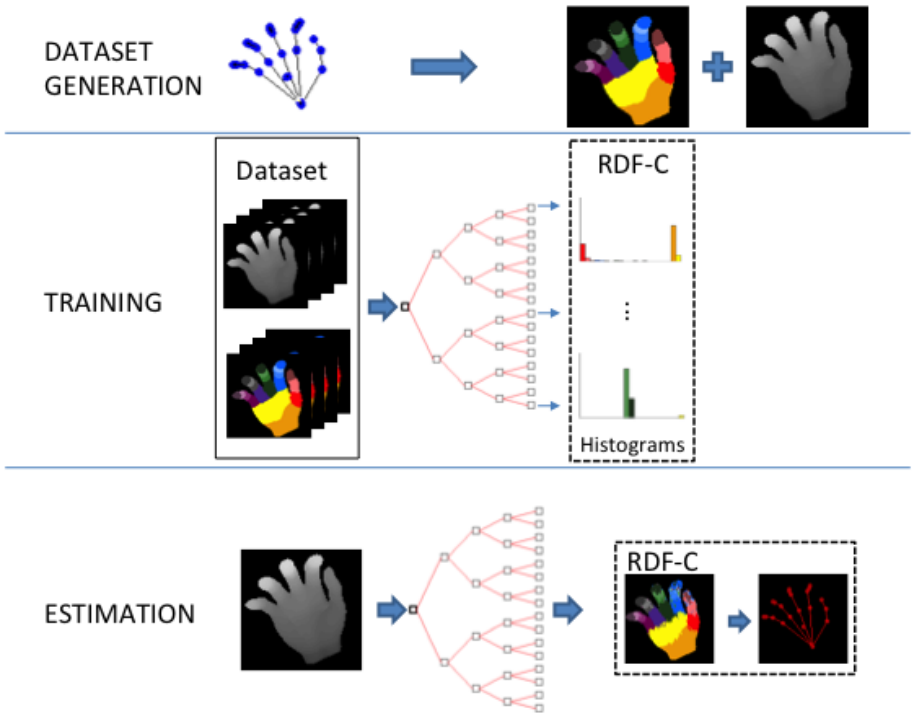

Figure 5.1. Overview of the RDF-C based pixel training and joint estimation.

First, a Gaussian kernel centered on a random point on the probability image is placed. Then, a weighted mean of the probability image under this Gaussian kernel is calculated. Weight indicates the importance of the pixel and is an estimate of the area the pixel covers. Weights are calculated as

$$w_{I,\boldsymbol{x},c_i} = P(c_i|I,\boldsymbol{x})I(\boldsymbol{x})^2. \tag{5.1}$$

The newly calculated mean point is used as the starting point of the next iteration. This is repeated until converging to a local maximum. For finding the global maximum, the algorithm runs several times, each time starting at a different initial point and the highest peak is selected. A sample convergence of mean shift algorithm is shown

in Figure 5.2 for the first bone of the thumb finger. Each pixel in the classification image evaluated by the RDF-C is normally represented by a probability distribution of joints. Each pixel is painted by its maximum likelihood estimate in the figure for facilitating the demonstration process. The bandwidth of each hand part is manually selected based on the size of each hand part. Figure 5.3 shows the final skeletal output found by the algorithm after each different hand region's centroid is estimated using mean shift. The depth of the found 2D coordinates of the joints are then approximated by looking at the pixel's corresponding depth value. Human hand's thickness does not vary much among its different joints. 3D position of the joint can be estimated by shifting its depth coordinate with a certain amount of length into the scene.

5.2. Hand Pose Estimation from Single Depth Image using Hybrid Classification Forests (RDF-H)

In this section, we propose a novel multi–layered hybrid approach to tackle the complexity problem. The idea is to reduce the complexity of the model by dividing the training set into smaller clusters, and to train RDF-Cs on each of these compact sets. Thus, the RDF-Cs need to model only a small amount of variation, requiring smaller memory. These *experts* accurately model a specific subset of the data, and infer significantly better pose estimates. The main challenge is to direct the input towards the correct experts, which can easily be done by training an RDF-S for detecting the clusters.

We use RDF-S in designing a multi–layered hybrid RDF network to tackle the articulated hand pose estimation problem. We divide the large dataset into simpler sub–problems by clustering the dataset first. Then, each such cluster corresponds to a hand shape that can be recognized with an RDF-S, and a separate hand pose estimator is trained on each cluster, forming skeleton experts. A similar approach is used in [61], which detects the hands in the first layer and then classifies hand shapes in the second layer. Our method classifies hand shapes in the first layer and then estimates the hand pose in the second layer.

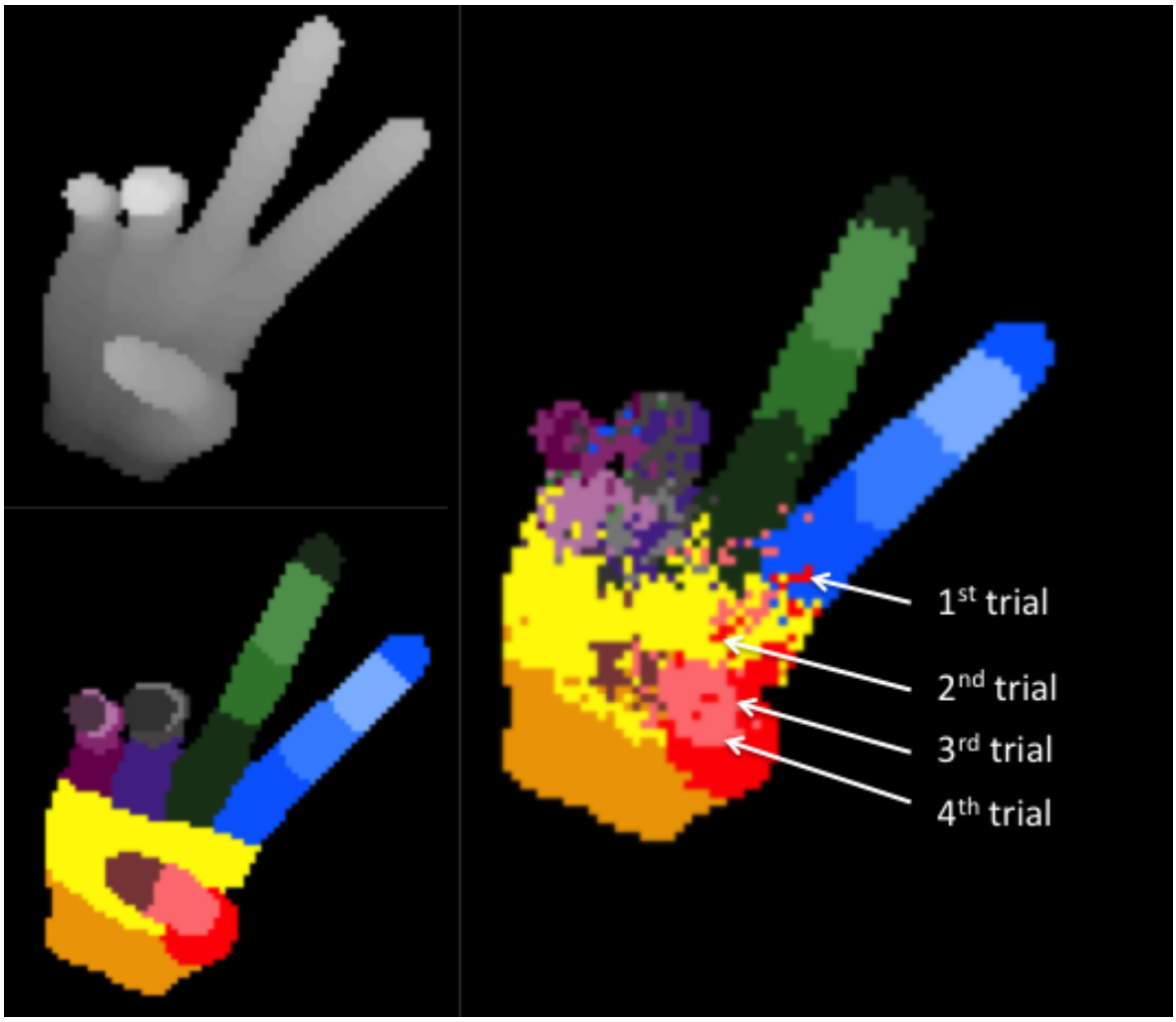

Figure 5.2. Overview of the mean shift convergence during joint estimation for the first bone of thumb shown with red color. At the left, corresponding depth and ground truth label images are shown. At the right, RDF-C results are shown on which mean shift runs.

A flowchart is given in Figure 5.4. Training consists of three phases: First, the training set is clustered according to hand skeleton similarity. Then, an RDF-S is trained that can assign cluster labels to input images. Finally, RDF-Cs are trained on each cluster, forming the experts. In the hand pose estimation process, there are four main steps: First, the RDF-S assigns a cluster label to each pixel. Then, either experts corresponding to the majority of the pixels are selected, or each pixel is assigned to its respective expert. The selected experts form a forest and infer hand part labels. Finally, the part labels are used to estimate the joint positions, forming the hand skeleton.

(a) (b) (c) (d)

Figure 5.3. Hand pose estimation process. (a) is the depth image, (b) is the assignment of each pixel to a class region by some RDF-C, (c) shows the estimated joint locations, (d) depicts the skeleton.

5.2.1. Pose Clustering and Shape Classification Forest (SCF)

A shape classification forest (SCF) is the name assigned to the first layer of the multi–layer hybrid forest (RDF-H) which runs RDF-S algorithm. The output is a set of posterior probabilities for each shape class label C_k. The model is trained on a dataset consisting of depth image–class label pairs. Details of RDF-S is discussed in Chapter 4.

The performance of the novel shape classification method on the publicly available ASL dataset of [83] has been shown in Section 4.3 to achieve a success rate of 97.8%.

Hybrid framework aims to cluster the large training dataset and then train a classifier to map new input images to these clusters. In such settings, it is more desirable to pursue a model based clustering approach, where the fit between the data and the model is optimized. Hence, we simultaneously train an SCF and cluster the data by using the following procedure:

(i) Estimate an initial clustering of the data and label the images accordingly:

$$L_0^i = c, \qquad c \in \{C_1, C_2, \ldots, C_K\} \tag{5.2}$$

where L_0^i is the label of image i at iteration 0, and c is a label of one of the K

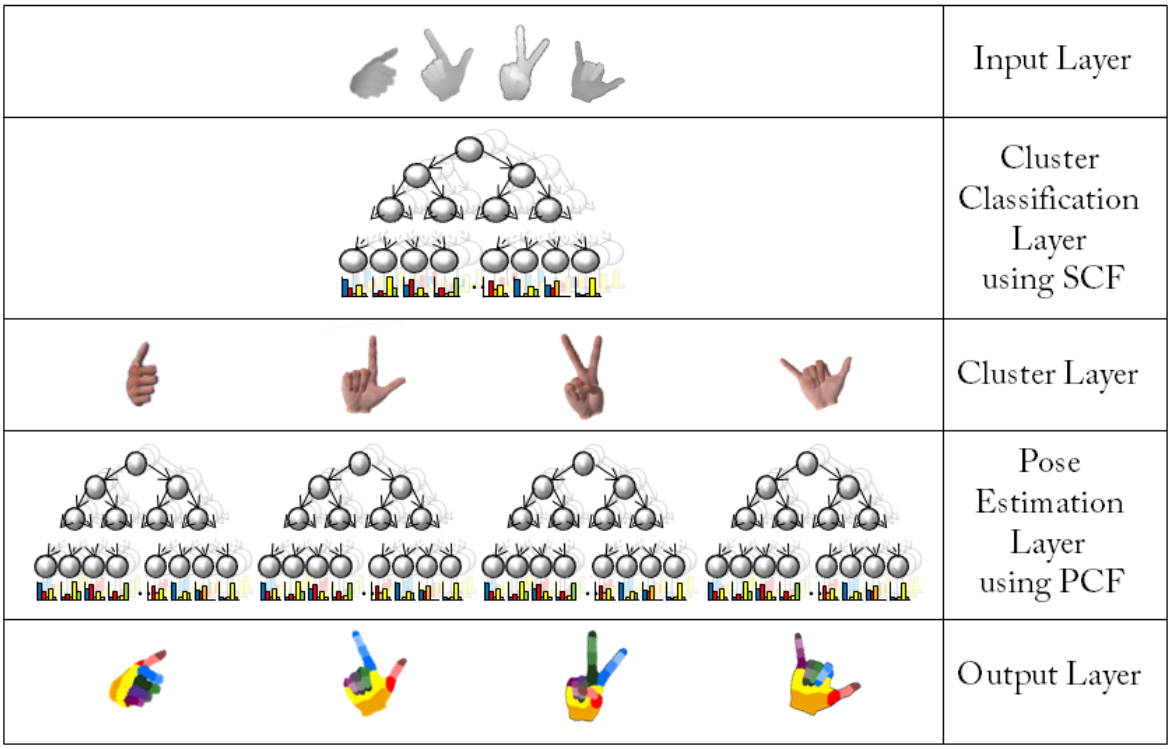

Figure 5.4. Flowchart of randomized hybrid decision forests (RDF-H).

clusters.

(ii) Train the SCF according to the image labels:

$$c_j = \arg\max_{c_k} P(c_k|I, \boldsymbol{x_m}) \tag{5.3}$$

such that c_j has the highest posterior probability for a pixel x_m in an image I^i, if I^i belongs to cluster corresponding to c_j.

(iii) Evaluate every image in the dataset using the SCF and assign new labels:

$$L_n^i = \arg\max_{c_j} \frac{1}{M} \sum_{m=1}^{M} P(c_j|I^i, \boldsymbol{x_m}) \tag{5.4}$$

(iv) Calculate the number of labels that have changed:

$$\Delta = \sum_{i=1}^{T} \delta_{L_n^i, L_{n-1}^i} \tag{5.5}$$

where δ is the Kronecker delta and T is the number of images in the dataset.

(v) If $\Delta > 0$, go to Step 2. Otherwise, return.

This method iteratively estimates new clusters and models them until the model and the clusters fit and no label changes in an iteration. To supply the algorithm with initial clusters, we apply spectral clustering. Spectral clustering methods are based on the Min–Cut algorithm, which partitions graph nodes by minimizing a certain cost associated with each edge in the graph [86]. This is a binary clustering method, which can be used to hierarchically cluster data into multiple clusters. We use a related algorithm that has been proposed by Meila *et al.* [87], which can estimate multiple clusters. In this method, a similarity matrix is formed for the samples to be clustered, where each entry S_{ij} in the matrix corresponds to the similarity of samples i and j. As the similarity measure, the reciprocal of a distance measure can be used.

The distance between two skeletal configurations is taken to be the weighted sum of the absolute differences of each angle pair. Using the pairwise distances of each configuration, we can estimate a clustering as follows:

$$D_{ij} = ||\mathbf{W}(\boldsymbol{v_i} - \boldsymbol{v_j})||_1 \tag{5.6}$$

$$\alpha = \max(\mathbf{D}) \tag{5.7}$$

$$S_{ij} = 1 - \frac{1}{\alpha} D_{ij} \tag{5.8}$$

$$R_{ii} = \sum_j S_{ij} \tag{5.9}$$

$$\mathbf{P} = \mathbf{S}\mathbf{R}^{-1} \tag{5.10}$$

Here, $\boldsymbol{v_i}$ and $\boldsymbol{v_j}$ are the vectors formed by all the angles of a skeleton. $\mathbf{W}$ is a diagonal matrix, such that W_{ii} is the weight of the angle i. α is the maximum amount of distance recorded in $\mathbf{D}$. $\mathbf{S}$ is the similarity matrix formed by normalizing the distance matrix $\mathbf{D}$ according to α and subtracting each element from 1. Then, each column c_i of $\mathbf{S}$ is normalized using the sum of elements in row r_i to form the matrix $\mathbf{P}$. We find the eigenvectors corresponding to the m largest eigenvalues of this matrix in the form of a $N \times m$ matrix. Each row of this matrix is a m dimensional representative of one of

the N samples. The rows of this matrix are clustered using the conventional k–means method.

5.2.2. Pose Estimation with Pose Classification Forests (PCF)

We compare the success of the RDF-H with the results in [5]. Whereas the method of [5] achieves a per pixel classification rate of 68.0% on a large synthetic dataset, the multi–layered method achieves a classification rate of 91.2%.

5.2.3. Pose Estimation Using a Hybrid RDF Network (RDF-H)

First, we simultaneously train an SCF (Φ) and cluster a dataset D into K clusters D^k, $k = 1, \ldots, K$, using the method of Section 5.2.1. Next, we train K PCFs, depicted as Ψ^k, on the clusters D^k.

Upon encountering a new input depth image, Φ classifies the image into one of the K clusters using by assigning a label C_i to it, using the method in Section 4.4. Instead of assigning a hard label, we take labels that correspond to the largest three of the average posterior probabilities $\rho_j = \frac{1}{M}\sum_{m=1}^{M} P(c_j|I, \boldsymbol{x_m})$. Without loss of generality, we call these labels C_1, C_2 and C_3 with posterior probabilities ρ_1, ρ_2 and ρ_3. The weighted sum of the hand part posteriors as estimated by the corresponding PCFs Ψ^1, Ψ^2 and Ψ^3 is taken to be the final posterior probability for each pixel, where the weights are ρ_1, ρ_2 and ρ_3:

$$P(c_j|I, \boldsymbol{x}) = \sum_{i=1}^{3} \rho_i P(c_j|I, \boldsymbol{x}, \Psi^i) \tag{5.11}$$

Finally, these posterior probabilities estimated by a collection of forests are used to estimate the hand pose as explained in Section 5.2.2.

The SCF assigns a cluster label to each pixel in an input image. This information can be used in two different ways: (i) a pose label for the entire image can be estimated

via voting, (ii) individual pixels can be sent to the corresponding expert PCFs according to their labels. We call these the Global Expert Network (GEN) and Local Expert Network (LEN) respectively. These networks are illustrated in 5.5.

The training of the multi–layered hybrid model requires three steps: (i) clustering of the training data, (ii) training an SCF with the clusters as shapes as in Section 5.2.1, (iii) training separate PCFs on each cluster.

5.2.4. Forest Parameter Selection

To verify the efficacy of the novel methods proposed, we first optimize each model with respect to their parameters through a grid search. The important parameters of SCFs and PCFs are as follows: (i) the tree height h; (ii) limits of feature vectors $\boldsymbol{u}$ and $\boldsymbol{v}$; (iii) the depth threshold τ; (iv) the number of trials ϵ. $\boldsymbol{u}$, $\boldsymbol{v}$ and τ are selected the same as reported in [5]. ϵ is the number of times the features are randomized during training of a node, and should be high to increase the chance of randomly selecting good features that better partition the data. We typically set $\epsilon = 2000$ to 10000. h directly limits the number of rules a tree contains and is essential to capture the variation of data: the more challenging a dataset, the higher the tree should be. The final parameter is the number of trees in the forest. Increasing this number gives an accuracy boost at the cost of CPU time. Our typical forest consists of three trees for the SCFs and two trees for the PCFs, as variation is much lower at the second layer.

5.2.5. Datasets

We use real data to train stand–alone SCFs that aim at hand shape classification, and synthetic data to train both the SCF and PCF in the multi–layered setting for hand pose estimation. Real data is captured with Kinect by performing the hand shape for 10–15 seconds, whereas synthetic data is generated using the hierarchical hand model by following the same methodology as in [5]. We typically use about 50 different hand poses and their interpolations to attempt to capture the large pose variations due to articulation. The number of images required to train the SCF is much lower, as each

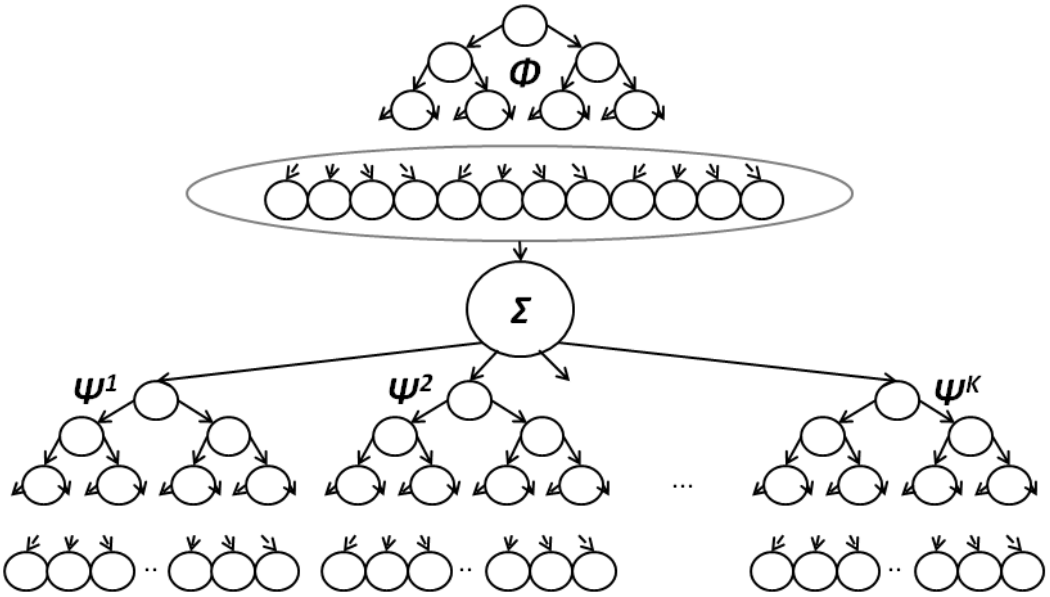

(a)

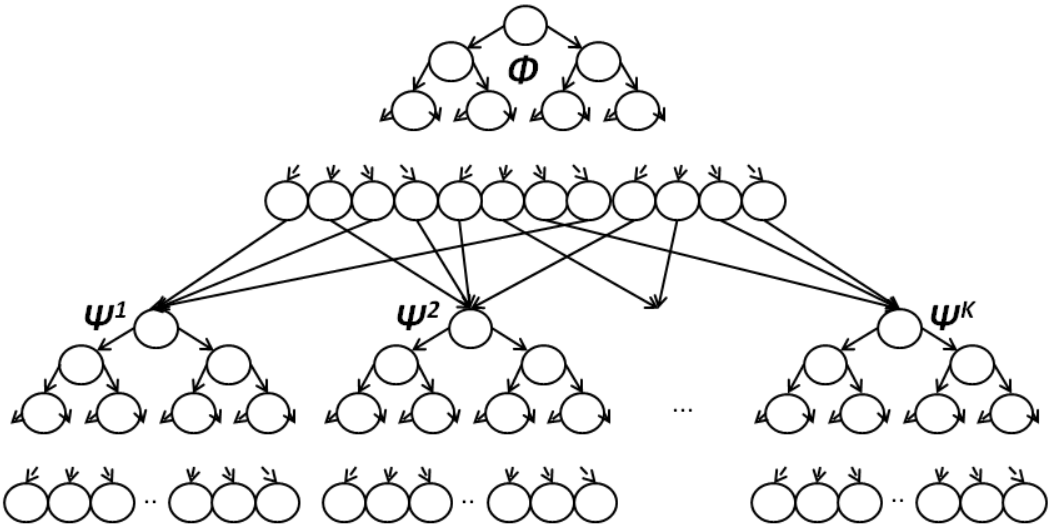

(b)

Figure 5.5. Different types of hybrid RDF networks. Φ depicts the SCF, and Ψ^i depicts the expert PCF corresponding to the cluster C_i. (a) Global Expert Network: The experts are selected according to the pose label. (b) Local Expert Network: Each pixel is sent to its own expert.

class label receives sufficiently many pixels. This contrasts the problem of small size of finger tips for PCFs.

5.2.6. Shape Classification Performance

Shape classification layer is already trained and tested in Section 4.4.1. We use directly the results of RDF-S as the first layer of our RDF-H.

5.2.7. Hand Pose Estimation

Two new factors introduced by the hybrid framework are the number of clusters K and the diagonal matrix $\mathbf{W}$ used in estimating the pairwise distances of two skeletons. Increasing K reduces the complexity of the PCFs in the second layer, while increasing that of the SCF in the primary layer. On the other hand, the individual elements of the weight matrix $\mathbf{W}$ determine the type of variation a cluster will contain: if we penalize the global rotation angles with large weights, pose clusters will contain variations in fingers mostly. Likewise, giving lower weights to the global rotation angles causes the clusters to contain more camera view point changes. By conducting several experiments, we determined that global rotation is the type of variation that is harder to capture by PCFs, mainly due to the rotation variant features used in the training phase. Therefore, we penalize the global angles with larger weights. We gradually decrease the weights from the palm to the fingers, allowing the finger tips to move rather freely.

Moreover, we proposed two different flavors of information passing from the first layer to the second layer, namely GEN and LEN. A preliminary test is devised for choosing between GEN and LEN. Per pixel classification rates are given in Table 5.1. Previously implemented model in the literature from [5] achieves a success rate of 68.0% on this dataset, whereas GEN achieves 91.2% and LEN achieves 90.9%. As expected, the expert networks perform significantly better. On the other hand, the difference between GEN and LEN is negligible in this case. Since LEN uses a different tree for each different pixel, its runtime performance is slower. For the sake of less complexity,

Table 5.1. Per pixel classification rates of each hand pose estimation method. Single–layered RDF is the PCF as proposed in [5]. The accuracy of both GEN and LEN are substantially higher than a single PCF.

Method	RDF-C	RDF-H (GEN)	RDF-H (LEN)
Per Pixel Classification Rate	68.0%	91.2%	90.9%

we chose to concentrate on GEN method as it is more concise and faster.

To verify and visualize the increase in accuracy of the new method, we first create a synthetic dataset consisting of 60k depth images formed by interpolating 10 hand poses corresponding to the ASL digits. We set K to be 5, 10, 20, and 30 and apply spectral clustering. Global rotations are penalized more than the movements of finger tips. If SCF is too shallow, it will not be able to learn the initial cluster labels. This means that it is not sophisticated enough to capture the variation of the data and hence, we need to increase its height. Motivated by this observation, we gradually increase the tree complexities for automatic model selection. Model based clustering achieves simultaneous clustering of the data and training of the SCF. We ensure that the algorithm converges and the model fits the clusters. For each of the clusters, we train a PCF with two trees. The optimal tree heights for different values of K are given in Table 5.2.

To compare the system with [5], we also train a single PCF with the entire dataset. This model corresponds to $K = 1$ in the Table. We also tried to keep the time complexity spent per pixel constant. Each pixel travel through 33 different tree nodes. In other words 33 different conditions are checked per pixel in the hybrid forest. Whereas the method of [5] achieves a per pixel classification rate of 68.0%, our method has a classification rate of 81.3%, 86.6% and 91.2% for increasing values of K. This shows that clustering will produce much better skeletons, and the efficiency rises as we use more clusters up to a point. However, it becomes increasingly harder for the SCF to learn the clustering for large values of K. Increasing the number of clusters from 20 to 30 does not improve performance but decrease it considerably even below $K = 1$ case.

Table 5.2. Optimal SCT and PCT heights for different number of clusters K, and per pixel classification rates (PPCR) achieved. $K = 1$ implies a single layer approach. Single layer approach uses 3 trees whereas the hybrid one uses 3 trees for SCF and 2 trees for PCF.

Clusters (K)	**1**	**5**	**10**	**20**	**30**	**30**
SCF Height	N/A	15	16	17	18	19
PCF Height	20	18	17	16	15	14
Total Height	20	33	33	33	33	33
Relative Memory	1.00	0.87	0.90	0.96	0.88	0.81
Relative Recognition Time	1.00	1.35	1.37	1.38	1.40	1.42
Per Pixel Classification Rate	68.0%	81.3%	86.6%	91.2%	77.4%	64.3%

Another important aspect of the hybrid framework is its ability to assign soft clusters in the first layer and find a weighted posterior probability for the pixels in the second layer. For previously unseen poses, this is a crucial feature that enhances generalization capability.

5.2.8. Results

In this chapter, we attempted to tackle the hand shape recognition and hand pose inference problems together. We utilized RDF-S based hand shape classification method that achieves very high recognition rates on real datasets. We proposed an iterative RDF based method to cluster hand poses according to their articulations and camera view point changes, which simultaneously handles model selection and training of the RDF. We devised a multi–layered hybrid framework that can estimate the hand pose significantly better than its predecessors, that can assign labels to previously unseen poses, estimate their skeletal configurations and use this for one shot learning of a gesture from a single image or video.

We have used synthetic hand model for our training. This hand model is pre-labeled with individual colored regions so that each hand part is at the center of a region. We have rendered this model and used it for training.

Specifically, our shape classification method contrasts the approach in our previous work [5] such that: (i) it does not rely on the efficiency of the hand pose estimation module; (ii) the models can be trained using real data, which simplifies the training process and gives more accurate results; (iii) evaluation is faster; iv) fewer samples are needed for training.

Furthermore, hybrid framework solves the problem of large memory requirements and manages to capture the large pose and camera view point variations of the hand. Hybrid hand pose estimation framework uses a novel model based clustering technique that simultaneously clusters the data and trains the SCF to assign cluster labels to data. For each cluster, we train a separate PCF that learns to assign pixels to hand part labels. As the training set is much smaller for clusters, training is much faster, the PCTs formed are shallower, and the per pixel classification accuracy of the PCFs is higher.

We focused on optimizing the speed and pixel classification accuracy of the system, in particular by performing grid search over all model parameters. The resulting framework is capable of retrieving images from the depth camera [2], apply per pixel classification using the multi–layered hybrid RDFs, estimate the joint locations from several hypotheses in the mean shift phase, and finally use these locations for pose classification at 30 fps, which is the limit of the depth camera.

Achieving a higher per pixel classification rate also improves the performance of mean shift algorithm. This also improves the quality of the pose estimation. More detailed analysis about the effects of pixel classification quality on estimated joints will be discussed in Chapter 6.

The novel shape classification and 3D hand pose estimation methods introduced in this paper significantly improve the performance of hand shape recognition and hand pose estimation tasks, and are general enough to be applied to other generic shape recognition or body pose estimation problems.

Despite RDF-C's, and therefore RDF-H's, favorable specialties, they have some major problems. RDF-Cs and RDF-Hs cannot effectively detect small body parts and they tend to mix some of the body parts producing structurally unacceptable skeletal inference as illustrated in Figure 5.6. They also perform bad under occlusion. Coping with the mixing of the hand parts problem requires employing certain pixel area thresholds which may produce missing hand joints.

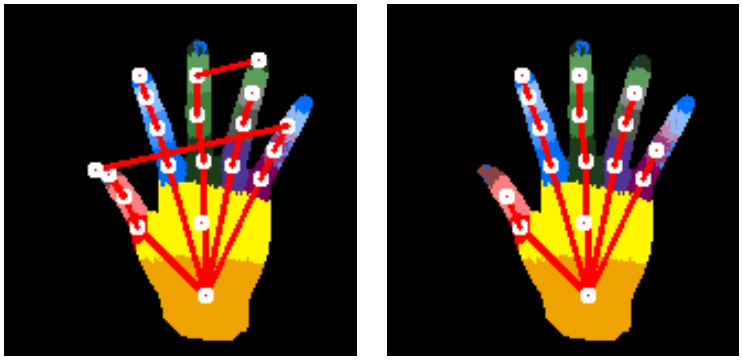

(a) (b)

Figure 5.6. Problems of RDFs for pixel classification: (a) Parts may be mixed, (b) Small parts may not be found.

6. HAND POSE ESTIMATION WITH REGRESSION BASED METHODS

In this chapter, we will integrate the methods that we introduced in previous chapters to build a better joint estimator. RDF-S, RDF-C, and RDF-H all rely on pixel classification. In the case of human hand, this transient pixel classification phase comes with a big disadvantage. The human hand is a highly deformable and self-occluding limb. Therefore, pixel classification based joint estimation is prone to the occlusion problem. If the regions of the hand is not seen in the captured depth image then there is no easy way to predict the unseen joints. In this chapter, we will develop a regression based randomized forest for skipping the pixel classification phase. The resulting joint estimator will therefore be robust against self-occlusion. In addition to that, we will also incorporate the hierarchical structure of the human hand into joint pose estimation methodology, instead of estimating all the joints independently.

In Section 6.1, we implement a regression based approach. Then we introduce hierarchical constraints of the hand into consideration for further improving the performance of this method as illustrated in Section 6.2. We then compare the performances of all the methods we introduced so far. In Section 6.3, we give the details of the hand data generation step and introduce the datasets that we use. Section 6.4 discusses the fine-tuning of the essential training parameters, namely the forest size, the tree depth, the probe distance, the depth threshold, and the mean shift bandwidth. In Section 6.5, the fine-tuned RDFs are tested on four different datasets. We first test on the training dataset to gather information about the characteristics of the methods, and then extend our tests to two different synthetic and one real test datasets.

6.1. Hand Pose Estimation using Randomized Decision Forest for Regression (RDF-R)

[24] proposed a new method for the human body pose estimation problem. This technique directly infers the joint coordinates using random decision trees without an intermediate pixel classification representation, hence making it more robust against occlusion. This algorithm is suitable for application to human hand pose estimation. We adapt Randomized Decision Forest for Regression (RDF-R) for directly inferring hand joint positions from the depth image without the intermediary per pixel classification phase. RDF-R can learn and estimate the joint positions even under self-occlusions. Unlike RDF-Cs, RDF-Rs depend on the mean shift algorithm in the training phase, as well.

1: // Collect relative offsets
2: initialize $R_{lj} = \emptyset$ for all leaf nodes l and joints j
3: **for all** pixels q in all training images i **do**
4: lookup ground truth joint positions $\mathbf{z}_{ij}$
5: lookup 3D pixel position $\mathbf{x}_{iq}$
6: compute relative offset $\Delta_{iq \to j} = \mathbf{z}_{ij} - \mathbf{x}_{iq}$
7: descend tree to reach leaf node l
8: store $\Delta_{iq \to j}$ in R_{lj} using reservoir sampling
9: // Cluster
10: **for all** leaf nodes l and joints j **do**
11: cluster offsets R_{lj} using mean shift
12: take top K weighted modes as V_{lj}
13: **return** relative votes V_{lj} for all nodes and joints

Figure 6.1. Training joint positions.

6.1.1. Training of the Joint Positions

The structure of the trees, namely the features selected in the tree nodes, is the same as described in Section 4.2. Therefore, the structure is learned in such a way that

leaves are favored to store pixels belonging to the same part of the hand shape.

```
// Collect absolute votes
initialize Z_j = ∅ for all joints j
for all pixels q in the test images do
    lookup 3D pixel position x_q = (x_q, y_q, z_q)^T
    for all trees in forest do
        descend tree to reach leaf node l
        for all joint j do
            lookup weighted relative vote set V_lj
            for all (Δ_ljk, W_ljk) ∈ V_lj do
                if ||Δ_ljk||_2 ≤ distance threshold λ_j then
                compute absolute vote z = Δ_ljk + x_q
                adapt confidence weight w = w_ljk · z_q^2
                Z_j := Z_j ∪ {(z, w)}
// Aggregate weighted votes
sub-sample Z_j to contain N votes
aggregate Z_j using mean shift on  Equation (6.2)
return weighted modes as final hypotheses
```

Figure 6.2. Direct estimation of joint positions.

RDF-Rs do not store hand part histograms at each leaf node l but a distribution over the relative 3D offsets, called a vote, to each hand joint j. These votes are the positions of joints relative to the pixel in question. Each training pixel q is propagated through the tree branches until it reaches a leaf node l. The pixel then casts a relative vote for each distinct joint j. The relative vote can be evaluated using as:

$$\Delta_{iq \to j} = \mathbf{z}_{ij} - \mathbf{x}_{iq}, \tag{6.1}$$

where $\mathbf{z}_{ij}$ is the ground truth joint position, and $\mathbf{x}_{iq}$ is the 3D pixel position for a pixel q belonging to image i. For a leaf node l, a relative vote to joint j evaluated for pixel q belonging to image i is then stored in set R_{lj}. Examples of possible vote distributions

are illustrated in Figure 6.3.

We prefer to use large training sets since we want to infer joint positions of different hand pose configurations. All the information represented by a vote distribution of a leaf cannot be stored in memory. A consensus of relative votes has to be reached per tree leaf for information compression. Unfortunately the vote distributions are not unimodal. Representing the votes by fitting a Gaussian is therefore not suitable. The different clusters of votes have to be distinguished as a preliminary phase. Mean shift algorithm is a proper candidate for the task. After selecting a suitable kernel, the mean shift algorithm finds the number of different clusters and their means. The percentage of relative votes belonging to a cluster is the weight of that cluster. Unfortunately the training phase requires handling of great numbers of votes per tree leaf. In order to learn the relative votes in a reasonable time, the vote distribution R_{lj} is sub-sampled using reservoir sampling of [88]. Reservoir sampling is a single-pass $O(N)$ algorithm that facilitates speeding up the long training phase. Sub-sampling, once a reasonable sample size is chosen, does not affect the modes of the vote distributions, thus providing a considerable performance increase during the training phase without compromising quality.

Consequently, we initialize a set $R_{lj} = \emptyset$ for all leaf nodes l and joints j. A depth image pixel q is propagated to its respective tree leaf and casts a vote which is stored in R_{lj}. All the reservoir sampled pixels of a leaf l cumulatively represent vote distributions for all different joints j. For all leaf nodes l and joints j we cluster the reservoir sampled distributions R_{lj} using mean shift and take top K weighted modes as V_{lj}. The algorithm for learning the joint position votes is shown in Figure 6.1.

6.1.2. Direct Joint Position Estimation using RDF-R

We start by initializing $Z_j = \emptyset$ for all joints j. All the pixels in a test depth image are propagated to the tree leaves by starting at the root node and assigning the pixel either to the left or to the right child recursively until a leaf node l is reached. 3D pixel position of the depth image pixel is recalled from the depth image using

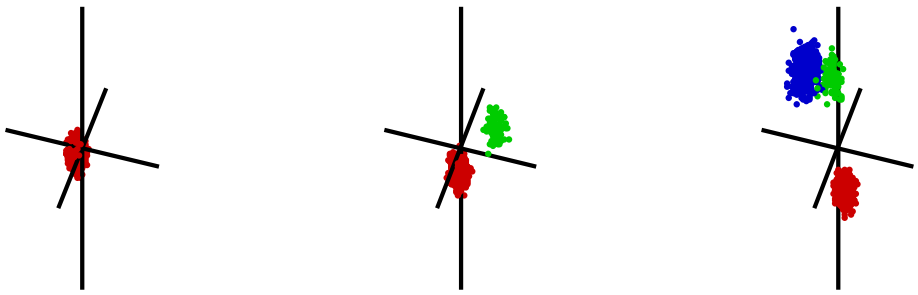

Figure 6.3. Sample multi-modal vote distributions for three different joints. Vote distributions may have multiple modes. Different colors indicate pixel clusters that are assigned to the same mode found by mean shift.

$\mathbf{x}_q = (x_q, y_q, z_q)^\mathsf{T}$. Each test-time depth pixel casts its per joint vote as represented by the stored weighted relative vote set V_{lj}. Absolute vote coordinate is evaluated using $\mathbf{z} = \Delta_{ljk} + \mathbf{x}_q$. The vote is not cast if $\|\Delta_{ljk}\|_2 \geq \lambda_j$, where λ_j is a distance threshold learned for each different hand joint. To aggregate the absolute votes Z_j, for each joint j we define a continuous distribution over world space using a Gaussian Parzen density estimator such as

$$P_j(z') = \sum_{(z,w)\in Z_j} w. \exp\left(-\left\|\frac{z'-z}{b_j}\right\|_2^2\right), \tag{6.2}$$

where b_j is a learned per-joint bandwidth. Running mean shift using Equation 6.2 produces the weighted modes as final hypotheses. The layout of inference algorithm is shown in Figure 6.2. A preliminary comparison of classification and regression based methods on a single pose is illustrated in Figure 6.4.

6.2. Hierarchical Mode Selection using Geometry Constraints (RDF-R+)

RDF-R method outputs posterior distributions of possible joint locations. Even though using the global modes of the multi-modal distributions seems to be the most straightforward approach, the correct position of the joint often corresponds to a local mode. However, considering local modes for the joint positions results in multiple skeletal configuration candidates, instead of a single one given by the global modes. For

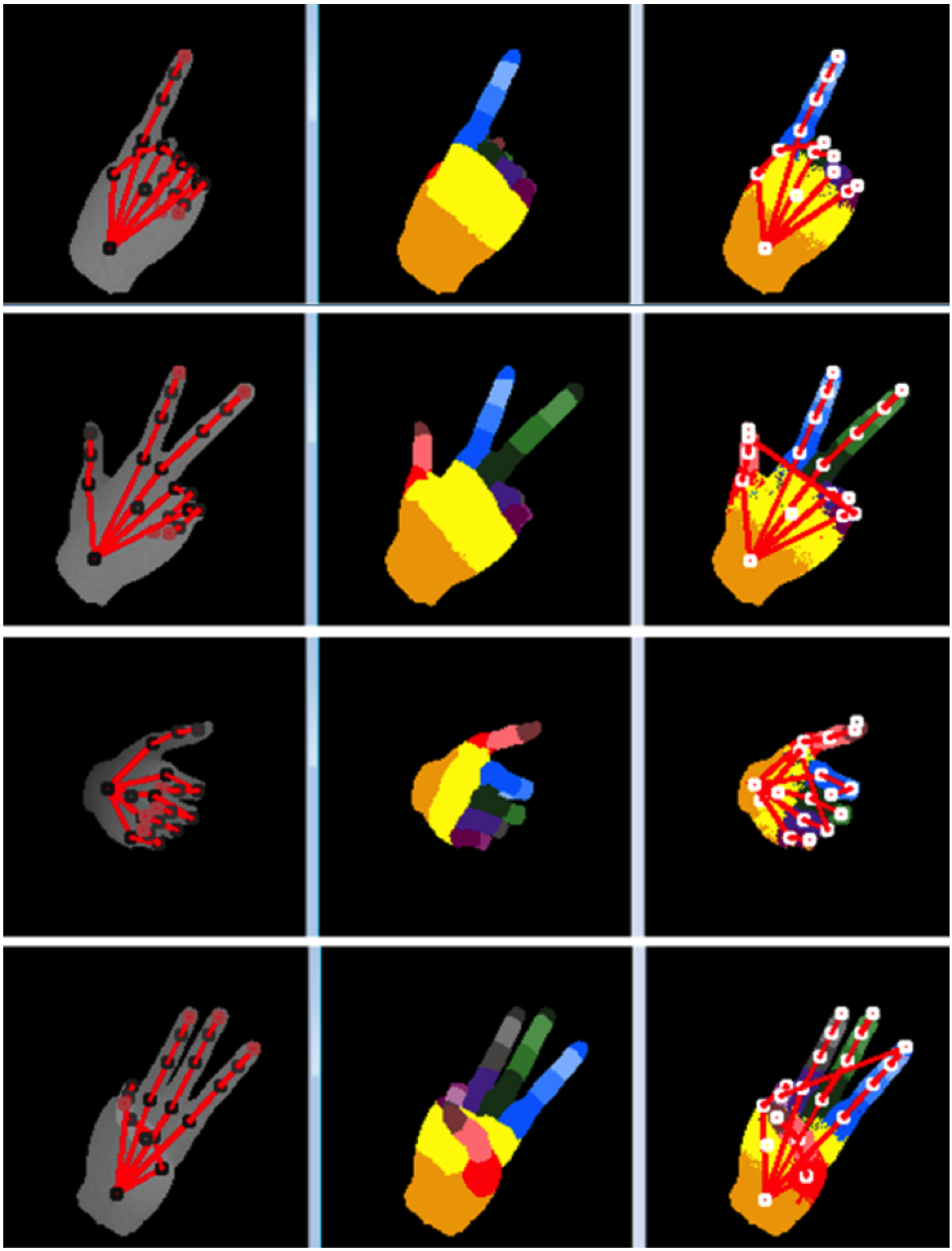

Figure 6.4. Preliminary comparison of classification and regression based methods: left) skeleton found by RDF-R directly from depth image, middle) ground truth of per pixel classification, right) skeleton extracted from pixel classification with RDF-C shows fingertip and self occlusion problems.

selecting a suitable configuration, we introduce a hierarchical mode selection method and define a constraint function based on our prior knowledge about the hierarchical structure of the 3D model. We penalize each candidate skeletal configuration according to our constraints and select the one with the smallest penalty to be the hand pose. The hierarchy of a skeleton can be defined as

$$H = \{(c, p) : p \text{ is the parent of } c\} \tag{6.3}$$

where c and p are joints.

Let j be a joint and $P(\cdot|j)$ be the posterior distribution of j's position. Assuming that the distribution has N_j modes, we define a mode of this distribution as $\boldsymbol{x}_j^{k_j}$ where $k_j \in \{1, \ldots, N_j\}$ and $P(\boldsymbol{x}_j^{k_j}|j) \geq P(\boldsymbol{x}_j^{k_j+1}|j)$. With this condition modes are ordered decreasingly according to their probabilities.

For finding the skeletal configuration, we want to select a mode for each $P(\cdot|j)$. This selection is performed by dynamic programming so that the total penalty of the hierarchical model is minimized for a given penalty function f,

$$(k_1', \ldots, k_J') = \underset{k_1,\ldots,k_J}{\operatorname{argmin}} \sum_{(c,p)\in H} f\left(\boldsymbol{x}_c^{k_c}, \boldsymbol{x}_p^{k_p}\right) \tag{6.4}$$

where J is the total number of joints and $k_1, \ldots, k_J$ are the mode indices of the related joints. Then, the most suitable skeletal configuration can be represented as

$$S' = (\boldsymbol{x}_1^{k_1'}, \ldots, \boldsymbol{x}_J^{k_J'}). \tag{6.5}$$

By defining a penalty function, different hierarchical constraints can be imposed. Let

us define two different penalty functions

$$f_1\left(\boldsymbol{x}_c^{i_c}, \boldsymbol{x}_p^{i_p}\right) = \begin{cases} 0, & i_c = 1 \text{ and } i_p = 1 \\ 1, & \text{otherwise} \end{cases} \tag{6.6}$$

$$f_2\left(\boldsymbol{x}_c^{i_c}, \boldsymbol{x}_p^{i_p}\right) = \left(||\boldsymbol{x}_c^{i_c} - \boldsymbol{x}_p^{i_p}|| - b_{cp}\right)^2 \tag{6.7}$$

where b_{cp} is the expected length of the bone between the joints c and p.

Since $\boldsymbol{x}_j^k$s are ordered according to their probability, the global mode of the posterior distribution is $\boldsymbol{x}_j^1$. Thus, f_1 behaves as the global mode finding approach used by [24]. f_2 tries to select the modes such that the distance between them is as close as possible to the expected bone length.

An example of the improvement made by RDF-R+ method is shown in Figure 6.5 which shows the vote distribution for tip of the index finger. As clearly seen, there are two different local modes in the distribution. The global mode is not the correct one to be selected. RDF-R wrongly selects the global mode whereas RDF-R+ considers the hierarchical dependencies of the joints and finds the appropriate local mode successfully.

In this section, we introduced a novel hierarchical mode selection method which introduces the use of constraints imposed by the hand skeleton geometry. RDF-Rs extract multi-modal joint position distributions per joint. They only consider the global mode. However, disregarded local modes of the joint distribution provide invaluable information in the case of self-occlusions and missing data. Knowing all joint configurations are sampled from the same skeletal constraints provides a strong prior knowledge about the hierarchy of the modes over different joints. We investigate possible skeleton configurations that fit not only on the global modes but also on the local modes. The probable configurations are then filtered out using distance constraints based on a priori positions from the hand skeleton model. For the single frame estimation case, the best skeletal configuration is selected to be the hand pose using dynamic programming. In addition to that we also propose a low dimensional GPLVM based manifold

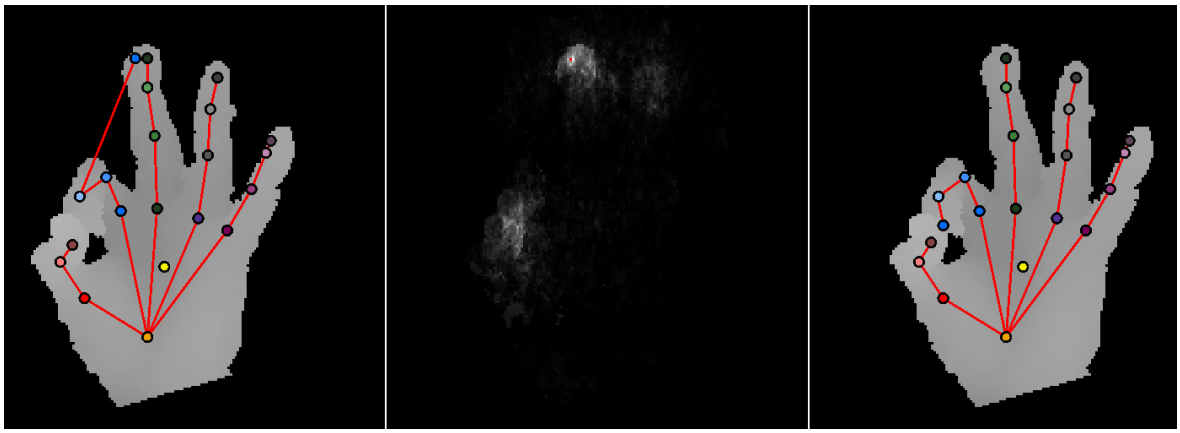

Figure 6.5. Improvement of RDF-R+ method over RDF-R is shown for tip of the index finger: left) incorrect fingertip estimation of RDF-R, middle) accumulated votes for index fingertip, right) correct fingertip estimation of RDF-R+.

extraction from specific dynamic gestures of the hand. We then implement a temporal domain tracker that runs on the learned manifold with greater accuracy.

6.3. Data Generation and the Datasets

Training the decision trees for classification and regression requires a great amount of training data. Capturing such a big dataset and labeling different parts of the depth images is a problem on its own. In order to cope with this problem, a synthetic 3D hand mesh is modeled and a realistic skeleton is rigged. The produced skeletal object is animated. In this approach, the difficult pixel labeling problem reduces to creating a label texture that is mapped to the hand mesh. We generate the label texture such that each skeleton joint is at the center of one of the labeled parts. The variation of the human hand across different individuals is significantly less than the body. An average sized hand is selected whose length from the bottom of the palm to the tip of the middle finger is 20 cm. Each different joint of the hand is restricted in a manner to mimic the constraints of the human hand. The synthesizer program designed for this study allows for different poses to be stored in keyframes along a timeline. Once an animation is designed, we animate it using linear interpolation between different keyframes.

In this chapter, we use 40 different hand poses. Poses are mainly selected from the American Sign Language alphabet. 26 poses represent the letters from A to Z, and 10 poses are for the numbers between 1 and 10. We also include four widely used hand poses, namely the closed-hand, open-hand, approval gesture, and all finger tips touching pose. For each pose, the model is rotated up to 32, 64, and 64 degrees along the x, y, and z axes, respectively. Various samples are collected for different angles with steps of six degrees. Center of the palm is always aligned with the center of the images created. We also add Gaussian depth noise to the depth image pixels with a mean of 10 mm, and a standard deviation of 5 for improving the generalization of the trained classifiers. During hand pose configuration setup, Gaussian noise is introduced to the angles of the skeleton for the unconstrained degree of freedoms with a mean of 2 degrees and a standard deviation of 1 degree. The resulting training (TRAIN) dataset consists of 29766 image samples. Rendered depth and label images are 160x160 pixels in resolution. In Figure 6.6, we show sample frames from the TRAIN dataset.

Training and validation are done on the TRAIN dataset using 10–fold cross validation. For testing the performance of different methods, we created two different datasets. The first one is the cropped (CROP) dataset. It is generated by retaining the center 80x80 pixels and erasing the outer pixels of each image from the TRAIN dataset. On the average, 81.09% of the pixels from each image are kept with a standard deviation of 8.91. The CROP dataset is used for testing the performance of different methods under missing data conditions.

The second test dataset is the Rock-Paper-Scissors-Lizard-Spock (RPSLS) dataset. The Rock-Paper-Scissors-Lizard-Spock game is invented by [89]. The RPSLS dataset is a completely new dataset synthesized from 5 different well-known poses not contained in the training set. All possible transitions between pose pairs are considered and animated using 3 frames per transition. The same rotation conditions are also applied to the pose animations, resulting in a dataset of 30492 images with 160x160 resolution. The poses of the RPSLS dataset are not used during the training of the decision trees. This dataset is used to benchmark the generalization performance of different methods.

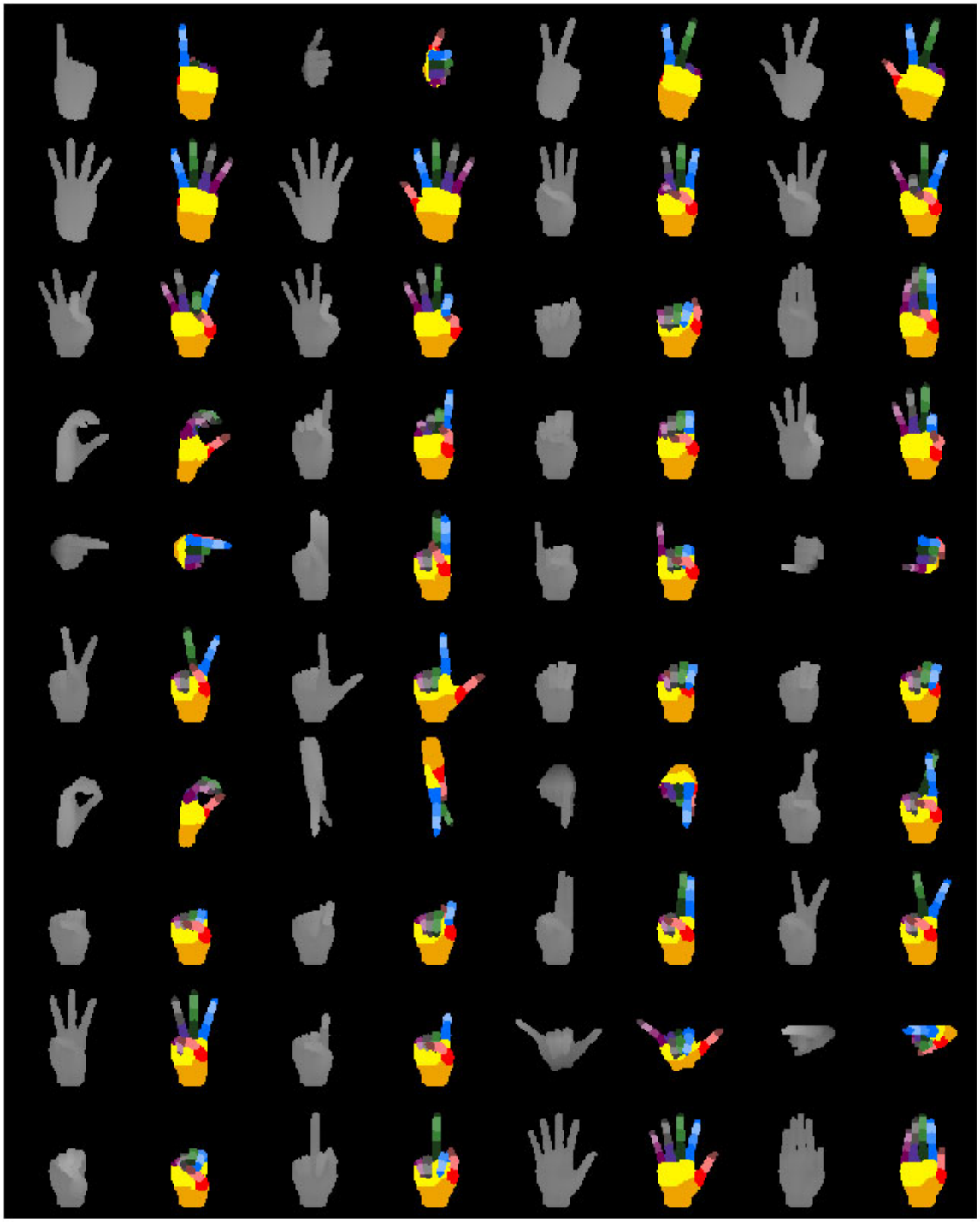

Figure 6.6. Sample frames from the TRAIN dataset.

Additionally, we tested the methods on a subset of ASL Finger Spelling Dataset of [83] for reporting the performance on real data. The dataset contains sample frames of 5 annotators for 24 finger spelling signs. Since 3D annotation on depth data is a tedious task, we only annotated a 55 frame subset of the dataset. The annotated subset consists of one sample for a, d, e, f, i, l, s, u, v, w, and y signs of each annotator.

There is also a well-known ChaLearn [90] multi-modal gesture recognition dataset. This dataset includes dynamic hand gestures rather than static ones. It provides both depth and color cues. Unfortunately, the depth images in the dataset are normalized to 8-bits of resolution. Moreover, most of the static hand shapes in the dataset are located far from the camera which forbids us to effectively use the depth variations. Since the scope of this thesis is mainly static hand gesture analysis, we couldn't use this dataset for experimentation.

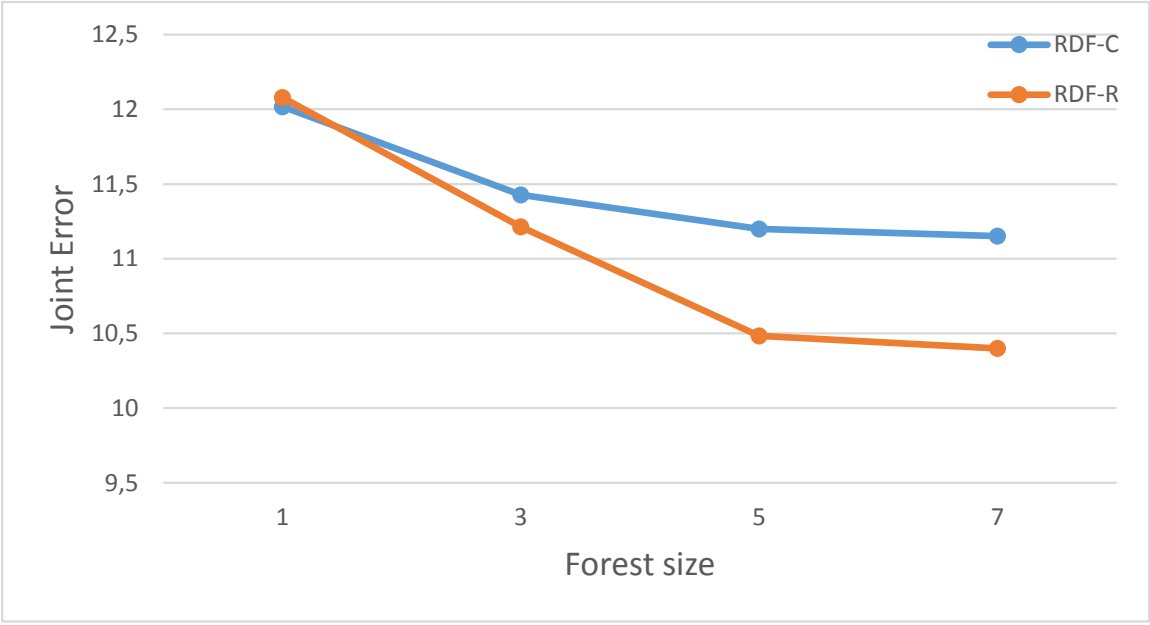

Figure 6.7. Effect of the forest size.

6.4. Parameter Selection

We do 10–fold cross validation for fine-tuning the essential training parameters. We investigate the effects of the forest size, the tree depth, the probe distance, the depth threshold, and the mean shift bandwidth parameters.

Figure 6.8. Effect of the tree depth.

6.4.1. The Effect of the Forest Size

An advantage of random forests is that the inference performance can be enhanced by combining multiple random trees. Both the generalization capability and the accuracy of the inference improves as the number of trees used is increased. There is a trade-off between inference time and the inference accuracy. Figure 6.7 shows the effect of number of trees on the accuracy of the system. Accuracy, recognition time, and memory usage are jointly optimized when the number of trees is selected to be 5.

6.4.2. The Effect of the Tree Depth

The depth of the trees is also an essential parameter. The representation capability increases as the depth of the trees increase. Unfortunately, increasing the depth of the trees also increases the inference time. Selecting an optimal depth is important for balancing the inference accuracy and the recognition time. In addition to that, the memory requirement also increases exponentially. If the training data complexity and size are not adequate for the utilization of the desired tree depth, numerous empty sub-branches in the forest structure appear. This under-utilization causes ineffective

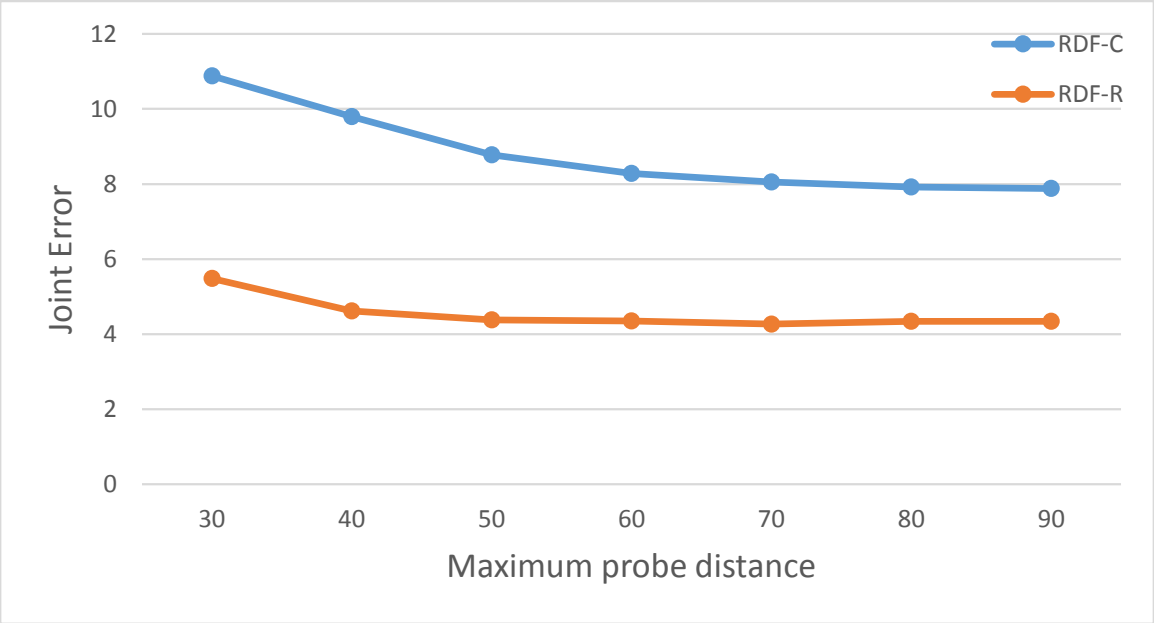

Figure 6.9. Effect of the probe distance.

use of the allocated memory. For instance, selecting a tree depth of 20 consumes approximately 256 MB of memory per tree.

The validation performance of both RDF-C and RDF-R stabilizes after a tree depth of 20 levels. They both slowly converge to their maximum accuracy as we increase the tree depth. However, it is not feasible to further increase the tree depth as the memory required increases exponentially. We selected a tree depth of 21 for our tests as it is a good trade-off between the accuracy, recognition time, and memory requirement.

Another interesting behavior is that RDF-Cs perform better than RDF-Rs when tree depth is less than 13 as shown in Figure 6.8. This behavior is due to the fact that RDF-Cs store class label histograms whereas RDF-Rs store 3D relative votes. For a high quality histogram, leaves should have numerous pixels, which is the case in a shallow tree. On the other hand, RDF-Rs work better with just enough data.

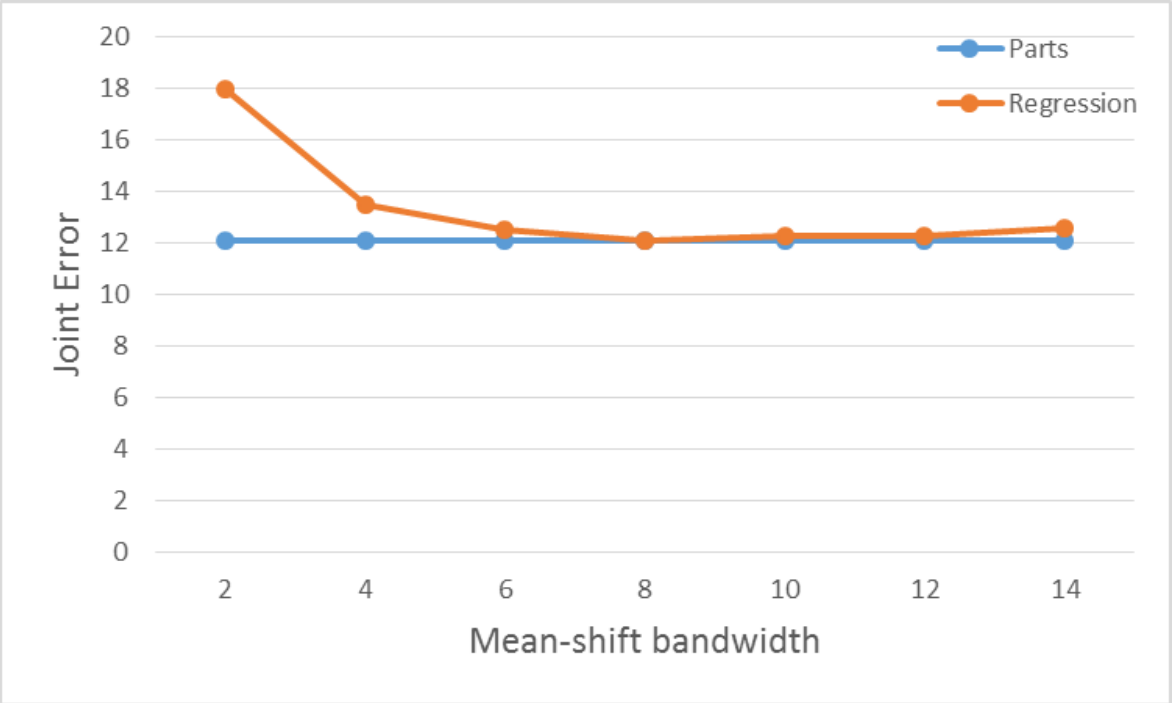

Figure 6.10. Effect of the bandwidths of joints.

6.4.3. The Effect of the Probe Distance

Probe distance is an important parameter which defines the learning amount from spatial relations. As we increase the probe distance, even more distant depth pixel couples are utilized for inference. With a small probe distance value, a more localized recognizer is trained which cannot infer successfully using correlation of distant parts or joints of the model. On the other hand, selecting a bigger than needed maximum probe distance value increases the training time. Both the RDF-C and RDF-R methods converge to their optimal performances when probe distance is selected to be 60 for our dataset as seen in Figure 6.9.

6.4.4. The Effect of the Depth Threshold

Depth threshold is similar to the probe distance. It controls the amount of learning based on depth variations. A very small value forces the learning not to depend on depth differences which produces a silhouette learner. A big value may learn the noise along the depth axis. We selected 30 as the depth threshold.

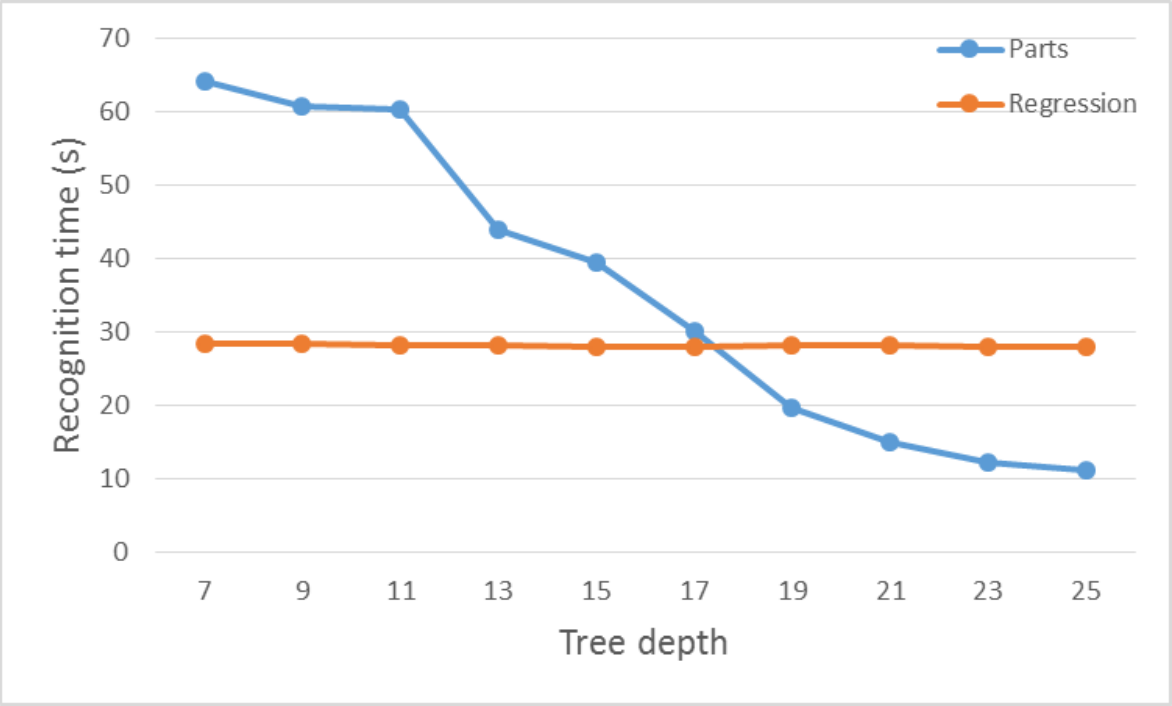

Figure 6.11. Effect of the tree depth on the recognition time.

6.4.5. The Effect of the Mean Shift Bandwidth

We used a shared bandwidth parameter for all joints. RDF-C algorithm produces less multi-modal and smoother distributions when compared to RDF-R. RDF-Rs form multi-modal distributions where the distribution peaks are clearly distinguished. Selecting an appropriate bandwidth has a greater influence on the performance of RDF-Rs. Performance of RDF-Cs do not change for reasonable values of bandwidth values whereas the performance of RDF-Rs are clearly dependent on the bandwidth parameter. We selected the bandwidth parameter to be 8.

6.5. Hand Pose Estimation Test Results

We start by testing all methods with the training dataset for demonstrating the amount of learning each method can achieve. We use CMC curves that report successful joint localization versus an acceptance threshold. For instance, the acceptance rate at 10 mm shows the percentage of joints that are closer than 10 mm to ground truth locations. RDF-C achieves a performance rate of 76.6% at 10 mm acceptable

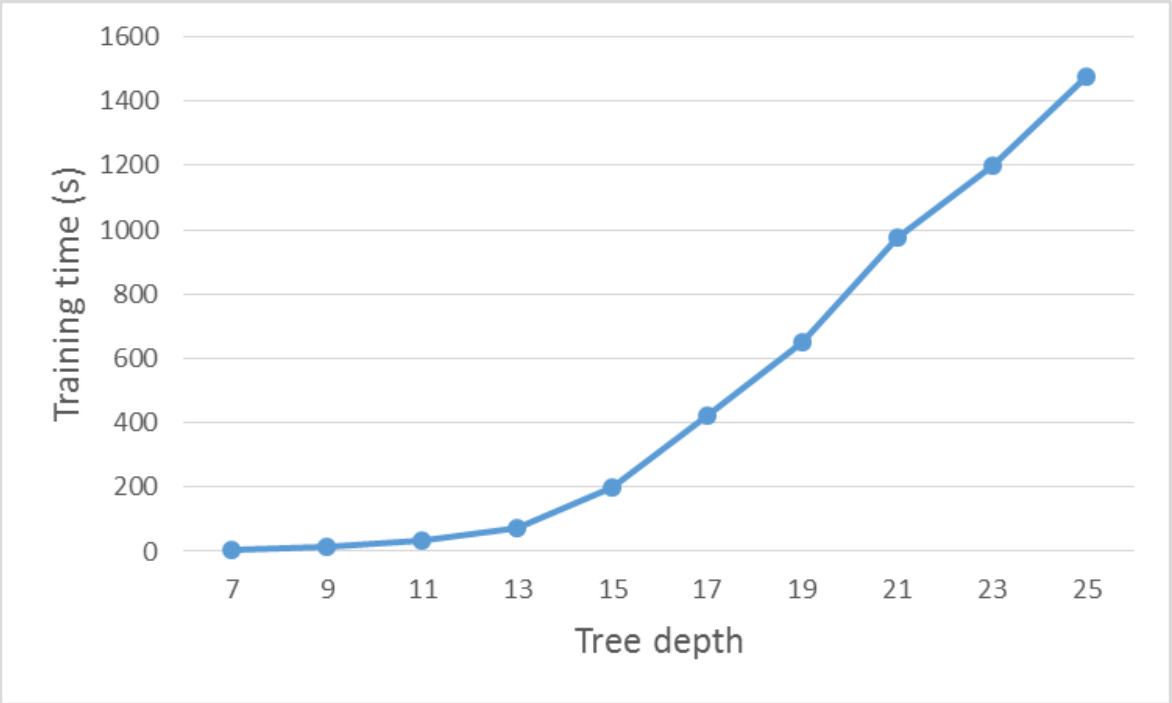

Figure 6.12. Effect of the tree depth on the training time.

distance threshold. For RDF-R and RDF-R+, this performance increases to 98.0% and 98.1% respectively. These results clearly show that RDF-C under-performs due to self-occlusions of the hand poses. Both regression forest based methods are robust to self-occlusion, hence, can learn all of the joints with a high accuracy. Figure 6.13 shows the CMC curve for the TRAIN dataset.

6.5.1. CROP Dataset

The hand is a limb that inherently produces self-occlusions. Moreover, depth data may be partly missing due to various other reasons. Parts of the hand may be out of sight of the camera. Similarly hand may be very close to the camera. Depth cameras have zero planes. The pixels closer than the zero plane are clipped. Another common cause of missing data is occlusion imposed by other objects in the environment. Depth cameras provide qualitative information where significant depth differences among neighboring regions occur. Given a depth image, segmentation algorithms are able to mark those regions occluded by other objects with a high accuracy. When those occluded regions are removed, the resulting depth image is an image where some

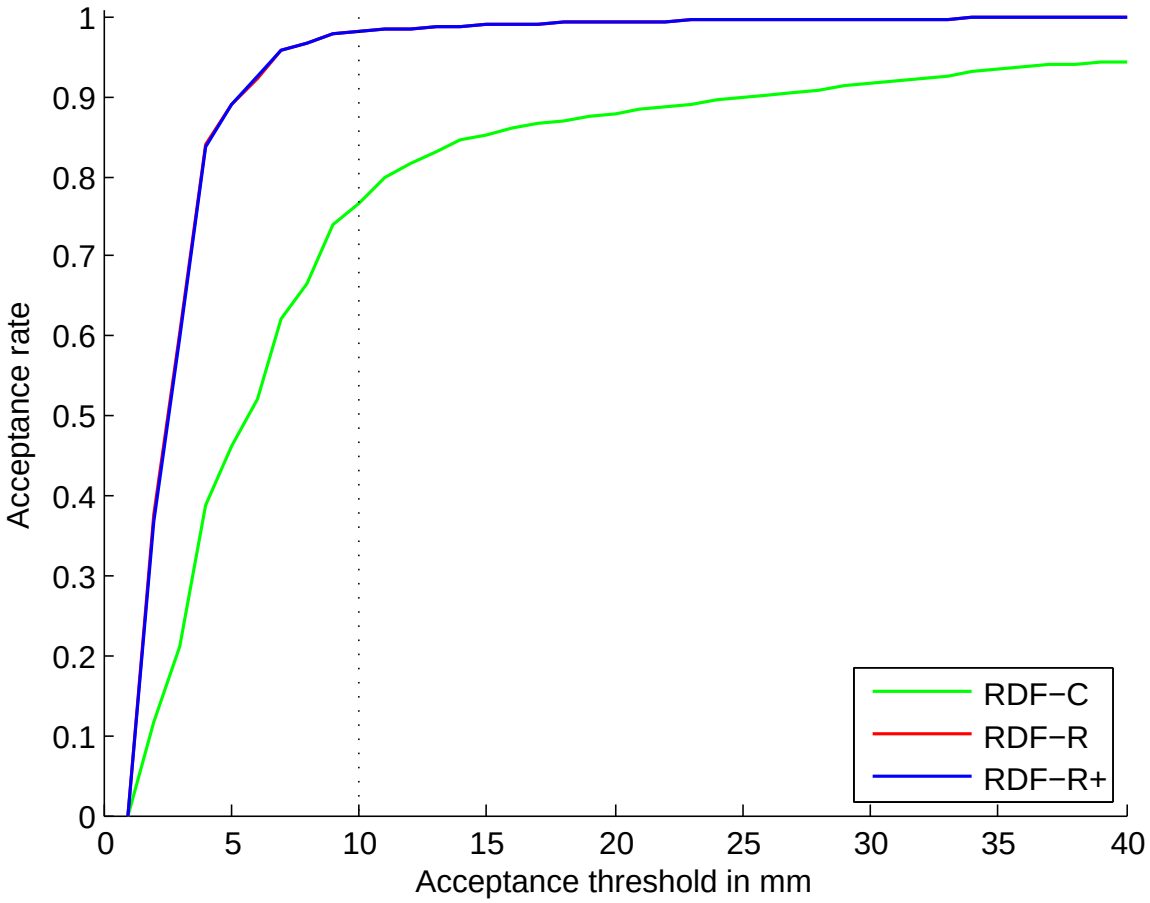

Figure 6.13. CMC curve for the TRAIN dataset.

of the valuable data is missing. The CROP dataset is specially designed for testing the inference performance of methods in the case of large amount of occlusions. The RDF-C method is by design not robust against missing data. It produces a transient state of pixel classifications where the valuable information about occluded parts are lost. RDF-R is implemented to cope with this problem. It is robust to occlusion by design. In addition, RDF-Rs provide multi-modal posterior distributions that are suitable for imposing structural constraints. The prior information provided by structural constraints of the hand is applied to create a new algorithm, namely RDF-R+.

Figure 6.14 shows the CMC curve for the CROP dataset. The performance plots clearly demonstrate the strength of RDF-R over RDF-C. 50.4% of all joints recognized by the RDF-C method are in a neighborhood of 10 mm of ground truth coordinates. RDF-R method enhances this performance to 74.8%, which is a very

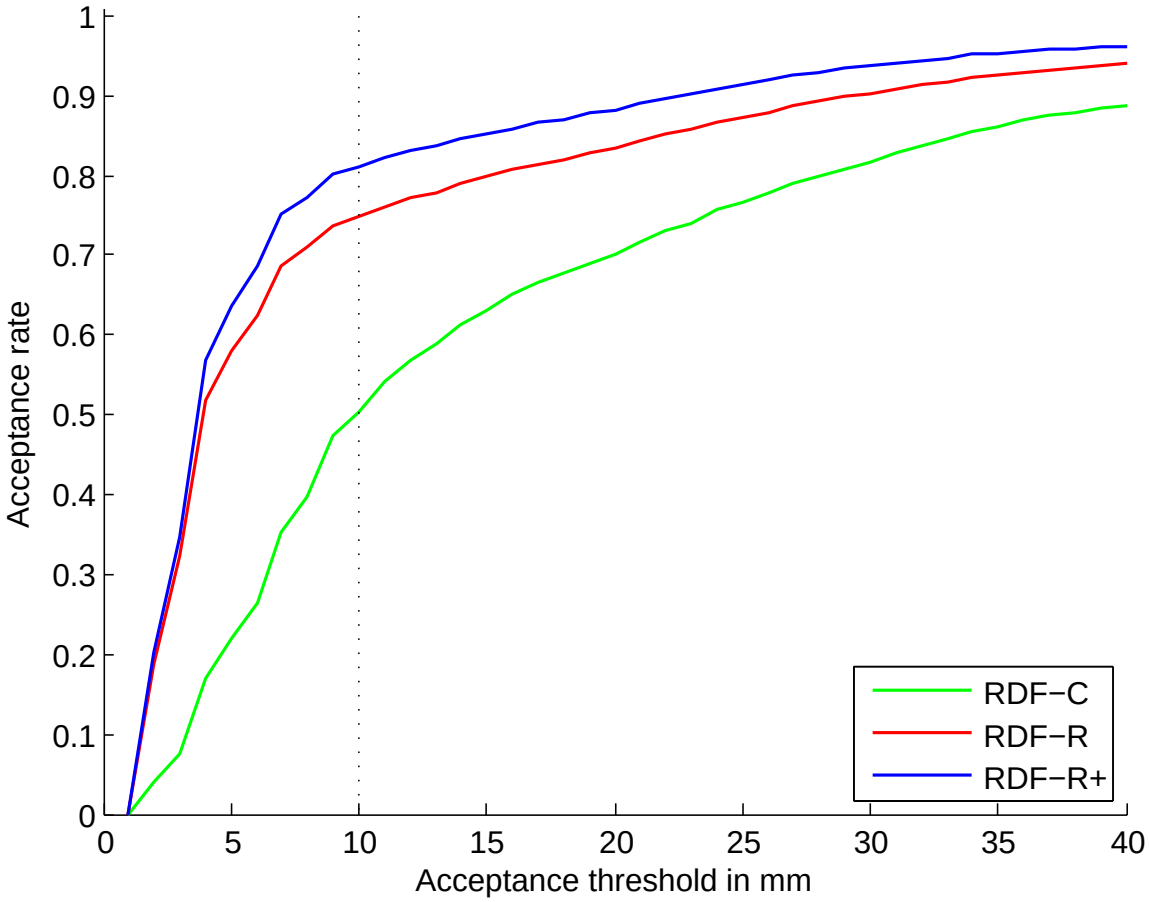

Figure 6.14. CMC curve for the CROP dataset.

significant improvement. Applying skeletal constraints still improves the results. RDF-R+ performs significantly better than RDF-R, increasing the performance to 81.3%.

6.5.2. Rock-Paper-Scissors-Lizard-Spock (RPSLS) Dataset

The RPSLS dataset is a difficult dataset to recognize by the trees trained with the TRAIN dataset. It is chosen to evaluate the sensitivity of the methods against extreme situations. The poses used during the creation of the dataset are either completely new poses or very similar but different poses. In either case the exact poses are not included in the training dataset.

Training dataset includes a thumb-up pose which means all right in English body language. This pose is similar to the rock-pose of RPSLS dataset. The open-hand pose

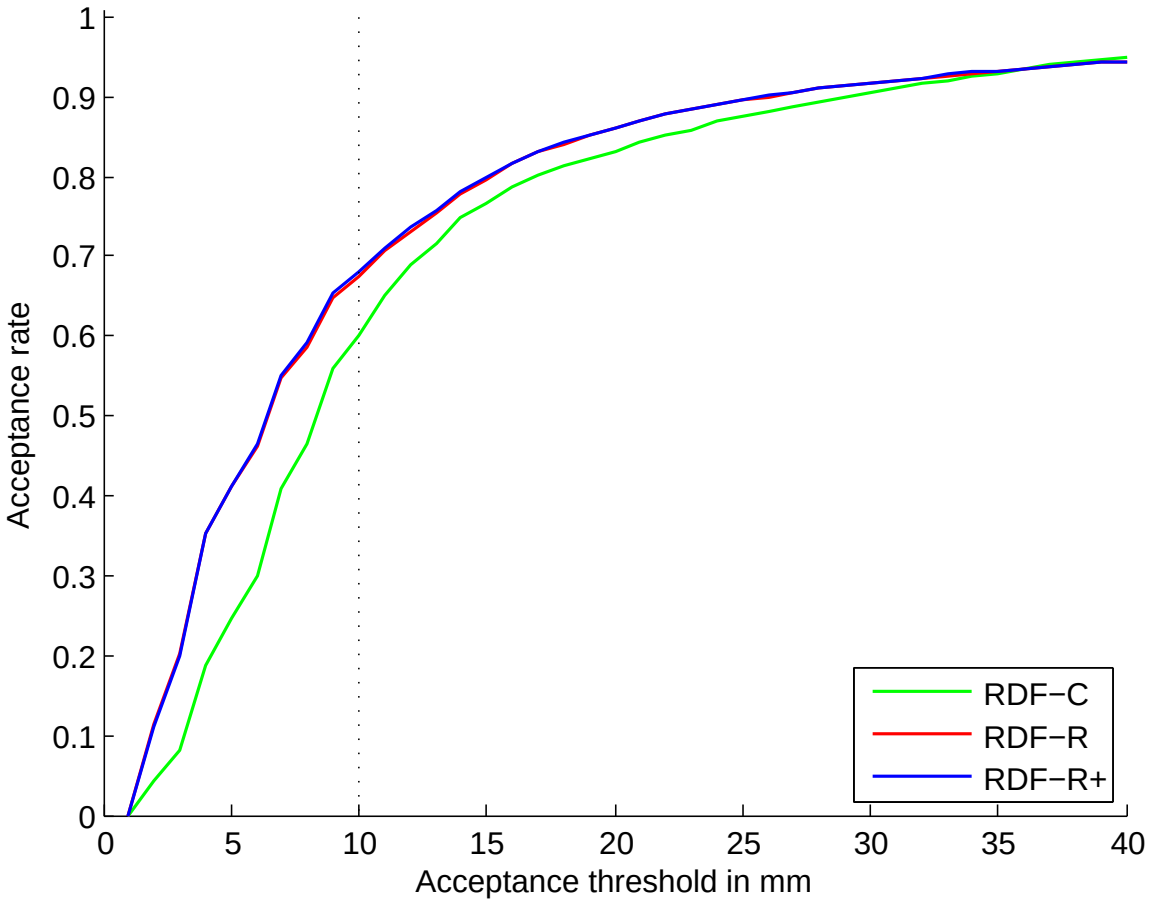

Figure 6.15. CMC curve for the RPSLS dataset.

of training dataset is similar to the Spock-pose of RPSLS dataset. The open-hand pose is not regarded as similar to the paper pose due to their different alignments around z-axis. Training set rotates the poses around z-axis only 32 degrees which cannot cover 90 degree difference between open-hand and paper poses. None of the poses in RPSLS dataset is included in training. During this test, we check for the generalization limits of different methods.

Figure 6.15 shows the CMC curve for the RPSLS dataset. The performance plots demonstrate the similar relative performance improvements between RDF-C, RDF-R. RDF-R+, however, behaves similar to RDF-R. 60.2% of all joints recognized by the RDF-C method are in a neighborhood of 10 mm of ground truth coordinates. RDF-R method increases the performance to 67.5%. An interesting result is that the performance of RDF-C is better on RPSLS dataset compared to the CROP dataset with

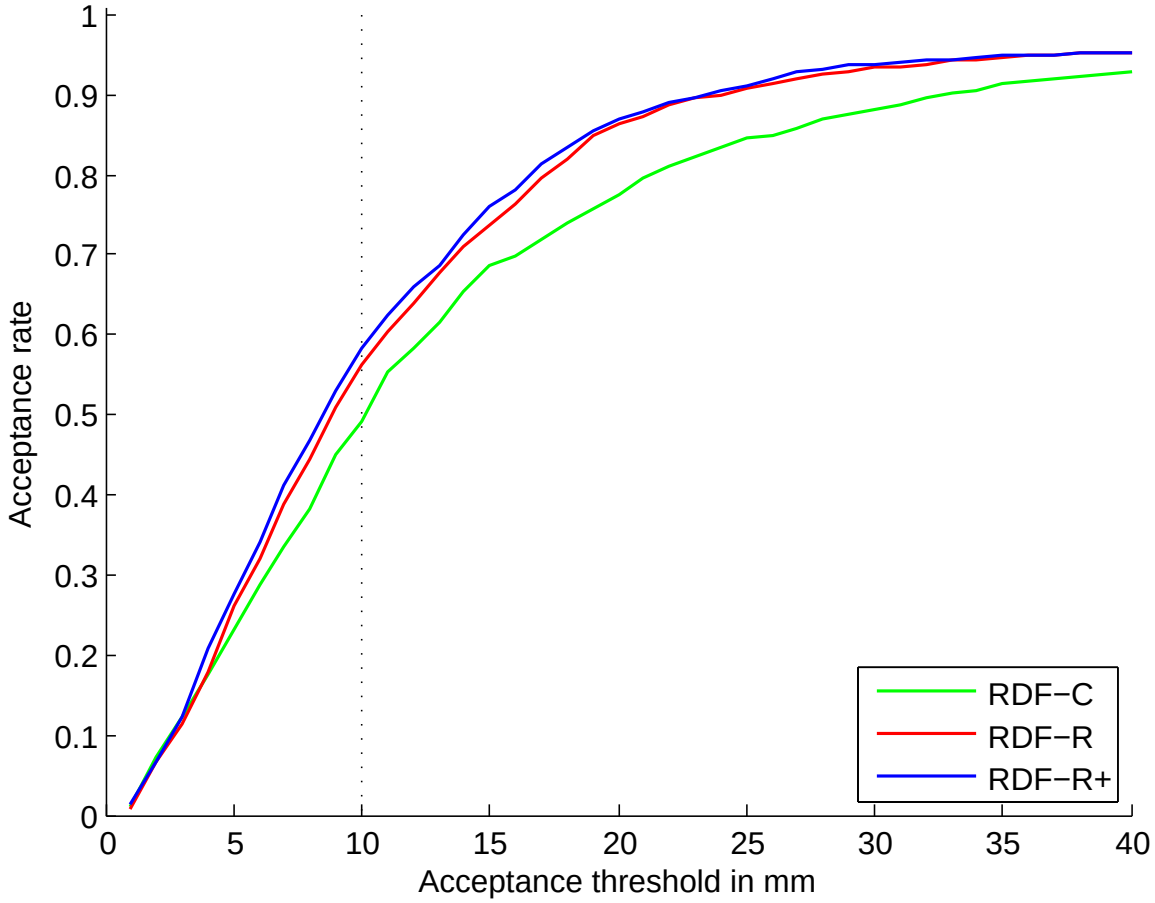

Figure 6.16. CMC curve for the SURREY dataset.

their respective values of 60.2% and 50.4%. This is caused due to successful recognition rate on poses that are similar to the training poses and absence of cropping. Inferring in case of missing data is where RDF-C is weak. Applying skeletal constraints this time improves the results not so significantly, as its performance is 67.7%. When we examine the multi-modal posterior distributions of different joints, we see that the joint configurations are either detected with a high confidence or not detected at all with a high variance. Constraints cannot improve the performance significantly since similar poses are already detected well enough.

6.5.3. ASL Finger Spelling Dataset (SURREY)

SURREY dataset is a challenging real dataset which includes both depth and color channels. For the purposes of our work we only concentrated on depth images.

Unfortunately depth images are very low resolution and come with difficult capture artifacts as shown in Figure 6.17. Figure 6.16 shows the CMC curve for the ASL Finger Spelling Dataset. The performance of all algorithms are lower than those for the CROP and RPSLS datasets. This performance degradation is due to several factors: The first, is the significantly different characteristics of the training and test datasets: The test dataset contains many different unseen poses, and variations. The second is the presence of 5 different subjects, with different hand geometries. To see which of these factors weighs more in performance degradation, we have looked at performance on different shapes and on different subjects. Instead of giving CMC curves, we provide performance figures at the 10 mm acceptance threshold in Table 6.1 and Table 6.2, for different shapes and different subjects, respectively.

Figure 6.17. Sample depth images from SURREY dataset. High variations in mean depths of hand centroids are difficult segmentation noise are illustrated.

As observed from Table 6.1 and Table 6.2, the performance varies among different hand shapes and subjects. For example, the ASL letters a and s perform the worst: Upon inspection, it is seen that these ASL letters have been performed differently than they are rendered in the training database. If one excludes these shapes from the test set, performance increases by 2.5%. Different subjects, on the other hand, affect performance; somewhat less. The hand size of the subject is an important factor. For instance, RDF-C performs better for subject 2. When subject 2's live samples are examined, it is seen that she has a considerably bigger palm and shorter fingers than the synthetic model used in training. In some rare cases RDF-R+ algorithm decreases

Table 6.1. Performances of methods for each sign in SURREY dataset: performance criterion is the percentage of joints that are closer than 10 mm to the ground truth.

ASL Letter	RDF-C	RDF-R	RDF-R+
a	46.3	44.2	**48.4**
d	49.5	**61.1**	**61.1**
e	41.1	**53.7**	52.6
f	48.4	47.4	**53.7**
i	41.1	52.6	**58.9**
l	54.7	65.3	**67.4**
s	35.8	**47.4**	45.3
u	55.8	**67.4**	63.2
v	58.9	58.9	**62.1**
w	51.6	64.2	**65.3**
y	58.9	55.8	**62.1**

the performance of RDF-R. It is due to imposing bone length constraints which are not very compatible with the test data that is estimated. It is apparent that the system would further benefit from more rigorous training, with poses closer to those in the test set, with different hand shapes, and with different hand sizes.

Overall real depth camera data performance of RDF-C, RDF-R, and RDF-R+ at 10 mm acceptance threshold are 49.3%, 56.2%, and 58.2% respectively. Comparing the different algorithms, we observe that RDF-R algorithms perform significantly better than RDF-C; and RDF-R+ has a 2% advantage over RDF-R.

Figure 6.18 illustrates sample problematic cases for different methods. The average joint estimation performance rates of methods for all four datasets are shown in Table 6.3. A more comprehensive performance illustration of different methods for SURREY dataset is illustrated in Figure 6.19. Note that some occluded joints may be located differently from ground truth in tests with real data (ASL Finger Spelling), especially when fingers are invisible due to self-occlusion. This is partly due to human

Table 6.2. Performances of methods for each subject in SURREY dataset: performance criterion is the percentage of joints that are closer than 10 mm to the ground truth.

Subject	RDF-C	RDF-R	RDF-R+
Subject 1	52.2	56.9	**61.7**
Subject 2	**50.2**	49.3	47.8
Subject 3	46.4	51.2	**56.5**
Subject 4	45.9	**57.9**	56.9
Subject 5	51.7	65.6	**67.9**

Table 6.3. Acceptance rates for the threshold of 10 mm. In all datasets, RDF-R+ method outperforms the other methods.

Dataset	RDF-C	RDF-R	RDF-R+
TRAIN	76.6	98.0	**98.1**
CROP	50.4	74.8	**81.3**
RPSLS	60.2	67.5	**67.7**
SURREY	48.7	55.8	**57.6**

errors in ground truth labeling.

6.5.4. Results

We have demonstrated an implementation of regression forests for estimating the articulated 3D pose of the human hand. Previous attempts at articulated hand pose estimation used RDF-Cs. We have adapted RDF-Rs to this problem and implemented an improved hierarchically constrained version for further enhancing the robustness against heavy occlusion by implementing an algorithm that exploits the prior knowledge about the hierarchy of human hand. Considering the hierarchical dependencies of the joints improved the joint position accuracy significantly. Skeletal constraints are exhaustively evaluated using dynamic programming in real-time. Tests with real data have shown us that although performance is lower with tests on real data, the results are consistent and performance is still acceptable. In order to improve performance, more

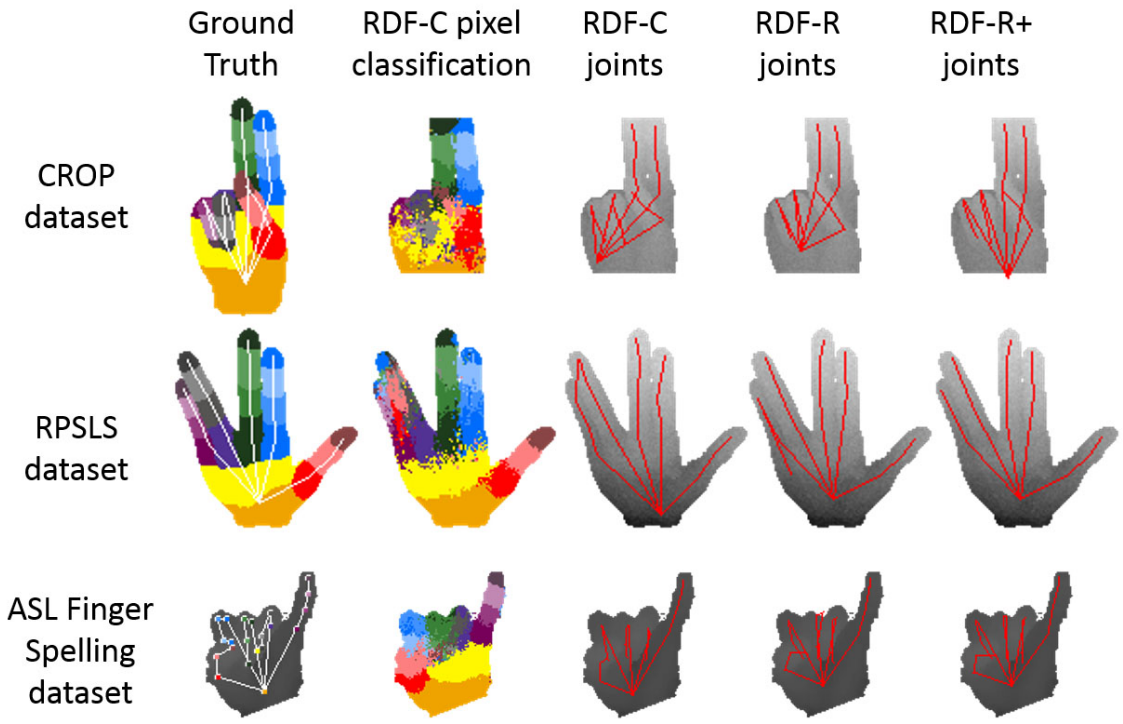

Figure 6.18. Joint estimation illustrations in the test datasets.

rigorous training with (i) more poses, (ii) different hand geometries and, (iii) real data is left as future work. The inference algorithms altogether run with an approximate speed of 200 FPS on a conventional notebook computer (Core i7 Quad 2.7 Ghz). Moreover the approach only uses a single depth image for inference. Temporal information can still be utilized for extra performance in future studies. Being able to detect the hand configuration without using a prior calibration step is important for commercial applications. Although this method works with a high accuracy, it can also be used as an initialization and/or observation step for a temporal domain tracker. For future studies, other skeletal constraints can be used and combined. Distances between all different joint pairs can be learned from the dataset for applying more restrictive hand configurations. Posterior distribution of joints can also be used as an observation step of a particle filter that fits a skeleton with a fast local search.

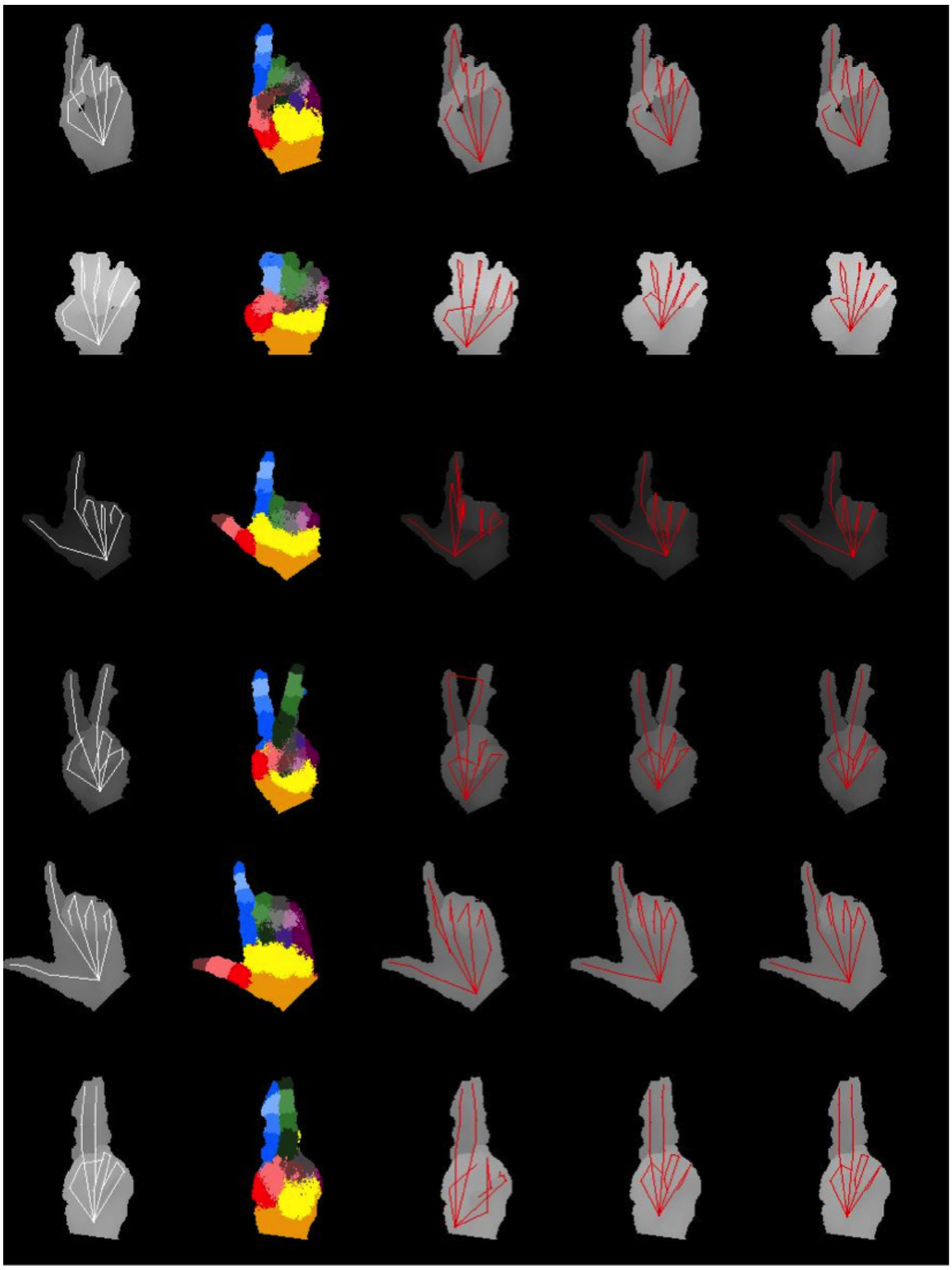

Figure 6.19. Joint estimation illustrations in SURREY dataset. From left to right; ground truth, pixel classification, RDF-C, RDF-R, RDF-R+ performances are shown.

7. TRACKING DYNAMIC HAND GESTURES

The methods discussed in previous chapters capture the pose configuration of the hand joints without using any temporal information. While this ability is essential for re-initialization of the pose estimation framework, it would be better if one could incorporate the temporal information using tracking. However, the hand pose vector is high dimensional and tracking in this space causes errors. While the hand can take arbitrary poses, it is well known that the correlation between joint angles is very high. Therefore, it is a good idea to reduce the dimensionality and to track hand pose on a reduced dimensionality manifold. Moreover, extracting a manifold provides additional benefits that it also captures the inter-dependencies of hand joint hierarchy. Previous methods such as RDF-C, RDF-H, RDF-R, all consider the joints as independent. RDF-R+ tries to force hand hierarchy into the pose configuration search but it is still possible to extract an unrelated pose.

In this section, GPLVM dimensionality reduction method is considered for reducing the dimensionality of the pose configuration model of a specific hand motion to a 2D manifold. Most pose estimation applications can benefit from the additional tracking performance gained by the prior knowledge of the underlying hand gesture. We use the GPLVM to represent the prior knowledge in terms of a hand gesture manifold.

We first start by summarizing GPLVM in Section 7.2 as published in [72]. In Section 7.3, we discuss a suitable representation of pose configuration. Learning the manifold of hand gesture is mentioned in Section 7.4. Projecting a pose configuration space vector onto the extracted manifold is explained in Section 7.5. We conclude by applying Kalman Filter in Section 7.6 and presenting our experiment results in Section 7.7.

7.1. Gaussian Processes

Gaussian Processes (GP) [91] are generalizations of Gaussian distributions defined over infinite index sets. Thereby a GP can be used to specify distribution over functions.

It is completely defined by its mean function $\mu(\mathbf{x}_i)$, which is often taken to be zero, and its covariance function $k(\mathbf{x}_i, \mathbf{x}_j)$. The covariance function k characterizes the nature of the functions that can be sampled from the process. One widely used covariance function is

$$k(\mathbf{x}_i, \mathbf{x}_j) = \theta_1 e^{-\frac{\theta_2}{2}\|\mathbf{x}_i - \mathbf{x}_j\|^2} + \theta_3 + \beta^{-1}\delta_{ij}, \tag{7.1}$$

where the parameters are given by $\phi = \{\theta_1, \theta_2, \theta_3, \beta\}$ and δ_{ij} is Kroneckers delta function. This covariance function combines an RBF function, a bias and a white-noise term. The parameters Φ of the covariance function k will be referred to as the hyper-parameters of the GP. By definition of a GP any finite number of variables specified by the process will have a joint Gaussian distribution [91]. For regression $y_i = f(\mathbf{x}_i) + \epsilon$, with noise $\epsilon \sim N(0, \beta^{-1})$, where $y_i \in \mathcal{R}$ and $\mathbf{x}_i \in \mathcal{R}^q$ placing a GP prior with zero mean and covariance function $k(\mathbf{x}_i, \mathbf{x}_j)$ (including a white-noise term with variance β^{-1}) over f, leads to the joint distribution,

$$\begin{bmatrix} \mathbf{y} \\ y_* \end{bmatrix} \sim \begin{bmatrix} \mathbf{K} & \mathbf{K}_* \\ \mathbf{K}_*^T & k(\mathbf{x}_*, \mathbf{x}_*) \end{bmatrix} \tag{7.2}$$

of a set of observed data $\{\mathbf{x}_i, y_i\}_{i=1}^N$ and an unseen point x_*, where $K_{ij} = k(\mathbf{x}_i, \mathbf{x}_j)$. Conditioning on the observed data leads to a posterior distribution over functions. From this posterior we obtain the predictive equations of a GP for an unseen point $\mathbf{x}_*$,

$$\bar{y}_* = k(\mathbf{x}_*, \mathbf{X})\mathbf{K}^{-1}\mathbf{Y} \tag{7.3}$$

$$\sigma_*^2 = k(\mathbf{x}_*, \mathbf{x}_*) - k(\mathbf{x}_*, \mathbf{X})^T\mathbf{K}^{-1}k(\mathbf{x}_*, \mathbf{X}) \tag{7.4}$$

where $\mathbf{X} = [\mathbf{x}_1, ..., \mathbf{x}_N]^T$ and $\mathbf{Y} = [y_1, ..., y_N]^T$, $\bar{y}_*$ is the mean prediction and σ_*^2 is the variance.

By maximizing the marginal likelihood over functions f,

$$P(\mathbf{Y}|\mathbf{X},\Phi) = \int P(\mathbf{Y}|f,\mathbf{X},\Phi)P(f|\mathbf{X},\Phi)df \tag{7.5}$$

$$P(f|\mathbf{X},\Phi) = N(0,\mathbf{K}), \tag{7.6}$$

the hyper-parameters Φ of the GP can be learned from the observed data. This is referred to as training in the GP framework. It might seem undesirable to optimize over the hyper-parameters as the model might over-fit the data. Setting the noise variance β^{-1} to zero the function f will pass exactly through the observed data $\mathbf{Y}$. Inspection of the logarithm of Equation 7.5,

$$\log p(\mathbf{Y}|\mathbf{X}) = -\frac{1}{2}\mathrm{tr}(\mathbf{Y}^T\mathbf{K}^{-1}\mathbf{Y}) - \frac{1}{2}\log|\mathbf{K}| - \frac{N}{2}\log 2\pi \tag{7.7}$$

shows two "competing terms", the data-fit and the complexity term. The complexity term measures and penalizes the complexity of the model, while the data-fit term measures how well the model fits the data. This "competition" encourages the GP model not to over-fit the data.

7.2. Gaussian Process Latent Variable Models (GPLVM)

Let $Y = [y_1, ..., y_N]^T$ be a matrix representing the training data, with $y_i \in \mathcal{R}^D$. Similarly, let $X = [x_1, ..., x_N]^T$ denote the matrix whose rows represent corresponding positions in latent space, $x_i \in \mathcal{R}^d$. The Gaussian Process Latent Variable Model relates a high-dimensional data set, $\mathbf{Y}$, and a low dimensional latent space, $\mathbf{X}$, using a Gaussian process mapping from the latent space to the data space. Given a covariance function for the Gaussian process, $k_Y(x, x')$, the likelihood of the data given the latent positions is,

$$P(\mathbf{Y}|\mathbf{X},\bar{\beta})\frac{1}{\sqrt{(2\pi)^{ND}\left|\mathbf{K}_Y\right|^D}}\exp\left(-\frac{1}{2}\mathrm{tr}(\mathbf{K}_Y^{-1}\mathbf{Y}\mathbf{Y}^T)\right), \tag{7.8}$$

where elements of the kernel matrix $\mathbf{K}_Y$ are defined by the covariance function, $(\mathbf{K}_Y)_{i,j} = k_Y(x_i, x_j)$. We use a kernel that is the sum of an RBF, a bias or constant term, and a noise term [72].

$$k_Y(x, x') = \theta_1 \exp(-\frac{\theta_2}{2}\|x - x'\|^2) + \theta_3 + \frac{\delta_{x,x'}}{\theta_4}, \tag{7.9}$$

where $\theta = \theta_1, \theta_2, ...$ comprises the kernel hyper-parameters that govern the output variance, the RBF support width, the bias, and the variance of the additive noise, respectively. The posterior can be written as

$$p(\mathbf{X}, \bar{\beta}|\mathbf{Y}) \propto p(\mathbf{Y}|\mathbf{X}, \bar{\beta})\, p(\mathbf{X})\, p(\theta). \tag{7.10}$$

Learning in the GPLVM consists of minimizing the log posterior with respect to the latent space configuration, $\mathbf{X}$, and the hyper parameters, θ,

$$\mathcal{L} = \mathcal{L}_r + \sum_i \ln \theta_i + \sum_i \frac{1}{2}\|x_i\|^2, \tag{7.11}$$

where we have introduced uninformative priors over the kernel hyper-parameters, and simple priors over the latent positions. These priors prevent the GPLVM from placing latent points infinitely far apart, i.e. latent positions close to the origin are preferred. The log likelihood associated with Equation (7.9) is,

$$\mathcal{L}_r = \frac{D}{2} \ln \mathbf{K}_Y + \frac{1}{2}\mathrm{tr}(\mathbf{K}_Y^{-1}\mathbf{Y}\mathbf{Y}^T). \tag{7.12}$$

Using a smooth covariance function the GPLVM will specify a smooth mapping from the latent space $\mathbf{X}$ to the observation space $\mathbf{Y}$, this means that points close in the latent space will be close in the observed space. Having a smooth generative mapping does not imply that an inverse functional mapping exists. Recently Lawrence *et al.* [92]proposed an extension to the GPLVM where the model is constrained by representing each latent point as a smooth parametric mapping from its corresponding observed data point, $\mathbf{x}_i = g(\mathbf{y}_i, \mathbf{W})$, where $\mathbf{W}$ is the mapping parameter set. This constrains points that

are close in the observed space to also be close in the latent space. The mapping from observed data Y to X is called the back-constraint.

7.3. Pose Representation Favorable for Dimensionality Reduction

GPLVM is selected as the non-linear manifold extraction tool since its behavior is well studied in recent studies. Its pose interpolation capability is especially high as presented in [93]. Our framework depends on good interpolation performance since it is infeasible to train with all the possible hand pose configurations. The framework designed must be able to generalize for poses which are not in the training dataset of manifold extraction, and GPLVM is a good candidate for having smooth interpolation performance.

Pose configuration can be defined using various different methodologies. One could store a 3D position of the root joint of the hand in the world coordinate space and then proceed by storing the relative angles of each degree of freedom per hand joint. Despite its compressed representation, this kind of pose definition is hard to utilize since even small errors in joints which are high in the hierarchy, accumulate. A very small error in the root joint would affect the whole hand configuration considerably. On the other hand, one can represent the hand pose configuration by storing all of the 3D joint coordinates, in addition to the fingertip coordinates. This kind of representation inherently includes the world space coordinates of the root hand joint, assuming that the hand size is known. Moreover, this representation style is also compatible with the RDF-C and RDF-R methods used for extracting the joint coordinates from a single depth image. Therefore, we used 3D hand joint coordinates in combination with fingertip coordinates as the pose configuration model.

Let us define $\hat{x}_t \in \mathcal{R}^m$ that represents the pose configuration of the human hand skeleton, where m is a sufficiently large number that includes 3D coordinates of all hand joints and all fingertips. In this work, m is set to be 60, which is enough to store the 3D coordinates of 15 hand joints and 5 fingertips in order to define a valid hand pose. Running a tracker on a high dimensional space such as $\mathcal{R}^m$ is a challenging task.

GPLVM is used for reducing the high dimensionality to a 2D manifold. GPLVM is initialized with Probabilistic PCA (PPCA) and a radial basis function (RBF) kernel is used as the non-linear covariance function generator. It is easier to design a robust tracker once the 2D pose manifold for a specific hand gesture is captured. The following sections describe briefly about the GPLVM for 2D pose manifold extraction and the details of the tracker running on 2D pose manifold.

7.4. Learning the 2D Gesture Manifold using GPLVM

Extracting a hand pose manifold from all possible meaningful hand configurations is a challenging task. We use the GPLVM toolkit for Matlab, designed by Neil D. Lawrence. The toolkit [72], does not support datasets of sizes greater than 500 points in feasible training times. Stability of the extracted manifold is also another problem. Therefore, in this section, we concentrated on tracking of a specific gesture, namely the grasping gesture of the hand. At first we created a 50 frame grasping animation as shown in the middle column of Figure 7.1. Applying GPLVM for reducing the dimensions to 2 produced the manifold as shown in Figure 7.2. Red dots are the projections of the original pose configuration points on the manifold space. We also want to track the grasping gesture from different camera angles. Another animation consisting of 650 frames is created where the hand is rotated around the y-axis between -30 and +30 degrees with 5 degree steps for adding some camera position invariance. This produces 13 different camera positions for the same grasping gesture. Rotated hand pose configurations are shown in Figure 7.1. Capturing the 2D manifold of the 663 frame grasping gesture data provides the manifold shown in Figure 7.4. Fortunately, the projections of the original pose configurations and their rotations do not get mixed up but display a nicely arranged set of 2D pose points on the manifold. This is a very favorable behavior of GPLVM that will increase our inference power as the tracking algorithm runs. One can understand the nature of the rotation of the hand and pose configuration of the grasping gesture just by observing the manifold space.

7.5. Projecting the Pose Observations onto the Gesture Manifold

GPLVM has many advantages, however, it only provides one-way mapping from the manifold space to the original space. Finding a mapping from the original space to the manifold remains as a global search problem. Given a pose configuration, we used a nearest neighbor classifier on the trained pose configurations for finding a suitable projection on the manifold. L_2 norm is used as the distance metric. Once the nearest pose is found, its corresponding projection on the manifold is used as the starting point of a local search. A small grid is located over the manifold space by taking the starting point as its center. Size of the grid is adjusted so that it at least contains 8 different training points. The grid is searched with a brute force algorithm, at each step mapping the 2D manifold point to its original space and evaluating the distance from the ground truth using L_2 norm. 2D coordinate which provides the smallest error is selected as the 2D mapping of the original pose configuration. Local search grid is illustrated in Figure 7.3.

7.6. Kalman Tracker on the 2D Pose Manifold

Tracking is the problem of generating an inference about the motion of an object given a sequence of data points.

In typical tracking problems, we have a model for the object's motion, and some set of measurements from a sequence of images. These measurements could be the position of some image points, the position and moments of some image regions, or pretty much anything else. They are not guaranteed to be relevant, in the sense that some could come from the object of interest and some might come from other objects, or from noise.

In this study, we used Matlab's Kalman Filter implementation with constant velocity motion model. The tracking is done in two dimensions where our extracted GPLVM gesture manifold lies. The prediction of a new pose configuration can be done by using the measurement history gathered from randomized forest outputs using the

motion model. The extracted GPLVM manifold is known to have a smooth mapping from latent space to data space. Close points in the latent space are also close in the data space. Therefore constant velocity model on the latent space assumption is valid. After the Kalman prediction phase, the predicted value is corrected with the latent projection of the newly observed measurement y_t from the randomized forests.

7.7. Experiments

A base dataset of grasping gesture that includes rotation of the hand around y-axis from -30 to 30 degrees with steps of 5 degrees is generated. This dataset is used for training RDFs and RDF-Rs which are 14 levels deep, each of them containing 5 trees.

Gaussian depth noise with a standard deviation of 2 mm is added since it provides us to create different depth images with the same animation parameters. We will be using this variation in the depth images for our cross validation needs. Effect of different depth noise values on the synthesized depth images are shown in Figure 7.5.

For testing the performance of the method discussed, 10 different grasping gesture animations are generated. The animation is the same grasping animation as the training set, however, this time the camera rotates around the y-axis from -25 degrees to +25 degrees with 0.5 degree steps producing an image sequence of 100 frames. Test animations have exactly the same hand and camera motions but each of them with its own depth noise sampled from the same Gaussian distribution. Gestures are animated with a Gaussian depth noise of 2 mm standard deviation. General direction over the extracted manifold is shown in Figure 7.6 Given a depth image of human hand, observations are done using two different techniques, namely by RDF-Cs and RDF-Rs. Observed hand pose configurations are mapped to 2D manifold using the technique described in Section 7.5. A Kalman Filter based tracker is run on the 2D manifold using constant velocity motion model. Error for a specific frame is calculated as the average of Euclidean distances of the 3D joint coordinates from their ground truth values over 10 different animations as shown in Equation (7.13). Performances

of different methods are illustrated in Table 7.1.

$$E_{f,i} = \frac{1}{k}\sum_{a=1}^{k} \|x_{a,f,i} - \bar{x}_{a,f,i}\|_2^2 \,, \tag{7.13}$$

where f is the frame index, k is the number of animations, $x_{a,f,i}$ is the 3D ground truth coordinate of the ath animation's ith joint in frame f whereas $\bar{x}_{a,f,i}$ is the measured 3D coordinate either by RDF-C, RDF-R, or RDF-R+. We cannot utilize hybrid forests RDF-H in this chapter since they require vast amounts of data. In this chapter due to limitations of GPLVM toolbox we can capture the manifold using only a small amount of training pose configurations. Usage of RDF-H's over this amount of data is not applicable.

Table 7.1. Errors of the different methods in mm.

Method	Plain Error	After GPLVM	After GPLVM+Kalman
RDF-C	5.42 ± 0.118	2.13 ± 0.052	1.45 ± 0.020
RDF-R	2.89 ± 0.059	2.01 ± 0.031	1.32 ± 0.018
RDF-R+	2.71 ± 0.073	1.95 ± 0.045	1.30 ± 0.028

7.8. Results

As we stated in previous chapters, regression based methods have an advantage against pixel classification based approaches when self occlusion is present. In this section, we designed the grasping gesture in a manner that minimal amount of self-occlusion is generated so that the performance comparison between RDF-Cs and RDF-Rs are to be made in a fair fashion. Besides all of the advantages, RDF-Rs are harder to implement and require considerably more time to be trained. In this chapter, we improved the performance of the hand pose estimation of single depth frame based methods by incorporating tracking for a known hand gesture. Prior knowledge about the hand gesture is added by using GPLVM for capturing the underlying manifold of the gesture. Tracking has been implemented using Kalman Filter that is working over the gesture manifold for three different scenarios, namely, using RDF-C, RDF-R, and RDF-R+ respectively. Using prior knowledge about the hands gesture dramati-

cally increases the performance of all methods as shown in Table 3.1. Employing a Kalman Filter on top of GPLVM projection further enhances the results as expected. Regression based methods RDF-R and RDF-R+ produce considerably better results compared to RDF-Cs as expected. Although the gesture animation is designed in favor of having no self-occlusions, the animation contains the occlusion of the tip of the thumb when the hand is fully closed. This is a major problem for RDF-Cs. They cannot find the tip of the thumb which increases their error rate. However, RDF-Rs are already known to produce better results when compared to RDF-Cs even without occlusion, as demonstrated in this study in Section 6.2. Mean of the error improves from 5.42 mm to 2.71 mm. Standard deviation also improves in regression based methods. An interesting result is that the standard deviation of RDF-R is better than RDF-R+. This can also be reasonably explained by the error induced with the application of dynamic programming. Dynamic programming of RDF-R+ method searches amount different hand joint distributions for minimizing a penalty function. Penalty function is a heuristic. A better penalty function may improve standard deviation performance of RDF-R+. A dramatic improvement is achieved by using GPLVMs gesture manifold. In the RDF-C case, the improvement is much greater than the improvement in the regression based methods. This is also reasonable since RDF-Cs are known to be relatively inaccurate compared to RDF-Rs. It is seen that the prior knowledge captured by the gesture manifold corrects most of the inaccuracy of the RDF outputs. Fortunately GPLVMs improvement still produces better performance on RDF-R and RDF-R+ as expected. Consequently, Kalman Filter further enhances the mean and the variance of the errors in both scenarios as well.

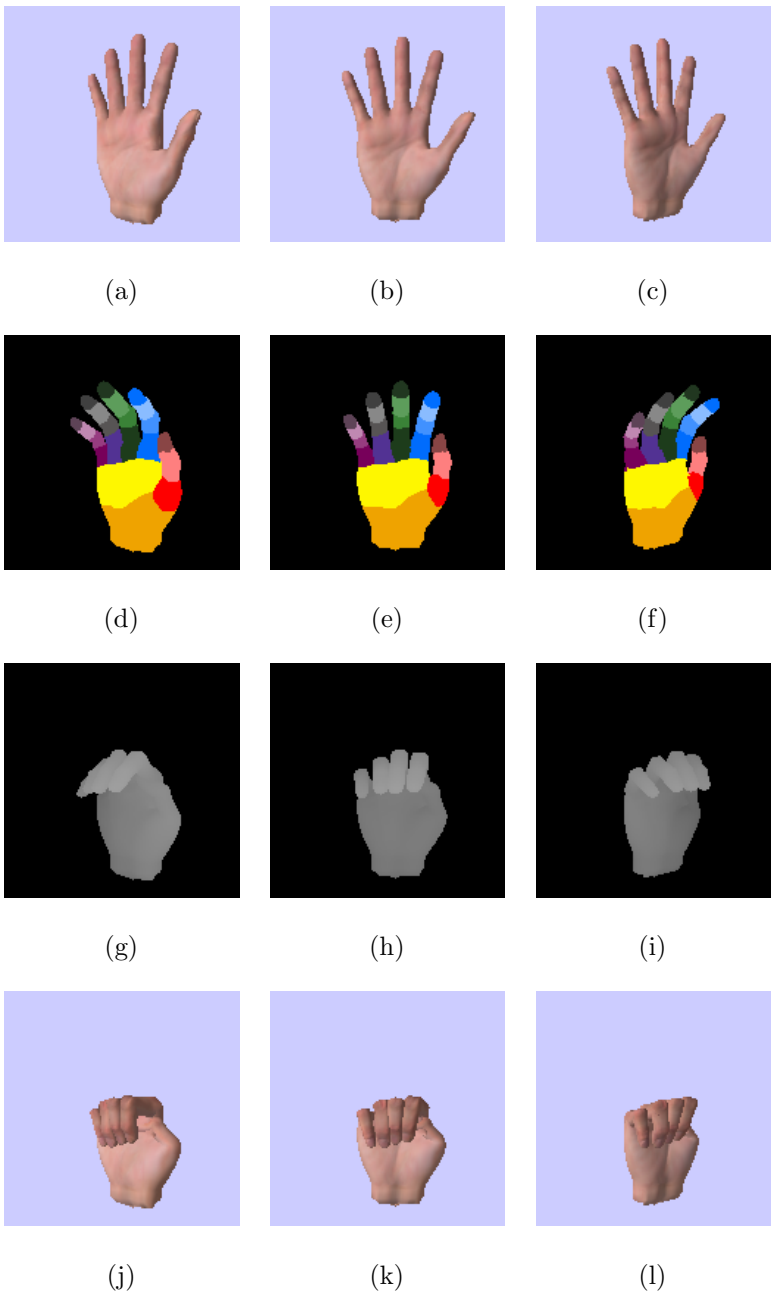

Figure 7.1. Grasping gesture of a hand demonstrated: first and last rows display realistic render of the hand, second row displays hand labels whereas third row shows corresponding depth images generated.

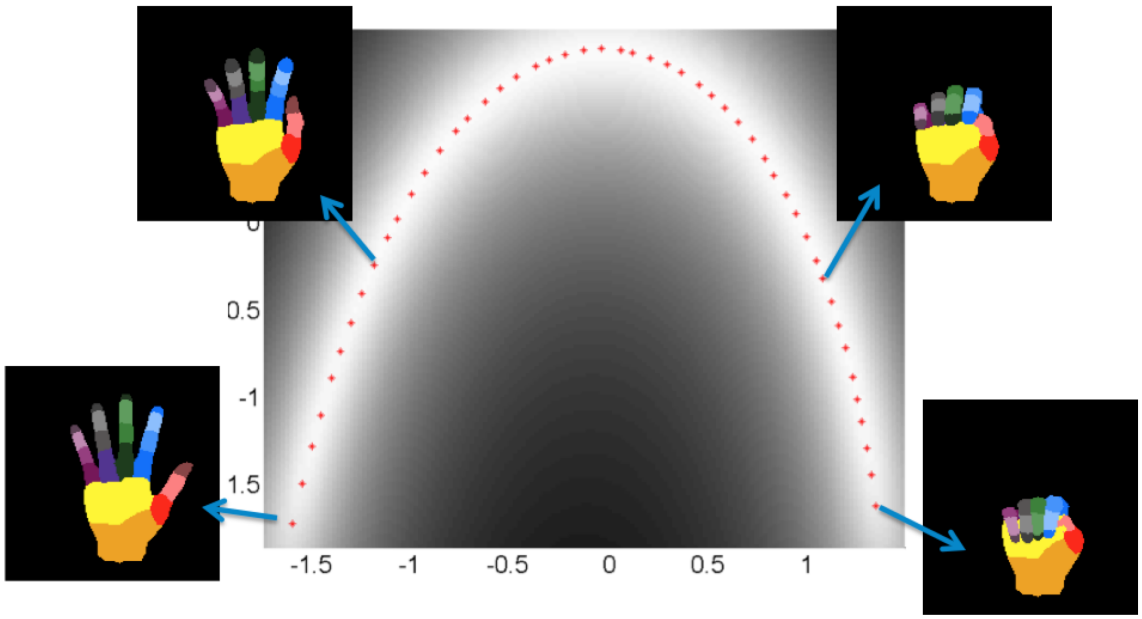

Figure 7.2. 2D manifold captured from a 50 frame grasping animation and corresponding gestures over it is illustrated.

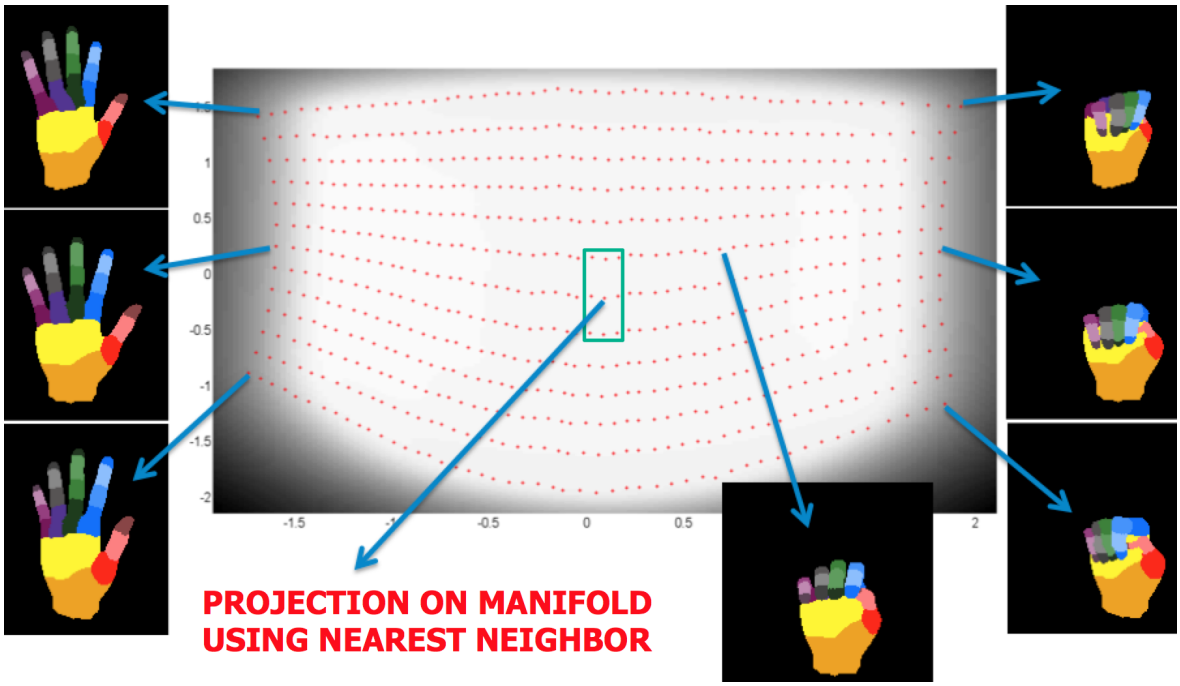

Figure 7.3. Illustration of projection onto the manifold using local search grid. Brute force search is done in the grid for fine tuning 2D GPLVM coordinates.

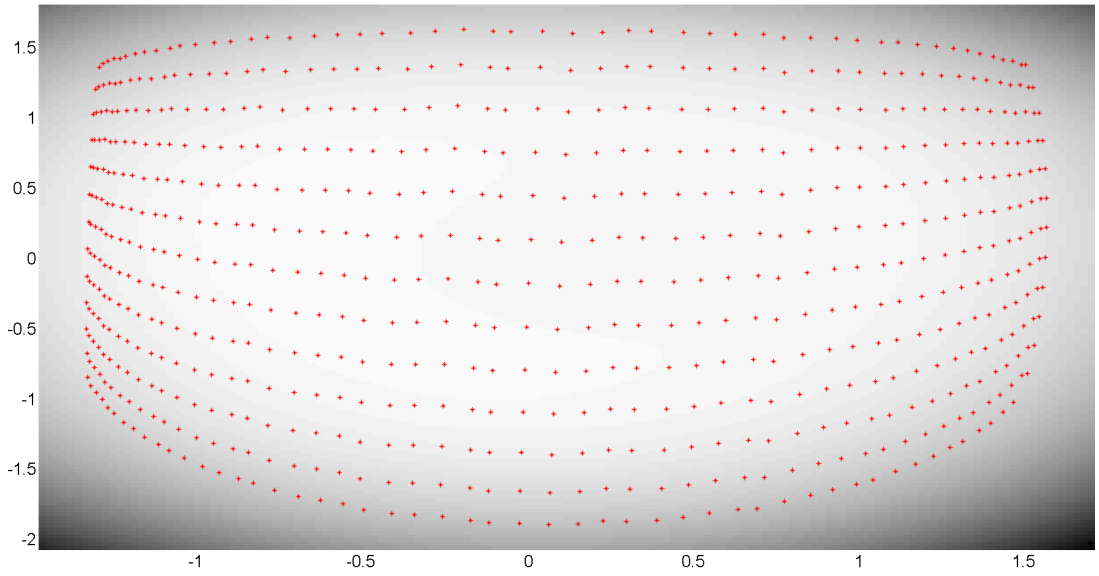

(a)

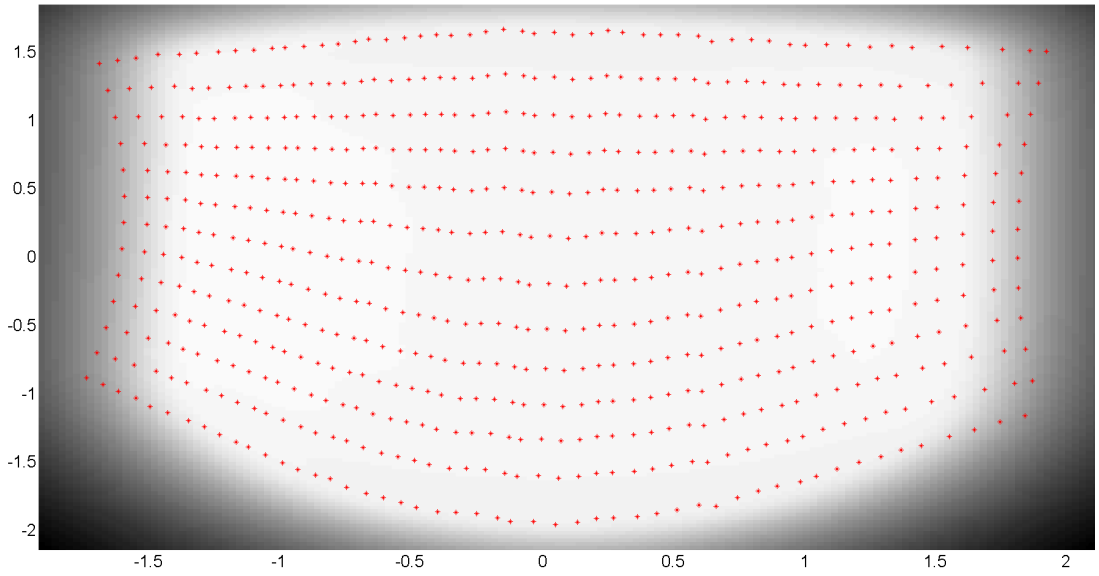

(b)

Figure 7.4. GPLVM convergence: (a) intermediate manifold, (b) converged manifold.

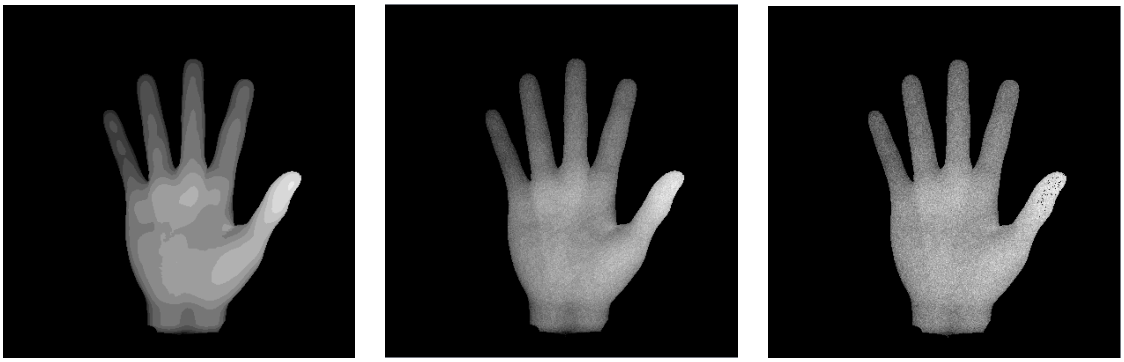

(a) (b) (c)

Figure 7.5. Effects of the Gaussian depth noise: (a) no noise, (b) 1 mm, (c) 2 mm.

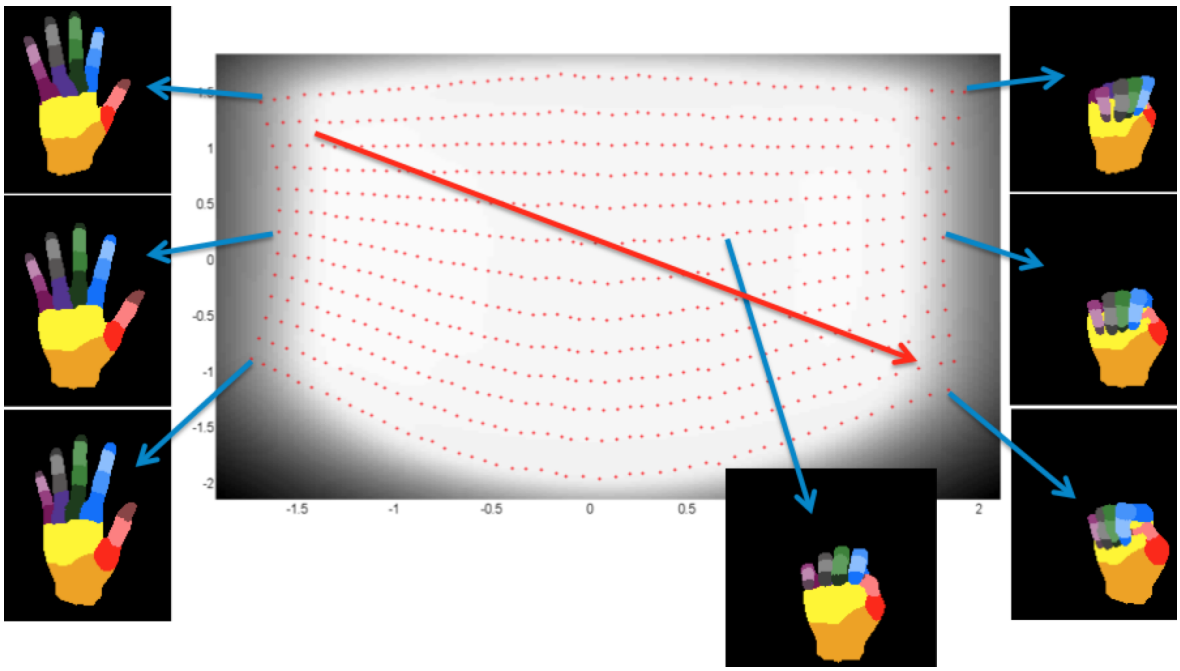

Figure 7.6. General direction of the tracked animations over the manifold as they are animated.

8. CONCLUSIONS AND FUTURE WORK

In this concluding chapter we summarize the contributions of this thesis. We finalize by discussing the important future work directions.

8.1. Summary of the Thesis Contributions

The main problem attacked in this thesis is super real-time extraction of the human hand pose from depth images. We then utilize our single frame based framework for tracking dynamic hand gestures.

We have used Randomized Decision Forests in our work. First, we have used them for inferring the shape of the hand. At the training time, we can associate a shape of the hand with its ground-truth pose configuration. Therefore, capturing the shape of the hand from the depth image can also provide us with its configuration. Unfortunately, this approach is not scalable. In the case of wrong shape classification, this approach would fail catastrophically. For a small number of different hand shapes, the method is feasible, and we call it RDF-S. We test our shape recognition framework on a dataset consisting of 65K depth images corresponding to 24 of the 26 ASL letters (omitting non–static letters j and z) performed by five subjects [83]. Pugeault *et al.*have reported their results on this dataset using both leave–one–subject–out cross–validation and by using half of the set for training and half for validation. For the former validation technique, our shape recognition framework achieved a recognition rate of 84.3%, while Pugeault *et al.* [83] report 47.0%. For the latter, an RDF-S consisting of a single tree reached 97.8%, compared to 69.0% using only depth features, and 75.0% using both depth and color features [83].

RDFs can also be used to infer the articulated pose of the hand. In order to achieve this, we start by extending our shape recognition framework so that it can recognize different shapes in a single depth image. We then map different parts of the human hand as different shapes, and basically train a shape recognizer for distin-

guishing between different regions of the human hand, and call it RDF-C. Carefully designing the regions, we assume the centroids of the different parts of the inferred regions map to their corresponding hand joints. The centroids of the regions are found by the mean shift mode finding algorithm. We choose mean shift due to its resistance to outliers. The surface depth of the joint is acquired from the depth image, and the correct 3D depth coordinate of the hand joint is evaluated by shifting the surface coordinate by a predefined value. We assume this value for all of the human hand joints to be constant.

We then combine our shape recognizer RDF-S and classification based pose estimator RDF-C for building a hybrid joint estimator, named as RDF-H. RDF-H uses two layers of RDFs. In the first layer we utilize an RDF-S for choosing the cluster of the hand pose. We then switch to an expert RDF-C which is specifically trained for that cluster of the hand poses. Clustering the hand poses is done by employing spectral clustering on the poses. RDF-H provides very good performance boost. It can improve per pixel classification rates from 68.0% up to 91.2% in certain trials. Unfortunately, RDF-Hs require vast amounts of data to be trained and are not suitable for small and medium sized datasets.

RDF-Cs and RDF-Hs are basically designed for shape recognition in single depth images. They are successful if the shapes are completely seen. In the case of the human hand, the shapes are its different regions. These regions are prone to be invisible due to self occlusion. The shape based methods are not adequate in the case of occlusion. Unfortunately, the human hand is a very deformable object that produces self occlusions all the time. For coping with this problem, we try to bypass the pixel classification phase and try to directly infer the joint coordinates. We incorporate regression based approaches. We change the training and testing framework of our RDFs so that they now do direct inference. We call this type of regression based RDFs as RDF-R. RDF-Rs skip the pixel classification, hence, the shape recognition phase. They are resistant to self occlusion by design. RDF-Rs, as expected, provide a great amount of accuracy increase. However, all the methods we designed so far consider the different joints of the hand as independent, which is clearly not the case. We try to incorporate

the hierarchical dependencies of different hand joints into our estimation process. We call the new regression based method as RDF-R+. Fortunately, it further enhances the accuracy [94].

We compare our different methods for joint estimation such as RDF-C, RDF-R, RDF-R+. We carefully design different datasets for benchmarking their advantages and disadvantages. RDF-R+ method achieves best accuracy performance both on synthetic and real datasets.

As an additional improvement, we add temporal domain knowledge into the joint estimation process by extracting a gesture manifold of the hand using GPLVM. We run a Kalman tracker over the extracted manifold for successfully tracking a specific grasping gesture of the hand. For the case of the grasping gesture, we achieve very promising accuracy results. The best single image algorithm we designed, namely RDF-R+, achieves 2.71 ± 0.073 mm average accuracy where manifold tracking method achieves 1.30 ± 0.028 mm average accuracy.

8.2. Conclusions

Estimating the joint configuration of a very deformable object such as the human hand is a tedious task. Most examples in the literature use exemplar-based approach. Our shape recognition chapter, Chapter 4, describes a framework for exemplar-based approach. Recognizing a specific hand shape inherently tells us about the pose configuration. However, we further employ more sophisticated strategies for capturing individual hand joint coordinates independently. Trying to estimate each joint on its own comes with its advantages and disadvantages. As an advantage, this approach is more generic. If a suitable learning scheme can be employed that can handle high dimensionality without over-fitting the training data, this can be a great advantage. Then we can generalize hand configurations as describing each and every different pose of a human hand using exemplar-based methods is not feasible. Fortunately, randomized decision forests are known to be resistant to over-fitting. We also utilize their massive parallelization potential for our super real-time speed target. These benefits

come with a big disadvantage that each joint is now independently estimated, hence, losing the very valuable information of hierarchical constraints of our hand model.

Losing inter-dependencies of joints as we are gaining a more generic estimation framework is a quality limiting bottleneck. Especially in the case of the human hand, which can be captured in low resolutions due to limitations of the sensors, this approach is prone to produce abnormal pose configurations from time to time. Extra constraints must be imposed to the estimation layer which utilizes the hierarchical structure of the model as we priorly know from the model. Our novel contribution RDF-R+ tries to achieve that in a very fast manner without sacrificing from our super real-time speed target. RDF-R+ guarantees to find a pose estimation which is compatible with the bone lengths of the learned model. However it does impose a bone length constraint blindly. The resulting skeleton, which is compatible with the model, can still not be the combination of joints that are originally looked for.

A better approach would be to model the pose configurations that a human hand can be in by extracting a low dimensional manifold. In Chapter 7, we both try to learn the pose configuration manifold and track a specific dynamic hand gesture with successful results. Learning the pose manifold using GPLVM is a tedious task. The human hand pose configurations can easily generate a sample set of thousands of different poses. GPLVM, a non-linear manifold extraction method, can generate qualitative manifolds that can interpolate successfully between different training samples. Unfortunately, there are two major drawbacks of GPLVM. First, its training phase takes increasingly long times as we use thousands of different pose configurations for representing the very complex hand pose configurations. Second, GPLVM learns only a mapping from the reduced manifold space to the original pose space. Going from the original pose space to the manifold space is not straightforward, though projecting the poses to the extracted manifold provides very promising results. Due to our super real-time aim, we test with a subset of the human hand poses with a very fast manifold projection method in Chapter 7. Surprisingly we achieve promising results in a small subset of gestures.

The framework is optimized for multi-core systems and is capable of running on conventional notebooks without experiencing frame drops. Further enhancement is possible through the utilization of the GPU, and this framework can be used along with more CPU intensive applications such as games and modeling tools. Usage of depth cameras has the extra benefit of not being affected by illumination also.

8.3. Directions for Future Works

8.3.1. Theoretical Investigation

A possibility for open theoretical research arises from the work presented here. Jointly learning the underlying pose configuration manifold and the randomized forests at the same time would be interesting. In our work, we were restricted in that fashion due to manifold extraction's high computational cost with our vast amount of training samples.

Multi-layer hybrid approach showed us that combining different concepts in a single architecture can boost the performance. In our case we utilized a shape recognition layer preceding the original joint estimation phase and showed its performance increase and better memory utilization. Combining two different trees actually produces another tree. We can further generalize this approach by looking at the hybrid forests as a single forest whose different layers are optimized by different criteria. For instance, training a single tree of depth 20, whose first 10 levels are trained using an entropy gain objective for shapes and the last 10 layers with an entropy gain objective of specific joints is also an interesting way to investigate. Dynamically switching between optimization criteria during training could be beneficial. More interestingly, each layer's optimization criterion can also be treated as a hyper-parameter.

Latent variable models (LVM) are valuable tools to investigate further. Recent advances in LVMs provide incorporating constraints into the learning phase such as in [95]. Non-linear dimensionality reduction area also has recent improvements as presented by Geiger *et al.* [96]. Such works are a good direction for further investigation.

Physically-based motion models are also another area of recent research. As the computational power increases we are able to design better but more complex problems. State-of-the-art computer graphics hand models are using muscle models. They model the physics of the muscles and animate the model by applying necessary forces to the underlying muscles. This gives better interaction of the model with its environment during a grasping or collision scenario. An interesting work concentrating on 3D tracking combined with kinematic models is presented in [97].

8.3.2. Evaluation

We believe that a number of interesting additional experiments would be useful to better understand the differences between algorithms and the conditions under which each algorithm is best applicable. Such experiments include an evaluation of hybrid forests more thoroughly. An investigation about different manifold extraction methods is also needed. GPLVM is a state-of-the-art tool for non-linear manifolds recently. However there are newer methods for classification and regression such as [98] and [96].

We investigated the performance of RDF-Hs comparatively with RDF-Cs in Section 5.2. However both RDF-Cs and therefore RDF-Hs are not resistant to self-occlusion. Another research area for performance evaluation can be combining the power of hybrid forests with regression based methods.

Another aspect of empirical evaluation that should be improved is in the area of comparing pose estimation algorithms in the literature. Although lack of a standard articulated pose benchmark with known ground truth (neither real images nor realistic synthetic ones) makes this difficult, it is important to compare alternative approaches. We tried to compare our results with the live Surrey dataset by manually labeling the ground truth of a small subset of poses in Section 6.5.3. A more comprehensive live benchmark is still needed.

REFERENCES

1. Oikonomidis, I., N. Kyriazis and A. A. Argyros, "Markerless and Efficient 26-dof Hand Pose Recovery", *Asian Conference on Computer Vision*, pp. 744–757, 2011.

2. Microsoft Corporation, Kinect for Xbox 360, RedmondWA, http://www.xbox.com/en-US/kinect, 2011.

3. Shotton, J., A. Fitzgibbon, M. Cook, T. Sharp, M. Finocchio, R. Moore, A. Kipman and A. Blake, "Real-time Human Pose Recognition in Parts from Single Depth Images", *Computer Society Conference on Computer Vision and Pattern Recognition*, Vol. 2, p. 3, 2011.

4. Ho, T. K., "Random Decision Forests", *International Conference on Document Analysis and Recognition*, Vol. 1, pp. 278–282, IEEE, 1995.

5. Keskin, C., F. Kıraç, Y. E. Kara and L. Akarun, "Real Time Hand Pose Estimation Using Depth Sensors", *International Conference on Computer Vision Workshops*, pp. 1228–1234, IEEE, 2011.

6. Shotton, J., T. Sharp, A. Kipman, A. Fitzgibbon, M. Finocchio, A. Blake, M. Cook and R. Moore, "Real-time Human Pose Recognition In Parts from Single Depth Images", *Communications of the ACM*, Vol. 56, No. 1, pp. 116–124, 2013.

7. Catmull, E., "A System for Computer Generated Movies", *Proceedings of the ACM Annual Conference*, Vol. 1, pp. 422–431, ACM, 1972.

8. Lee, D., M. Glueck, A. Khan, E. Fiume and K. Jackson, "A Survey of Modeling and Simulation of Skeletal Muscle", *ACM Transactions on Graphics*, Vol. 28, No. 4, pp. 1–12, 2009.

9. Heap, T. and D. Hogg, "3D Deformable Hand Models", *Gesture Workshop*, Vol. 13,

pp. 131–139, 1996.

10. Lin, J., Y. Wu and T. S. Huang, "Modeling the Constraints of Human Hand Motion", *Proceedings of Workshop on Human Motion*, pp. 121–126, IEEE, 2000.

11. Badler, N. I. and M. Morris, "Modelling Flexible Articulated Objects", *Proceedings of Online Conference on Computer Graphics*, pp. 305–314, 1982.

12. Magnenat-Thalmann, N., R. Laperrire, D. Thalmann *et al.*, "Joint-dependent Local Deformations for Hand Animation and Object Grasping", *Proceedings on Graphics Interface*, 1988.

13. Rijpkema, H. and M. Girard, "Computer Animation of Knowledge-based Human Grasping", *SIGGRAPH Computer Graphics*, Vol. 25, No. 4, pp. 339–348, 1991.

14. Gourret, J.-P., N. M. Thalmann and D. Thalmann, "Simulation of Object and Human Skin Formations in A Grasping Task", *SIGGRAPH Computer Graphics*, Vol. 23, pp. 21–30, ACM, 1989.

15. Foley, J. D., *Computer Graphics: Principles and practice, in C*, Vol. 12110, Addison-Wesley Professional, 1996.

16. Cooney, W. P., M. J. Lucca, E. Chao and R. Linscheid, "The Kinesiology of the Thumb Trapeziometacarpal Joint", *J Bone Joint Surg Am*, Vol. 63, No. 9, pp. 1371–81, 1981.

17. Buford Jr, W. L., L. M. Myers and A. Hollister, "3-D Computer Graphics Simulation of Thumb Joint Kinematics", *International Conference of the Engineering in Medicine and Biology Society*, pp. 833–834, IEEE, 1989.

18. Thompson, D. E., W. L. Buford Jr, L. M. Myers, D. J. Giurintano and J. A. Brewer III, "A Hand Biomechanics Workstation", *SIGGRAPH Computer Graphics*, Vol. 22, pp. 335–343, ACM, 1988.

19. Albrecht, I., J. Haber and H. Seidel, "Construction and Animation of Anatomically Based Human Hand Models", *Eurographics/SIGGRAPH Symposium on Computer Animation*, 2003.

20. Thalmann, N. M. and D. Thalmann, "Hidden Surfaces, Reflectance, and Shading", *Computer Animation*, pp. 87–99, Springer, 1990.

21. Deutscher, J., A. Blake and I. Reid, "Articulated Body Motion Capture by Annealed Particle Filtering", *Proceedings of the Computer Vision and Pattern Recognition*, Vol. 2, pp. 126–133, IEEE, 2000.

22. Pavlovic, V. I., R. Sharma and T. S. Huang, "Visual Interpretation of Hand Gestures for Human-computer Interaction: A Review", *Transactions on Pattern Analysis and Machine Intelligence*, Vol. 19, No. 7, pp. 677–695, 1997.

23. Torus Knot Software, Ogre3D (Version 1.8.1), http://www.ogre3d.org/.

24. Girshick, R., J. Shotton, P. Kohli, A. Criminisi and A. Fitzgibbon, "Efficient Regression of General-activity Human Poses from Depth Images", *International Conference on Computer Vision*, pp. 415–422, IEEE, 2011.

25. Fergus, R., P. Perona and A. Zisserman, "Object Class Recognition by Unsupervised Scale-invariant Learning", *Computer Society Conference on Computer Vision and Pattern Recognition*, Vol. 2, pp. II–264, IEEE, 2003.

26. Winn, J. and J. Shotton, "The Layout Consistent Random Field for Recognizing and Segmenting Partially Occluded Objects", *Computer Society Conference on Computer Vision and Pattern Recognition*, Vol. 1, pp. 37–44, IEEE, 2006.

27. Liu, X. and K. Fujimura, "Hand Gesture Recognition Using Depth Data", *International Conference on Automatic Face and Gesture Recognition*, pp. 529–534, IEEE, 2004.

28. Grest, D., J. Woetzel and R. Koch, "Nonlinear Body Pose Estimation from Depth

Images", *Pattern Recognition*, pp. 285–292, Springer, 2005.

29. Knoop, S., S. Vacek and R. Dillmann, "Sensor Fusion for 3d Human Body Tracking with An Articulated 3d Body Model", *International Conference on Robotics and Automation*, pp. 1686–1691, IEEE, 2006.

30. Zhu, Y. and K. Fujimura, "Constrained Optimization for Human Pose Estimation from Depth Sequences", *Asian Conference on Computer Vision*, pp. 408–418, Springer, 2007.

31. Bourdev, L. and J. Malik, "Poselets: Body Part Detectors Trained Using 3d Human Pose Annotations", *International Conference on Computer Vision*, pp. 1365–1372, IEEE, 2009.

32. Siddiqui, M. and G. Medioni, "Human Pose Estimation from A Single View Point, Real-time Range Sensor", *Computer Society Conference on Computer Vision and Pattern Recognition Workshops*, pp. 1–8, IEEE, 2010.

33. Plagemann, C., V. Ganapathi, D. Koller and S. Thrun, "Real-time Identification and Localization of Body Parts from Depth Images", *International Conference on Robotics and Automation*, pp. 3108–3113, IEEE, 2010.

34. Ganapathi, V., C. Plagemann, D. Koller and S. Thrun, "Real Time Motion Capture Using A Single Time-of-flight Camera", *Conference on Computer Vision and Pattern Recognition*, pp. 755–762, IEEE, 2010.

35. Suryanarayan, P., A. Subramanian and D. Mandalapu, "Dynamic Hand Pose Recognition Using Depth Data", *International Conference on Pattern Recognition*, pp. 3105–3108, IEEE, 2010.

36. Doliotis, P., V. Athitsos, D. Kosmopoulos and S. Perantonis, "Hand Shape and 3d Pose Estimation Using Depth Data From A Single Cluttered Frame", *Advances in Visual Computing*, pp. 148–158, Springer, 2012.

37. Gallo, L. and A. P. Placitelli, "View-independent Hand Posture Recognition from Single Depth Images Using PCA and Flusser Moments", *Signal Image Technology and Internet Based Systems (SITIS), Eighth International Conference on*, pp. 898–904, IEEE, 2012.

38. Billiet, L., M. Oramas, M. Hoffmann, W. Meert, L. Antanas *et al.*, "Rule-based Hand Posture Recognition Using Qualitative Finger Configurations Acquired with The Kinect", *Proceedings of the 2nd International Conference on Pattern Recognition Applications and Methods*, pp. 1–4, 2013.

39. Yao, Y. and Y. Fu, "Real-time Hand Pose Estimation from RGB-D Sensor", *International Conference on Multimedia and Expo*, pp. 705–710, IEEE, 2012.

40. Liang, H., J. Yuan and D. Thalmann, "Hand Pose Estimation by Combining Fingertip Tracking And Articulated ICP", *Proceedings of the 11th ACM SIGGRAPH International Conference on Virtual-Reality Continuum and its Applications in Industry*, pp. 87–90, ACM, 2012.

41. Breiman, L., "Random Forests", *Machine learning*, Vol. 45, No. 1, pp. 5–32, 2001.

42. Ye, M., X. Wang, R. Yang, L. Ren and M. Pollefeys, "Accurate 3d Pose Estimation from A Single Depth Image", *International Conference on Computer Vision*, pp. 731–738, IEEE, 2011.

43. Lopez-Mendez, A., M. Alcoverro, M. Pardas and J. R. Casas, "Real-time Upper Body Tracking with Online Initialization Using A Range Sensor", *International Conference on Computer Vision Workshops*, pp. 391–398, IEEE, 2011.

44. Bregler, C. and J. Malik, "Tracking People With Twists and Exponential Maps", *Computer Society Conference on Computer Vision and Pattern Recognition*, pp. 8–15, IEEE, 1998.

45. Sigal, L., S. Bhatia, S. Roth, M. J. Black and M. Isard, "Tracking Loose-limbed

People", *Computer Society Conference on Computer Vision and Pattern Recognition*, Vol. 1, pp. I–421, IEEE, 2004.

46. Wang, R. Y. and J. Popović, "Real-time Hand-tracking with A Color Glove", *Transactions on Graphics*, Vol. 28, p. 63, ACM, 2009.

47. Brubaker, M. A., D. J. Fleet and A. Hertzmann, "Physics-based Person Tracking Using the Anthropomorphic Walker", *International Journal of Computer Vision*, Vol. 87, No. 1-2, pp. 140–155, 2010.

48. Erol, A., G. Bebis, M. Nicolescu, R. D. Boyle and X. Twombly, "Vision-based Hand Pose Estimation: A Review", *Computer Vision and Image Understanding*, Vol. 108, No. 1, pp. 52–73, 2007.

49. Suarez, J. and R. R. Murphy, "Hand Gesture Recognition with Depth Images: A Review", *RO-MAN*, pp. 411–417, IEEE, 2012.

50. Athitsos, V. and S. Sclaroff, "Estimating 3d Hand Pose from A Cluttered Image", *Computer Society Conference on Computer Vision and Pattern Recognition*, Vol. 2, pp. II–432, IEEE, 2003.

51. de Campos, T. E. and D. W. Murray, "Regression-based Hand Pose Estimation from Multiple Cameras", *Computer Society Conference on Computer Vision and Pattern Recognition*, Vol. 1, pp. 782–789, IEEE, 2006.

52. de La Gorce, M., D. J. Fleet and N. Paragios, "Model-based 3d Hand Pose Estimation from Monocular Video", *Transactions on Pattern Analysis and Machine Intelligence*, Vol. 33, No. 9, pp. 1793–1805, 2011.

53. Thippur, A., C. H. Ek and H. Kjellström, "Inferring Hand Pose: A Comparative Study of Visual Shape Features", *International Conference on Face and Gesture*, 2013.

54. Singh, V. K. and R. Nevatia, "Action Recognition in Cluttered Dynamic Scenes

Using Pose-specific Part Models", *International Conference on Computer Vision*, pp. 113–120, IEEE, 2011.

55. Stenger, B., P. R. Mendonça and R. Cipolla, "Model-based 3d Tracking of An Articulated Hand", *Conference on Computer Vision and Pattern Recognition*, Vol. 2, pp. II–310–II–315, IEEE, 2001.

56. Rosales, R., V. Athitsos, L. Sigal and S. Sclaroff, "3d Hand Pose Reconstruction Using Specialized Mappings", *Proceedings of the Eighth IEEE International Conference on Computer Vision*, Vol. 1, pp. 378–385, IEEE, 2001.

57. Virtual Technologies, VirtualHand Software Library Reference Manual, http://www.scribd.com/doc/100401915/Virtual-Hand, 1998.

58. Mo, Z. and U. Neumann, "Real-time Hand Pose Recognition Using Low-resolution Depth Images", *Computer Society Conference on Computer Vision and Pattern Recognition*, Vol. 2, pp. 1499–1505, IEEE, 2006.

59. Malassiotis, S. and M. G. Strintzis, "Real-time Hand Posture Recognition Using Range Data", *Image and Vision Computing*, Vol. 26, No. 7, pp. 1027–1037, 2008.

60. Keskin, C., F. Kıraç, Y. E. Kara and L. Akarun, "Multilayered Randomized Classification Forests for Hand Pose Estimation Using Depth Sensors ", *International Conference on Computer Vision and Pattern Recognition Workshops on Gesture Recognition*, Springer, 2012.

61. Ong, E.-J. and R. Bowden, "A Boosted Classifier Tree for Hand Shape Detection", *International Conference on Automatic Face and Gesture Recognition*, pp. 889–894, IEEE, 2004.

62. Keskin, C., F. Kıraç, Y. E. Kara and L. Akarun, "Hand Pose Estimation and Hand Shape Classification Using Multi-layered Randomized Decision Forests", *European Conference on Computer Vision*, pp. 852–863, Springer, 2012.

63. MacKay, D. J., "Bayesian Neural Networks and Density Networks", *Nuclear Instruments and Methods in Physics Research Section A: Accelerators, Spectrometers, Detectors and Associated Equipment*, Vol. 354, No. 1, pp. 73–80, 1995.

64. Bishop, C. M., M. Svensén and C. K. Williams, "GTM: A Principled Alternative to The Self-organizing Map", *International Conference on Artificial Neural Networks*, pp. 165–170, Springer, 1996.

65. Bishop, C. M., M. Svensén and C. K. Williams, "GTM: The Generative Topographic Mapping", *Neural Computation*, Vol. 10, No. 1, pp. 215–234, 1998.

66. Kohonen, T., "The Self-organizing Map", *Proceedings of the IEEE*, Vol. 78, No. 9, pp. 1464–1480, 1990.

67. Tipping, M. E. and C. M. Bishop, "Probabilistic Principal Component Analysis", *Journal of the Royal Statistical Society: Series B (Statistical Methodology)*, Vol. 61, No. 3, pp. 611–622, 1999.

68. Tenenbaum, J. B., V. De Silva and J. C. Langford, "A Global Geometric Framework for Nonlinear Dimensionality Reduction", *Science*, Vol. 290, No. 5500, pp. 2319–2323, 2000.

69. Shi, J. and J. Malik, "Normalized Cuts and Image Segmentation", *Transactions on Pattern Analysis and Machine Intelligence*, Vol. 22, No. 8, pp. 888–905, 2000.

70. Elgammal, A. and C.-S. Lee, "Inferring 3d Body Pose from Silhouettes Using Activity Manifold Learning", *Computer Society Conference on Computer Vision and Pattern Recognition*, Vol. 2, pp. II–681, IEEE, 2004.

71. Grochow, K., S. L. Martin, A. Hertzmann and Z. Popović, "Style-based Inverse Kinematics", *ACM Transactions on Graphics*, Vol. 23, pp. 522–531, ACM, 2004.

72. Lawrence, N., "Probabilistic Non-linear Principal Component Analysis with Gaussian Process Latent Variable Models", *The Journal of Machine Learning Research*,

Vol. 6, pp. 1783–1816, 2005.

73. Teh, Y. W. and S. T. Roweis, "Automatic Alignment of Local Representations", *Advances in Neural Information Processing Systems*, pp. 841–848, 2002.

74. Sminchisescu, C. and A. Jepson, "Generative Modeling for Continuous Non-linearly Embedded Visual Inference", *Proceedings of the 21st International Conference on Machine Learning*, p. 96, ACM, 2004.

75. Urtasun, R., D. J. Fleet, A. Hertzmann and P. Fua, "Priors for People Tracking from Small Training Sets", *International Conference on Computer Vision*, Vol. 1, pp. 403–410, IEEE, 2005.

76. Wang, J. M., D. J. Fleet and A. Hertzmann, "Gaussian Process Dynamical Models for Human Motion", *Transactions on Pattern Analysis and Machine Intelligence*, Vol. 30, No. 2, pp. 283–298, 2008.

77. Urtasun, R., D. J. Fleet and P. Fua, "3d People Tracking with Gaussian Process Dynamical Models", *Computer Society Conference on Computer Vision and Pattern Recognition*, Vol. 1, pp. 238–245, IEEE, 2006.

78. Moon, K. and V. Pavlovic, "Impact of Dynamics on Subspace Embedding and Tracking of Sequences", *Computer Society Conference on Computer Vision and Pattern Recognition*, Vol. 1, pp. 198–205, IEEE, 2006.

79. Tian, T.-P., R. Li and S. Sclaroff, *Tracking Human Body Pose on A Learned Smooth Space*, Tech. rep., Boston University Computer Science Department, 2005.

80. Li, R., M.-H. Yang, S. Sclaroff and T.-P. Tian, "Monocular Tracking of 3d Human Motion with A Coordinated Mixture of Factor Analyzers", *European Conference on Computer Vision*, pp. 137–150, Springer, 2006.

81. Ek, C. H., P. H. S. Torr and N. D. Lawrence, "Gaussian Process Latent Variable Models for Human Pose Estimation", *Proceedings of the 4th International Con-*

ference on Machine Learning for Multimodal Interaction, pp. 132–143, Springer-Verlag, 2008.

82. Lee, C.-S., S. Y. Chun and S. W. Park, "Articulated Hand Configuration and Rotation Estimation Using Extended Torus Manifold Embedding", *21st International Conference on Pattern Recognition*, pp. 441–444, IEEE, 2012.

83. Pugeault, N. and R. Bowden, "Spelling It Out: Real-time ASL Fingerspelling Recognition", *International Conference on Computer Vision Workshops*, pp. 1114–1119, IEEE, 2011.

84. Uebersax, D., J. Gall, M. Van den Bergh and L. Van Gool, "Real-time Sign Language Letter and Word Recognition from Depth Data", *International Conference on Computer Vision Workshops*, pp. 383–390, IEEE, 2011.

85. Comaniciu, D. and P. Meer, "Mean Shift: A Robust Approach Toward Feature Space Analysis", *Transactions on Pattern Analysis and Machine Intelligence*, Vol. 24, No. 5, pp. 603–619, 2002.

86. Shi, J. and J. Malik, "Normalized Cuts and Image Segmentation", *Conference on Computer Vision and Pattern Recognition*, p. 731, Washington, DC, USA, 1997.

87. Meila, M. and J. Shi, "A Random Walks View of Spectral Segmentation", *AI and Statistics*, 2001.

88. Vitter, J. S., "Random Sampling with A Reservoir", *ACM Transactions on Mathematical Software*, Vol. 11, No. 1, pp. 37–57, 1985.

89. Kass, S., "Rock Paper Scissors Spock Lizard Game", http://www.samkass.com/theories/RPSSL.html, 1995.

90. Guyon, I., V. Athitsos, P. Jangyodsuk, B. Hamner and H. J. Escalante, "Chalearn Gesture Challenge: Design and First Results", *Computer Society Conference on Computer Vision and Pattern Recognition Workshops*, pp. 1–6, IEEE, 2012.

91. Rasmussen, C. E. and C. K. Williams, *Gaussian Processes for Machine Learning*, The MIT Press, 2006.

92. Lawrence, N. D. and J. Quiñonero-Candela, "Local Distance Preservation in The GP-LVM Through Back Constraints", *Proceedings of the 23rd International Conference on Machine Learning*, pp. 513–520, ACM, 2006.

93. Quirion, S., C. Duchesne, D. Laurendeau and M. Marchand, "Comparing GPLVM Approaches for Dimensionality Reduction in Character Animation", *Journal of WSCG.*, Vol. 16, No. 1–3, pp. 41–48, 2008.

94. Kıraç, F., Y. E. Kara and L. Akarun, "Hierarchically Constrained 3D Hand Pose Estimation Using Regression Forests from Single Frame Depth Data", *Pattern Recognition Letters Special Issue on Depth Image Analysis*, 2013.

95. Varol, A., M. Salzmann, P. Fua and R. Urtasun, "A Constrained Latent Variable Model", *Conference on Computer Vision and Pattern Recognition*, pp. 2248–2255, IEEE, 2012.

96. Geiger, A., R. Urtasun and T. Darrell, "Rank Priors for Continuous Non-linear Dimensionality Reduction", *Conference on Computer Vision and Pattern Recognition*, pp. 880–887, IEEE, 2009.

97. Salzmann, M. and R. Urtasun, "Physically-based Motion Models for 3d Tracking: A Convex Formulation", *International Conference on Computer Vision*, pp. 2064–2071, IEEE, 2011.

98. Urtasun, R. and T. Darrell, "Discriminative Gaussian Process Latent Variable Model for Classification", *Proceedings of the 24th International Conference on Machine Learning*, pp. 927–934, ACM, 2007.